SOUTHAMPTON OCEANOGRAPHY CENTRE

INTERNAL DOCUMENT No. 51

Seasonal to Interannual Variability in the SOC Air-Sea Flux Dataset and Hadley Centre Atmospheric Model Version 3

S A Josey

1999

James Rennell Division for Ocean Circulation and Climate
Southampton Oceanography Centre
University of Southampton
Waterfront Campus
European Way
Southampton
Hants SO14 3ZH
UK

Tel: +44 (0)023 80596409
Fax: +44 (0)023 80596400
Email: Simon.A.Josey@soc.soton.ac.uk

DOCUMENT DATA SHEET

AUTHOR

JOSEY, S A

PUBLICATION DATE

1999

TITLE

Seasonal to Interannual Variability in the SOC Air-Sea Flux Dataset and Hadley Centre Atmospheric Model Version 3.

REFERENCE

Southampton Oceanography Centre Internal Document, No. 51, 38pp. & figs. (Unpublished manuscript)

ABSTRACT

Results from a comparison of surface heat flux forcing variability in the SOC flux dataset with an ensemble mean of runs of the Hadley Centre Atmospheric Model 3 (HadAM3) with prescribed sea surface temperature (SST) for 1980-1995 are presented. The ability of HadAM3 to represent the detailed time evolution of the major atmospheric pressure oscillations over this period has been tested. Time series of the HadAM3 model and SOC observational indices for the Southern Oscillation are in fairly good agreement ($r^2 = 0.52$). In contrast, the North Atlantic Oscillation (NAO) indices are essentially uncorrelated ($r^2 = 0.02$). The correlation between model and observed North Pacific indices ($r^2 = 0.16$), is intermediate between these two cases. Despite the poor model representation of the NAO index time series, composite fields constructed from the HadAM3 and observed NAO indices reveal similar patterns in the dominant components of the heat exchange. However, the composite SST fields differ, suggesting that the anomalous heat exchange in the model is not strongly forced by SST anomalies. The major North Atlantic and North Pacific modes of variability in the model have been characterised by Empirical Orthogonal Function (EOF) analysis. The leading modes in the model surface fields tend to be similar, both in terms of spatial pattern and proportion of variance explained, to the observational modes characterised by Kent et al. (1999). Thus, HadAM3 appears to capture the spatial characteristics of the main modes of variability but not their time evolution. The difference in the relative ability of the model to represent the Southern Oscillation and NAO suggests that the latter process is not strongly coupled to the SST at interannual timescales. Causal relationships between the first four SST, pressure and net heat flux modes have been investigated for the North Atlantic using lag correlation analysis. Several coupled modes are found in the observational dataset in which the SST is lead by the pressure and net heat flux at intervals of 1-3 months. Little evidence is found for the SST leading atmospheric modes in either HadAM3 or the SOC dataset. The causal connection between SST, pressure and net heat flux anomalies associated with the NAO maximum state has been further investigated by a lead/lag composite analysis of the SOC dataset. Statistically significant SST anomalies with a persistent spatial pattern at lags of up to 5 months relative to the NAO index maximum are observed. These anomalies are caused by changes in surface heat exchange arising from the altered atmospheric circulation during the NAO maximum state. Prior to the NAO maximum significant SST patterns are not found. Thus, the NAO forces an ocean response via the SST field but is not driven by anomalies in this field at seasonal to interannual timescales.

KEYWORDS

AIR-SEA FLUXES, HADAM3, INTERANNUAL VARIABILITY, NORTH ATLANTIC OSCILLATION, SOC CLIMATOLOGY

ISSUING ORGANISATION

Southampton Oceanography Centre
University of Southampton
Waterfront Campus
European Way
Southampton SO14 3ZH
UK **Telephone: 023 80596116**

Not generally distributed - please refer to author

Table of Contents

ABSTRACT

Results from a comparison of surface heat flux forcing variability in the SOC flux dataset with an ensemble mean of runs of the Hadley Centre Atmospheric Model 3 (HadAM3) with prescribed sea surface temperature (SST) for 1980-1995 are presented. The ability of HadAM3 to represent the detailed time evolution of the major atmospheric pressure oscillations over this period has been tested. Time series of the HadAM3 model and SOC observational indices for the Southern Oscillation are in fairly good agreement (r^2 = 0.52). In contrast, the North Atlantic Oscillation (NAO) indices are essentially uncorrelated (r^2 = 0.02). The correlation between model and observed North Pacific indices (r^2 = 0.16), is intermediate between these two cases. Despite the poor model representation of the NAO index time series, composite fields constructed from the HadAM3 and observed NAO indices reveal similar patterns in the dominant components of the heat exchange. However, the composite SST fields differ, suggesting that the anomalous heat exchange in the model is not strongly forced by SST anomalies. The major North Atlantic and North Pacific modes of variability in the model have been characterised by Empirical Orthogonal Function (EOF) analysis. The leading modes in the model surface fields tend to be similar, both in terms of spatial pattern and proportion of variance explained, to the observational modes characterised by Kent et al. (1999). Thus, HadAM3 appears to capture the spatial characteristics of the main modes of variability but not their time evolution. The difference in the relative ability of the model to represent the Southern Oscillation and NAO suggests that the latter process is not strongly coupled to the SST at interannual timescales. Causal relationships between the first four SST, pressure and net heat flux modes have been investigated for the North Atlantic using lag correlation analysis. Several coupled modes are found in the observational dataset in which the SST is lead by the pressure and net heat flux at intervals of 1-3 months. Little evidence is found for the SST leading atmospheric modes in either HadAM3 or the SOC dataset. The causal connection between SST, pressure and net heat flux anomalies associated with the NAO maximum state has been further investigated by a lead/lag composite analysis of the SOC dataset. Statistically significant SST anomalies with a persistent spatial pattern at lags of up to 5 months relative to the NAO index maximum are observed. These anomalies are caused by changes in surface heat exchange arising from the altered atmospheric circulation during the NAO maximum state. Prior to the NAO maximum significant SST patterns are not found. Thus, the NAO forces an ocean response via the SST field but is not driven by anomalies in this field at seasonal to interannual timescales.

1. INTRODUCTION

The role that the ocean plays in determining atmospheric variability at seasonal to interannual timescales remains a topic of strong debate. In certain regions of the Tropics, the ocean and atmosphere are known to be strongly coupled and the processes associated with this coupling, as manifest most strongly in the El Nino Southern Oscillation (ENSO) cycle are becoming understood. However, in the Extratropics the level of feedback from sea surface temperature anomalies onto atmospheric modes of variability such as the North Atlantic Oscillation (NAO) remains poorly determined. The pioneering work of Bjerknes (1964) suggests that the ocean does not affect the atmosphere on interannual timescales but does become important at the interdecadal level and this viewpoint has been developed in a number of other studies (Cayan, 1992; Kushnir, 1994). However, another school of thought holds that the ocean also plays a significant role at the interannual level and Rodwell et al. (1999) have recently suggested a mechanism by which this feedback may take place.

It is in this context that the research described in this report has been conducted. The primary aim has been to ascertain whether an atmospheric model which is representative of those employed in climate studies at the Hadley Centre in recent years provides a reasonable description of the observed air-sea flux variability at seasonal to interannual timescales. To this end an intercomparison of the surface variability in the Southampton Oceanography Centre (SOC) flux dataset with that from the Hadley Centre Atmospheric Model Version 3 (HadAM3), run with prescribed sea surface temperature (SST) fields over the period 1980-1995, has been carried out. A secondary aim has been to investigate the causal connection between the ocean and atmosphere using the SOC dataset (Josey et al., 1998). Note that the model output is of limited use for assessing such connections as the SST fields are specified as a boundary condition rather than being free to evolve in response to changes in the surface fluxes.

Several aspects of the variability have been considered for both the North Atlantic and North Pacific although the focus of the causal response part of the study has been on the North Atlantic. The ability of the model to represent the observed time evolution of the major atmospheric pressure oscillations is first considered. A composite analysis is then used to investigate similarities between the model and observed (i.e. SOC) surface field anomalies during NAO extremes independently of their timing. The primary modes of variability in the model (including the NAO) have then been determined using Empirical Orthogonal Function (EOF) analysis and compared with the SOC modes characterised by Kent et al. (1999). Finally, the question of whether the atmosphere forces the ocean or vice versa has been addressed via both a lag correlation analysis of the first four SST, pressure and net heat flux EOFs and a lead/lag composite study centred on the NAO maximum state.

Use of the SOC fields limits the analysis to 1980-1995, thus we are not able to study all aspects of the major pressure oscillations as the time scale for prolonged shifts between extreme states is typically of order 20-30 yrs (Trenberth and Hurrell, 1994 ; Dickson et al., 1996). However, we are able to investigate the variability at seasonal to interannual timescales and the improved regional accuracy of 10-20 Wm^{-2} in the SOC fields, relative to earlier climatologies in which corrections were not made for ship report biases (Josey et al., 1999), warrants their use. This improvement represents a significant fraction of the signal associated with the various pressure oscillations. Within the period considered, the NAO has tended to be in a positive (also referred to as maximum) state (Hurrell and van Loon, 1997), that is to say a deeper than usual Iceland Low and stronger Azores High. Even so, other studies that have employed datasets occupying a similar interval have yielded useful insights into NAO related phenomena (Hurrell, 1995; Dickson et al., 2000). This is partly because large negative excursions do occur within this period, allowing both states of the NAO to be sampled even though the negative state might not be fully representative of the full range of conditions.

The manner in which ocean and atmosphere are linked on seasonal to interdecadal timescales is of particular interest. It has been suggested that even at short timescales the ocean plays a significant role in forcing the atmosphere with recent claims in the literature that knowledge of the SST fields at lead times of 2-3 yrs could lead to significant improvements in long term forecasts (Rodwell et al., 1999). However, this idea contradicts the results of earlier studies which suggest that it's only at the interdecadal scale that the ocean becomes important (Kushnir, 1994). In an attempt to resolve this issue the importance of SST anomalies at short timescales has been tested using the SOC flux dataset as will be described later.

Regarding the structure of the report, in the following section the model and observational datasets are described. In Section 3, results from the comparison of major modes of variability are presented. The causal connection between surface anomalies is then explored in Section 4. Finally, the implications of the results obtained are discussed in Section 5.

2. MODEL AND OBSERVATIONAL DATASETS

2.1. Hadley Centre Model

The atmospheric model used for this analysis is the HadAM3 version of the UKMO unified forecast and climate model. The model is run with a horizontal grid spacing of 3.75^{o} x 2.5^{o} , 19 vertical levels and a timestep of 30 minutes (Pope et al., 1999). The fields employed are averages over a six member ensemble of model runs (the so-called 'Climate of the 20th Century' runs) in which the Global sea-Ice and Sea Surface Temperature dataset (GISST, Rayner et al., 1996) was used to prescribe the lower boundary conditions. Each member of the ensemble was

initialised with slightly different atmospheric conditions. The model output used here is a subset of the full run consisting of individual monthly mean surface fields over open ocean and ice covered regions for the period January 1980 - December 1995.

2.2. SOC Observational Dataset

The SOC observational dataset consists of monthly mean surface flux fields determined from ship meteorological reports on a global 1^o x 1^o grid for the same period, 1980 - 1995, as the model output. The last two years of this period represent an extension to the dataset employed by Kent et al. (1999). The surface fluxes have been estimated using a bulk formula approach and the method employed is described in detail in Josey et al. (1998). In addition, Empirical Orthogonal Functions (EOFs) generated by Kent et al. (1999) from the SOC dataset have been compared with parallel fields obtained from the HadAM3 output; see their report for details of the EOF calculation and a discussion of the limitations imposed by sampling density on EOF analyses using ship based fields. Note the SOC and HadAM3 EOF calculations are based on the slightly shorter period 1980 - 1993 than that used for the remainder of the analysis described here.

3. COMPARISON OF MAJOR MODES OF VARIABILITY

In this section, various aspects of the interannual variability in the HadAM3 model and the SOC observational datasets are compared. The time variation of several of the major pressure oscillations is considered first followed by a more general comparison of the main modes of variability in the surface fields using composite, EOF and cluster analysis techniques.

3.1. Time Variation of the Major Pressure Oscillations

a.) The Southern Oscillation

The ability of the model to represent the observed time series of the Southern Oscillation over the period 1980-95 was investigated using an index suggested by Zhang et al. (1997) for which the global zonal band between 20^o S and 20^o N is split into a Tahiti pole (extending eastwards from 178^o E to the South American Coast) and a Darwin pole (which covers the remainder of the band). In a given month, the anomalous pressure (i.e. the mean value for that month - the climatological monthly mean) is calculated for each grid cell. A monthly pressure anomaly is then determined for each pole by averaging over the set of anomalous pressures formed from all grid cells within the pole. The Southern Oscillation Index (SOI) used here is

defined to be the monthly pressure anomaly for Tahiti minus that for Darwin; the anomalies for each pole having first been normalised by the standard deviation of the full time series in each case. The latitude/longitude ranges of the poles are summarised in Table 1, note that there are minor differences between them due to differences in the observational and model grids.

Time series of the model and observed SOI are shown in Fig.1. The expected extremes of the SOI corresponding to known ENSO events are evident in each time series. The SOI is negative during the El Ninos in 1983, 1987 and 1992-93 and positive for the La Ninas of 1984 and 1988-89. The two time series are fairly well correlated (r^2=0.52) suggesting that the model is able to represent the observed ENSO related pressure variability within the Tropics at least for the period considered.

b.) The North Atlantic Oscillation

Non-seasonal oscillations in the Azores High - Iceland Low pressure distribution, i.e. the NAO, have been quantified using pressure anomalies averaged over the Azores and Iceland Boxes defined in Table 2a which have been normalised as for the SOI. Hurrell and van Loon (1997) have noted that there is some question over whether the Azores High is best represented by land based pressure measurements at Azores or at Lisbon with seasonal differences in the ability of each site to capture the main pressure variations. By choosing a box to represent the Azores High that spans the longitude range between these two locations it is hoped that this problem may be avoided. Further, the choice of locations for the boxes has been guided by the location of the poles in the first EOF of pressure from the analysis of Kent et al. (1999) which is well known to be closely related to the NAO (Wallace and Gutzler, 1981).

Time series of the model and observed NAO are shown in Fig.2a, winter (December-March) months are shaded black while the remaining months are shaded grey. The two time series are uncorrelated (r^2=0.02) and restricting the comparison to winter months, in which the NAO shows the most pronounced variation, does not improve the correlation (r^2=0.01). There are no immediately obvious trends in the full time series. However, there is some indication from the winter months that the SOC NAO index tends to increase from the mid-'80's until 1994 with a sharp downturn at the end of 1995 as has been noted in other studies e.g. Hurrell and van Loon (1997). In contrast, the HadAM3 NAO index tends to peak in the middle of the period considered (1984-1991) and fall away at either end. These trends are clearer in the winter mean time series shown in Fig.2b. In producing this plot an attempt has been made to allow for the interdecadal variation in the NAO by adding the 1980-1995 mean value, 2.0±1.8, determined from a subset of the century long Hurrell NAO index (obtained from http://goldhill.cgd.ucar.edu/cas/climind/nao_winter.html) to the SOC and HadAM3 values. The variation of the Hurrell index shows that aside from the 1985-1987 winters the long-term winter mean NAO index was positive throughout this period. The SOC and Hurrell winter indices are clearly well correlated (r^2=0.88) indicating that the ship based NAO index can be used as a proxy

for that obtained from land station data. HadAM3 clearly does not capture the timing of the interannual variations in the winter index when compared either with SOC (r^2=0.05) or Hurrell (r^2=0.01). Note that the model does slightly better at representing the variation of the pressure anomaly for the Iceland Low box, r=0.19, than the Azores High, r=0.07.

c.) The North Pacific Index

Interannual variations of the pressure field over the North Pacific are closely associated with the larger scale Pacific - North American (PNA) teleconnection pattern which has its main centre of action at approximately (45° N, 165° W). Variations of the PNA pattern are effectively captured by the North Pacific index (NPI) defined by Trenberth and Hurrell (1994, hereafter TH) to be the area weighted mean pressure within the region (30 - 65° N, 160° E - 140° W). TH note that the major observed variations in this index are between values averaged over winter (November - March). Several authors have found 'regime shifts' (i.e. changes in the predominant sign) of the winter mean NPI at intervals of several decades. A significant shift occurred in 1977 to the negative state, in which the Aleutian Low intensifies and shifts south-eastward from its normal position giving cooler SSTs in the central Pacific and warmer values along the American Coast north of about 40^0 N. The negative state persisted until about 1988 after which the NPI has remained close to normal. Thus the period considered in the current analysis is dominated by the negative phase of this oscillation.

Values of the North Pacific Index for each individual month within the period 1980-1995 have been determined for the SOC and HadAM3 datasets using the boxes defined in Table 2b. Comparisons have been made with the TH NPI values over the same period which were obtained from http://goldhill.cgd.ucar.edu/cas/climind/np.html. The pressure fields in the SOC flux dataset are based on the same data source, i.e. ship meteorological reports, as those employed by TH. Thus, unsurprisingly, there is strong correlation between the NPI determined from SOC and TH, r^2=0.99 for the individual monthly values. Both datasets have been compared separately with HadAM3, only results for the SOC comparison are presented as those obtained using the TH index are very similar. At the level of individual months, for which time series of anomalous index values (where anomalies are defined with respect to the 1980-1995 monthly means) are shown in Fig.3a, there is essentially no correlation between the HadAM3 and observed indices (r^2=0.05). The poor correlation may reflect a sampling problem with the observational datasets noted by TH, namely that monthly means do not adequately represent the dominant 20 day period planetary wave at these latitudes. These authors suggest that use of a five-month winter mean avoids this problem. The correlation between HadAM3 and the observed winter mean NPI time series, see Fig.3b, is slightly higher, r^2=0.16, although still not strong. Thus, the model's ability to represent the interannual variability of the major pressure oscillation in the mid-latitude North Pacific is intermediate between that for the SOI and NAO. This may reflect a stronger coupling of the PNA to the prescribed SST signal via a teleconnection with ENSO (see the review of Trenberth et al., 1998) than is the case for the NAO.

3.2 Temporal Correlation of the Global Surface Fields

The comparison of model and observed oscillation indices indicates a regional dependence in the ability of HadAM3 to represent the observed time variation of pressure anomalies. This facet of the model performance has been further investigated by averaging the 1^o x 1^o SOC pressure dataset onto the 2.5^o x 3.75^o HadAM3 grid and determining correlation coefficients between the SOC and HadAM3 time series of non-seasonal pressure anomalies in coincident grid cells, see Fig.4a. Correlation fields have also been determined for the heat flux components and SST (Fig.4b-g).

The model and observed pressure variations are positively correlated throughout the tropics with the best agreement ($r > 0.5$) occurring in the Warm Pool (centred at about 155^o E) and Cold Tongue (about 90^o W) regions of the Tropical Pacific. In the extratropics, the agreement is generally poor and this probably reflects a weakening of the extent to which the atmospheric pressure variations are coupled to sea surface temperature anomalies. In the North Atlantic and North Pacific mid-latitudes, pressure variations in the Eastern half of the basin are better represented than in the West where they are weakly anticorrelated . Regarding the heat exchange components, the latent and sensible fluxes exhibit similar patterns with the model and observations being positively correlated throughout the tropics (with $r > 0.5$ in the Cold Tongue region of the Pacific for the latent heat) but typically in poor agreement elsewhere. For the radiative fluxes, there is not such a clear cut latitudinal dependence although the model and observed shortwave is also most strongly correlated in the Tropical Pacific. The net heat flux pattern is very similar to that for the latent which implies that anomalies in the latter tend to dominate variability in the overall heat exchange. Finally, the correlation between the SOC SST dataset and the version of GISST used as a boundary condition on the model is shown in Fig.4g. The expected pattern of weaker correlation in regions where there are few ship observations (c.f. Fig.2 of Josey et al., 1999) is seen, with r values dropping to close to zero in the Southern Ocean and at high latitudes in the Northern Hemisphere.

3.3. Composite Analysis of HadAM3 and SOC NAO Fields

The results presented in the previous section indicated that HadAM3 does exhibit non-seasonal pressure variations between the Azores and Iceland although their timing is not in agreement with that observed. In this section, HadAM3 and SOC composite fields of the surface variables at NAO extremes within the period 1980-1995 are compared in order to establish whether the model NAO related air-sea interactions are similar to those observed. As noted in the introduction, such composites may underestimate the magnitude of the difference between

extreme NAO states as the period of analysis was confined to a predominantly positive phase, the last persistently negative state occurring in the late 1960s to early 1970s (Hurrell and van Loon, 1997). However, composite analyses have been effectively employed in other studies using post 1980 datasets to characterise NAO related phenomena (e.g. Dickson et al., 2000) thus we expect the technique to be of use here.

Composite anomaly fields have been generated by separately selecting winter months in the period 1980-1995 with normalised NAO index > 1.5 for the NAO+ state (< -1.5 for the NAO- state) from the SOC and HadAM3 datasets and averaging over the resulting subset. The months selected and the value of the NAO index for each are listed in Table 3. Kent et al. (1999) carried out composite analyses of the SOC fields using extremes of the first EOF of pressure as an indicator of the NAO within the slightly shorter period 1980-1993. Note that several months (including January 1984, December 1989 and December 1993) with high index values employed here were not selected in their analysis.

Plots of the difference (NAO+ - NAO-) in the composite fields for selected surface variables are shown in Fig.5. Note that the HadAM3 anomalies are typically smaller in magnitude than their SOC counterparts by a factor $\sqrt{6}$ due to the use of an ensemble mean over 6 model runs, for ease of comparison they have been multiplied by this factor in Fig.5. The exception to this rule is the SST which being a prescribed field is the same for all model runs, thus the HadAM3 SST composite anomalies have not been scaled by $\sqrt{6}$.

a.) Surface Meteorological Fields

The anomalous pressure fields (Fig.5ab) both show the familiar dipole structure associated with the NAO with differences between the NAO+ and NAO- states of order 20mb for the Iceland Low pole and somewhat weaker, about 12 mb, for the Azores High. The main difference between the two datasets is in the location of the high pressure anomaly which is shifted NE towards the bay of Biscay in HadAM3 relative to SOC. The composite anomalies for the other surface meteorological fields are as expected from the anomalous atmospheric circulation associated with the pressure dipole and similar to those found by Kent et al. (1999) on the basis of the EOF analysis. The primary features (see Fig.5c,e) are anomalously warm, moist air in the West Atlantic adjacent to the US coast and in the mid-high latitude East Atlantic, with cold, dry air occurring in the Labrador Sea and North-West Atlantic. The HadAM3 air temperature and specific humidity fields also show these features (Figs.5d,f) although in addition HadAM3 has a weak dipole in air temperature in the sub-tropical east Atlantic that is not seen in the observations.

In contrast to the atmospheric meteorological fields the composite anomalies for SST (Fig.5gh) are noticeably different between HadAM3 and SOC Equatorwards of about 45^{o} N. The SOC composite shows a quadropole structure that is similar to the air temperature composite with the addition of a tongue of cold water in the East Atlantic at about 20^{o} N. The model composite, i.e. the GISST fields composited on the months when the model is in an NAO extreme state, show

some similarities with the SOC fields at mid-high latitudes but fail to capture the dipole between the US and West African coasts.

b.) Heat Flux Fields

The composites for the net heat flux field and its components are shown in Fig.6. The dominant feature in both the SOC and HadAM3 net heat flux composites is a dipole between the US and Greenland Coasts showing anomalous heat gain / loss of up to 100Wm^{-2}. In addition there are secondary regions of enhanced heat gain in the Greenland/Iceland/Norwegian (GIN) Seas and coastal Europe, and heat loss extending westward from the West African coast. The enhanced/reduced heat loss in the Labrador/GIN Seas is consistent with the enhanced/reduced rates of water formation in these regions during an NAO+ state which have been noted from the observational record by Dickson et al. (1996).

Decomposition of the net heat flux anomaly into components reveals that the primary contribution comes from the latent heat flux (Fig.6cd), which peaks at 60-70 Wm^{-2}. Composites of the wind speed and sea - air humidity difference reveal that the latent heat flux anomalies are primarily a response to drier air / stronger winds enhancing heat loss south of Greenland and moister air / weaker winds reducing heat loss off the US coast (see Fig.6kl for the SOC wind and humidity difference fields, the HadAM3 fields are similar). Anomalies in the sensible heat flux field (Fig.6ef) make a significant contribution, of order 30 - 40 Wm^{-2} to the net heat exchange at mid-high latitudes but not in the tropics as the sea-air temperature difference anomalies at low latitudes are relatively small (see Fig.6m). Both the latent and sensible heat flux HadAM3 composites are in good agreement with the SOC fields. The radiative flux anomalies are relatively small with enhanced longwave loss (Fig.6gh) in both sets of fields in the North-West Atlantic adjacent to Greenland and reduced shortwave gain (Fig.6ij), due to a fractional increase in cloud cover of order 0.1 (not shown), in the SOC field in a thin band at 10^{o}N. The HadAM3 radiative fields show several differences with respect to the SOC composites, in particular there is a band of increased shortwave gain at approximately 35^{o}N in HadAM3 that is not seen in the current analysis although a similar feature does occur in the composites based on EOF extremes (Kent et al., 1999).

To conclude this section, the main result is that HadAM3 appears to contain a reasonable representation of the meteorological variable and dominant surface heat flux anomalies that have been diagnosed as being associated with the NAO from the SOC dataset despite having a noticeably different SST composite field from the tropics to mid-latitudes. This suggests that the SST field does not have a strong influence on the ability of the model to produce an atmospheric pressure oscillation which interacts with the ocean in a manner similar to that observed for the NAO. This conclusion is consistent with the idea that in the North Atlantic the ocean responds passively to atmospheric anomalies at interannual timescales (Kushnir, 1994). The nature of the

causal relationships between the sea level pressure, net heat flux and SST will be explored in detail in Section 4.

3.4. EOF and Cluster Analyses of the HadAM3 Fields

Empirical orthogonal functions have been calculated for the North Atlantic, North Pacific and Global Ocean for each variable in the HadAM3 dataset, with the mean seasonal cycle removed, using data over the period January 1980 - December 1993. In the initial stages of the analysis a problem arose due to the inclusion of surface values over ice which dominated the variability in several fields, particularly the surface temperature and sensible heat flux. To avoid this problem, ice covered regions were masked from the dataset by imposing the restriction that the surface temperature be greater than -2^{o} C throughout the period considered. The model EOFs have been compared with the corresponding EOFs determined from the SOC dataset by Kent et al. (1999). Note that the same latitude/longitude ranges for the North Atlantic (10 - 80^{o} N, 90^{o}W - 40^{o} E) and North Pacific (10 - 80^{o} N, 100^{o} E - 90^{o}W) have been employed in each study although there are differences in area for which data are available due to the imposition of a sampling threshold in the SOC analysis. In addition to the EOF analysis, cluster analyses have also been carried out, primarily to provide further support for the conclusions reached.

a.) North Atlantic

i.) EOF Analysis

The prescribed model SST field i.e. GISST3.0 was the first to be considered as it was necessary to establish that the main spatial modes of variability and their time series for this field were similar to those for SOC before considering the EOFs for the freely evolving model fields. The leading six EOFs of SST from HadAM3 and SOC and the time series for each component are shown in Fig.7. There is a one-to-one correspondence between the EOFs from the two datasets with strong similarities in pattern and percentage of variance explained by each. The time series for the first three corresponding EOFs in each dataset are correlated with $r > 0.95$ while the fourth, fifth and sixth have $r > 0.76$; values for r are listed in Table 4.

Having established that the SST variability is very similar in each dataset, the first six EOFs for the other model fields were compared with the observations. The HadAM3 EOF modes tend to be spatially similar (although with occasional differences in sequencing) to SOC but their time series are different. Thus the model's ability to represent spatial variability for the NAO but not its timing tends to repeated for other modes. The strongest similarities between the HadAM3 and SOC EOFs are found for the meteorological fields; the agreement between the turbulent and net heat flux patterns is less good but typically the first two or three EOF modes can be matched,

while the radiative flux patterns do not show a strong correspondence. Selected results for key fields are presented below.

The leading six EOFs of pressure, and the net heat, latent heat and shortwave flux from HadAM3 and SOC, together with the time series for each are shown in Figs. 8-11. The expected close pattern similarity between the first EOF of pressure and the NAO composite anomaly fields (Fig.5ab and Fig.8a,g) is evident in both the model and observed fields. The correlation between the NAO index and EOF1 pressure time series is very similar in model and observations, for HadAM3 r^2=0.85 and for SOC r^2=0.86. Note also that the HadAM3 EOF1 of pressure shows the southern half of the dipole extended eastwards relative to SOC as in the composite analysis. The second and third HadAM3 pressure EOF modes are similar to the January Eastern Atlantic and Scandinavian patterns found by Rogers (1990) from an analysis of a combined land-sea surface pressure dataset covering the period 1899-1986. The first three EOF modes show a direct correspondence in terms of spatial pattern between SOC and HadAM3. However, the time series of the first three corresponding SOC/HadAM3 modes are essentially uncorrelated, $r^2 < 0.06$ (see Fig.8m and Table 4).

For the net heat flux, the first EOF is similar in HadAM3 and SOC (Fig.9) while the second and third show some resemblance although there is not a direct correspondence between the locations of the extremes. Comparison with the latent heat flux EOFs (Fig.10) confirms that the model net heat flux variability is primarily driven by variations in this component (EOF1/EOF2 and EOF3/EOF4 of the net heat correspond to EOF2/EOF1 and EOF4/EOF3 of the latent). Note that the first HadAM3 EOF of latent heat was flagged as not being distinct from the second according to the North et al. (1982) criterion described in Kent et al. (1999). The first two EOFs were found to be distinct in the SOC analysis and these are similar to HadAM3 but in reverse order. In contrast to the meteorological and turbulent heat flux fields, the leading HadAM3 and SOC EOFs for the radiative fluxes are not clearly related although for the shortwave (Fig.11) HadAM3 EOF2 and SOC EOF1 each show a dipole between the tropics and sub-tropics.

In conclusion, it appears that the major modes of North Atlantic interannual variability in the model meteorological, turbulent and net heat flux fields are spatially similar to those observed but that their time variation is not well represented. As the only time dependent information supplied to the model is the SST this suggests that the ocean does not play a major role in setting the time evolution of the model atmospheric variability at interannual timescales.

ii.) Cluster Analysis

The above conclusion has been further tested by means of a cluster analysis of the five leading EOFs of the model fields listed in Table 5. Details of the analysis technique are given in Kent et al. (1999), the particular version employed here requires that the average correlation between each member of a group and the other members falls above a particular level. The results of the cluster analysis are shown in Fig.12, which may be compared with Fig.4a in Kent et al.

(1999). Distinct groups, which are outlined in the figure, may be identified with each of the first three pressure EOFs. The main feature of the cluster plot of interest is that none of the SST EOFs are grouped with pressure. Rather they form separate groups containing in addition EOFs of the air temperature and humidity. This result provides further confirmation of the conclusion reached above that variations in the SST field do not play a major role in determining the variability of the sea level pressure in the model.

In addition to the pressure, the outlined groups tend to contain EOFs of the wind stress, turbulent heat, longwave and net heat flux as prominent members. Note that the pairing of EOF1/EOF2 and EOF3/EOF4 of the net heat with EOF2/EOF1 and EOF4/EOF3 of the latent heat flux found by subjective comparison of the spatial patterns earlier is repeated by the cluster analysis. As there are only a limited number of cases where the SOC and HadAM3 EOFs are correspondent, it is difficult to draw direct comparisons between membership of the HadAM3 groups and those found for the SOC cluster analysis. However, it is clear that as regards membership of the NAO group, similar modes of latent and net heat flux variability are included in the group in the analysis of both the SOC and HadAM3 datasets. Specifically, EOF1 of the net and EOF 2 of the latent heat flux in the HadAM3 analysis (shown in Figs. 9a & 10b) are similar modes to those found in the corresponding group for the SOC analysis i.e. EOF1 of the net and EOF1 of the latent heat flux (Figs. 9g & 10g). Thus, the results of the cluster analysis are consistent with the earlier finding that the net heat flux forcing of the ocean in the atmospheric model varies with the NAO in a similar manner to that observed.

b.) North Pacific.

i.) EOF Analysis

The model SST field was again considered first, the leading six EOFs of SST from HadAM3 and SOC and the time series for each component are shown in Fig.13. There is a strong correspondence between the spatial patterns and time series of the first five EOFs from the two datasets. The time series for the first three EOFs are correlated with $r > 0.95$ while the fourth and fifth have $r > 0.87$; values for r are listed in Table 4b.

Considering now the freely evolving model fields, the leading HadAM3 EOF modes show similarities with SOC but their time series are different as was the case for the North Atlantic. Results for selected fields follow. The leading six EOFs of pressure, and the net heat, latent heat and shortwave flux from HadAM3 and SOC, together with the time series for each are shown in Figs. 14-17. The first three EOFs of pressure in HadAM3 are similar to the central North Pacific Ocean (PAC), North Pacific Oscillation (NPO) and Bering Sea (BER) modes found by Rogers (1990). In his analysis, these three modes explain similar proportions of the variance while in the analyses of the HadAM3, and SOC, fields the PAC pattern dominates. Specifically, in HadAM3, EOF1 (PAC) of the pressure explains 49.0 % of the variance while EOF2 (NPO) and EOF3 (BER)

account for 12.7 and 9.3% respectively. The difference probably stems from the exclusion of land values from the analysis of the model fields. Both the NPO and BER patterns have significant components over land while the PAC pattern has a simple monopole structure centred over the ocean. Thus the latter is likely to dominate any analysis using ocean only data.

The correspondence in spatial pattern between SOC and HadAM3 pressure modes over the North Pacific is less clear cut than for the Atlantic. There is a clear similarity between the first EOF in each case, and between EOF4 of SOC and EOF5 of HadAM3. In addition there are features in common between EOF2 in each case, and between EOF3 of SOC and EOF4 of HadAM3. However, EOF3 of HadAM3, has no obvious counterpart in the SOC analysis. The time series in Fig.14 show a modest level of correlation between the first SOC/HadAM3 modes, r = 0.27 (see Table 4b), while the second modes have r=0.14.

For the net heat flux, the first three EOFs are broadly similar in HadAM3 and SOC (Fig.15) and the model fields share the pattern characteristics of the first three EOFs of latent heat flux (Fig.16). In contrast to the North Atlantic, the first three HadAM3 and SOC EOFs for the shortwave flux in the North Pacific (Fig.17) all show a degree of correspondence. This may reflect a more direct influence of SST variations on cloud cover via the strong ocean-atmosphere coupling associated with El Nino. In particular the first mode shows a dipole structure between the Tropical Eastern and Western Pacific which is consistent with cloud cover variations known to occur during an ENSO cycle.

In conclusion, it appears that, as was the case for the North Atlantic, the major modes of North Pacific interannual variability in the model surface fields are spatially similar to those observed but their time evolution differs.

ii.) Cluster Analysis

The results of a cluster analysis of the model North Pacific fields are shown in Fig.18, the corresponding diagram for the SOC fields is Fig.19a in Kent et al. (1999). As was the case for the North Atlantic, the SST EOFs are grouped with model air temperature and humidity rather than pressure. Two pressure related groups are outlined in the diagram. The first contains EOF1 of pressure, which is grouped with both the first and second EOFs of latent and total heat flux as was found to be the case in the SOC analysis. The other group contains both the second and third EOFs of the pressure ; these two were not grouped together in the SOC analysis but as noted above, EOF3 of pressure in the model represents the Bering Sea pattern which was not found in the analysis of the observational data. Although detailed interpretation of the cluster diagrams is problematic because of differences in EOF modes between SOC and HadAM3, the analysis is useful in the sense that it provides further confirmation that the model pressure variability is not strongly connected with that in SST.

c.) Global.

The focus of the analysis presented above has been the Northern Hemisphere basins. Global variability has also been briefly considered, EOFs of the net heat flux (Fig.19) have been calculated from the model dataset and these reveal the dominance of variability in the Tropics. The first two modes of the net heat flux show strong variability in the Tropical Pacific which a correlation analysis reveals is partly ENSO related. Values for the correlation coefficient between the time series for modes 1 and 2 and the SOI defined in Section 3.1 are r = -0.47 and -0.37 respectively. Given the poor sampling in the tropics and Southern Hemisphere in the SOC dataset, global analyses have not been carried out for the observational fields.

4. THE CAUSAL CONNECTION BETWEEN SURFACE ANOMALIES

4.1. Causal Relationships Between EOF Modes in the North Atlantic

In an attempt to gain some insight into the causal relationships between atmospheric, surface interaction and ocean modes in the model and observations, a lagged correlation analysis of the first four EOF modes of pressure (SLP), net heat flux (Qnet) and SST has been carried out. The notation used here is for SLPn to indicate the nth EOF of SLP and similarly for the other variables. The initial motivation for this analysis was the desire to establish whether the SST fields give rise to an atmospheric response in the model. As the model SST fields are prescribed it is not possible to test whether the model atmosphere forces an ocean response. In addition, the observational dataset has been tested for SST either leading or lagging the other modes in order to establish whether there are lead/lag relationships besides that between the first EOF of SLP and the second of SST lagged by one month noted in Kent et al. (1999).

Correlation analyses at offsets ranging from -6 to +6 months have been carried out for all combinations of the first four EOF modes for each variable pairing (e.g. SLP and SST) using subsets of the full EOF time series for HadAM3 and SOC that run from July 1980 to June 1993. At this stage a simple criterion that $r > 0.2$ has been used to look for paired modes, using a Student's *t*-test this threshold is significantly different from zero at the 5% significance level for the sample of 156 months considered.

First consider the cases where there is evidence that SST leads an atmospheric response. For the first two EOFs in the SOC dataset no SST/SLP pairings with $r > 0.2$ were found with SST leading. In HadAM3, the only indication of SST leading an atmospheric response is in the relationship between SST1 and SLP3 where the peak correlation occurs for a lead interval of 3 months, see Fig.20a. For SOC there are some signs of SST leading Qnet amongst the lower observational modes SST3/Qnet4 and SST4/Qnet3, these are shown in Fig.20bc. However, this behaviour is not reproduced in the analysis of HadAM3 output.

Now consider the cases for which there are significant correlations when the SST modes lag those in SLP and Qnet. Three main groups emerge from the analysis of the observational dataset which share the common feature that the SLP and Qnet modes have maximum correlation at lag zero and each individually leads the same SST mode with r > 0.2 at some point within a lead interval of 1-3 months. Lead/lag correlation plots for each group are shown in Fig.21, peak values for the correlation coefficients together with the lag at which they occur are listed in Table 6. The groups are as follows:

a) Group 1. SLP1 / Qnet1/ SST2 (Fig.21a-c). There is a strong correlation between SLP1 and Qnet1 at lag zero in both model (r=-0.59)and observations (r=-0.65). The lagged plots show that in the observational dataset both SLP1 and Qnet1 lead SST2 with peak correlation > 0.4 at a lag of 1 month. Note that this group was identified by Kent et al. (1999).

b) Group 2. SLP2 / Qnet2 / SST1 (Fig.21d-f). The second EOFs of SLP and Qnet are correlated at lag zero with r=0.47 in HadAM3 and r=0.41 in SOC. In the SOC dataset, each of these modes has r> 0.2 with lagged SST1, although on different timescales; SLP2 shows the strongest correlation with SST1 lagged by 1 month while Qnet2 peaks with SST1 lagged by 3 months.

c) Group 3. SLP3 / Qnet2 / SST3 (Fig.21g-i). Qnet2 is also correlated with SLP3 at zero lag in both datasets (r=-0.52/-0.47 in SOC / HadAM3). In the SOC dataset, each of these modes has a peak correlation with SST3 at a lag of 1 month (r=0.31/-0.28 for SLP3 / Qnet2).

In addition to the above groups, SLP2 was found to be strongly correlated with Qnet3 at lag zero in SOC (r=-0.54) but not HadAM3 (r=0.19), this pairing and that between Qnet2 and SLP3 discussed above was noted in Kent et al. (1999). Qnet3 has a weak lagged correlation relationship with SST1 (not shown), so there remains the possibility that it should be included in Group 2 rather than Qnet2.

The correlations discussed above are relatively weak. This is due in part to the shorter timescale for variability of SLP and Qnet relative to SST which is evident in the EOF time series (Fig.7c, 8c, 9c). When the SLP time series are smoothed with a 3 point running mean the peak lagged correlations (occurring at the same lags as those found for the unsmoothed dataset) for the three main pairings are SLP1/SST2 (r=0.58), SLP2/SST1 (0.45) and SLP3/SST3 (0.48).

The main conclusion from this section is that there is little evidence amongst the first four EOFs for SST leading an atmospheric response in the observations and only a weak relationship (between SST1 and SLP3) in the model. There is evidence for SST lagging the SLP/Qnet modes with a significant correlation in the observational dataset and three groups have been noted, one of which was identified in the earlier analysis of Kent et al. (1999). The relationship between these groups is shown schematically in Fig.21j.

4.2. Ocean - Atmosphere Lead/Lagged Relationships with the NAO

The role of the ocean in driving / responding to the NAO has been further investigated by means of a lead / lagged composite analysis of the SLP, SST and Qnet fields about the NAO+ state. Composites of these fields were formed for both the SOC and HadAM3 datasets using the extreme NAO+ months listed in Table 3, offset by between -6 and +6 months. The comparisons presented here focus on the NAO+ state as results obtained for the NAO- state showed a somewhat weaker signal. This probably reflects conditions during the period considered in which the NAO- states were not as strong as those regularly experienced during the long term (i.e. interdecadal) negative phase of the oscillation. The composite fields have been tested for statistical significance using a grid point two-tailed *t* test at the 5% significance level with the null hypothesis that the anomaly is not significantly different from zero (see e.g. von Storch and Zwiers (1999) for details of the test). Note that with the chosen significance level there is a 5% probability that the test will incorrectly reject the null hypothesis i.e. that the anomaly will be incorrectly interpreted as significant. Selected lead/lagged spatial fields are shown in Fig.22a-e.

a.) Sea Level Pressure

Composite SLP fields for SOC and HadAM3 at intervals of -1, 0 and 1 month with respect to the NAO maxima are shown in Fig.22a. At lag 0 both datasets show a similar dipole structure to that noted in Sec. 3.3a for the NAO+ - NAO- composite. At a lead interval of 1 month the dipole structure remains weakly present in the SOC dataset but in HadAM3 the only significant feature is a small positive pressure anomaly located roughly midway between the two poles of the zero lag dipole. This suggests that the development of NAO+ conditions is different in the model from that in the observed record. At a lag of 1 month after the NAO maximum, the HadAM3 field retains the dipole structure but shifted westward from its zero lag location, while SOC has no features of significant spatial extent. Note that at longer lead/lag times there were no features of interest in either dataset.

b.) Sea Surface Temperature

Composite SST fields for SOC and HadAM3 at leads of 0-2 months with respect to the NAO maxima are shown in Fig.22b. At lead 0, the SOC dataset shows features consistent with the quadropole structure noted in Sec. 3.3a. In contrast, the model's only significant feature is a high latitude zonal dipole between the Labrador and Norwegian Seas. This feature is weakly present at lead intervals of 1-2 months relative to the model NAO+ state. However, calculations of the lagged correlation coefficient between the difference in the mean Labrador and Norwegian Sea SSTs and the model NAO index show that the two are not significantly correlated i.e. this high latitude dipole is not driving the model NAO. For the lead intervals of 1-2 months shown here (and at longer leads of up to 6 months not shown) there are no large scale significant anomalies in either

dataset. Thus the result noted in Sec. 4.1., that there is no indication of any SST mode leading SLP1 (i.e. the NAO), finds wider support in the composite analysis.

In contrast, evidence for significant SST anomalies lagging the NAO maxima are found from the analysis of the SOC fields for which composites at lags of 1 to 6 months are shown in Fig.22c (recall that as the HadAM3 SST fields are prescribed they cannot usefully be analysed for lagged signals). At lags of 1-2 months the main elements of the lag 0 SST field persist and a warm anomaly develops in the GIN seas. Over subsequent months these features weaken on a timescale that increases with latitude, the cold anomaly to the SE of Greenland still being significant at a lag of 5 months.

c.) Net Heat Flux

Composite Qnet fields for SOC and HadAM3 at lead intervals of 2, 1 and 0 months with respect to the NAO maxima are shown in Fig.22d. At lag 0, the SOC dataset shows a dipole structure with enhanced heat loss south of Iceland and reduced loss at about (40^{o} N, 60^{o} W) ; this feature is evident to a limited extent at a lead of 1 month but there is nothing significant at 2 months or earlier. Although there is some indication of anomalous heat flux forcing preceding the NAO by 1 month there is no associated SST feature (Fig.22b), thus it appears likely that this pattern represents anomalous forcing of the ocean by the atmosphere associated with the anomalous pressure field at a lead of 1 month noted above (Fig.22a). For HadAM3 at lag 0 there is a weak tripole structure in the Qnet field but nothing of strong significance in the lead fields.

Finally, we consider the SOC Qnet fields at lags of 1 - 6 months (Fig.22e). One might expect to find an anomalous surface heat flux signal related to the persistent SST anomalies (Fig.22c). No such response is seen indicating that the SST anomalies do not exert a significant feedback on the atmosphere on these timescales. A partial explanation for this may be that lags of 1 - 6 months are likely to shift the season being considered from winter to spring or summer in which the magnitude of the turbulent heat flux forcing is somewhat weaker (see e.g. Josey et al., 1999). Thus although there are SST anomalies present they may be insufficient to result in strong heat flux anomalies due to seasonal weakening of wind speed and changes in air temperature and humidity that act to reduce the air-sea temperature and humidity gradients.

Although not significant at short lag intervals, it is possible that SST anomalies become significant in the winter following the NAO maximum via re-emergence of a signal with the winter deepening of the mixed layer. To investigate this possibility, lagged composites of SST and Qnet for intervals of 11 and 12 months after the NAO+ state maximum have also been determined and are shown in Fig.15f. Scattered positive anomalies of order 0.2-0.3^{o} C are observed in the SST field. However, these are not associated with significant Qnet anomalies. Thus, it appears that the SST anomalies generated by the NAO do not have a major feedback on the atmosphere in the following winter.

In conclusion to this section, we have found no evidence to support the notion that SST anomalies play a significant role in establishing the state of the North Atlantic Oscillation at seasonal to interannual timescales in either the observed or atmospheric model datasets considered. Note that interdecadal timescales have not been considered so there remains the possibility that the ocean does play a role on longer periods. We have found evidence that NAO related surface heat flux forcing anomalies result in SST anomalies that persist for up to 6 months after the NAO maximum. However, these anomalies were not found to exert a feedback heat flux forcing on the atmosphere thereby further confirming the ocean's passive role at interannual and shorter timescales with regard to this mode of ocean-atmosphere coupling.

5. DISCUSSION

In this study, a comparison of the variability in the air-sea heat flux and related meteorological fields in the HadAM3 model and the SOC observational dataset has been carried out for the period 1980 - 1995. The main aims have been to assess the model's ability to represent the observed variability and to explore causal relationships between the ocean and atmosphere in the North Atlantic using the SOC dataset. There are two main conclusions, the first is that the model provides a reasonable representation of the spatial but not the temporal variations of the principal modes of interannual variability in the North Atlantic and North Pacific. The second is that at seasonal to interannual timescales the ocean does not exert a strong influence on atmospheric variability over the North Atlantic as manifest most strongly in the NAO.

Regarding the model performance, comparisons of the HadAM3, SOC and Hurrell NAO indices reveal that the time evolution of the NAO in the model within the period 1980 - 1995 does not correspond to that observed. The implications of this result for the suggestion by Rodwell et al., (1999) that the European winter climate could be predicted 'up to several years in advance' using a similar model given a knowledge of the SST evolution need to be considered. There are several possible causes of the poor temporal simulation in the model, it may reflect a problem with the representation of ice (more recent results from a run of HadAM3 with an improved ice field suggest a better representation of the NAO time variability, C. Gordon, personal comm.). However, the main centres of action in the NAO are located away from the ice edge and it is the mid-latitude variability in the pressure that is most poorly represented in the model (see Fig.4a), this suggests that other factors are at work. Comparisons of the pressure variations in the North Atlantic and Pacific, indicate that one of these factors is that the atmospheric link between the two basins is too strong in the model. Time series of winter mean values for the NAO, NPI and SOI in both the observational and model datasets are shown in Fig.23. The correlation between the North Pacific and Southern Oscillation Indices noted in Sec. 3.1. is evident in both time series. In contrast, the NAO time series is not significantly correlated

with either of the Pacific indices in the SOC dataset but does show a strong correspondence in the model. Values for r^2 between the various time series are summarised in Table 7. Variations in the NPI account for 45% of the NAO variance in the model, while these indices are uncorrelated in the observations. Thus, the model's poor performance in representing the time evolution of the NAO appears to be largely due to an unrealistically strong link between the atmospheric variability over the Pacific and the Atlantic such that the NAO is being driven to a significant extent by the Southern Oscillation. This link is evident in global fields of the pressure difference between NAO+ and NAO- states shown in Fig.24. A broad band of anomalously high pressure extends across the entire North Pacific basin in HadAM3 while in the SOC analysis this region is much more isolated. In addition, the model has a broad area of anomalously low pressure in the Indian Ocean which has no observational counterpart. It is suggested that teleconnections between the Tropics and higher latitudes within the model might usefully be explored in the future to shed further light on the reasons for the model differences with respect to the observed record.

The model inability to represent the NAO time evolution further suggests a passive rather than an active role of the sea surface temperature at interannual timescales in the mid-latitudes ; i.e. that the coupled ocean-atmosphere system behaves in the manner originally suggested by Bjerknes (1964). The contrast with the model response in the Tropical Pacific, where the time series of the Southern Oscillation index is well represented, suggests that the model is able to capture interannual variability in regions where there is a strong response of the atmosphere to SST anomalies. In the mid-latitude North Pacific, where a teleconnection between variations in surface pressure and tropical SST is well recognized (Trenberth et al., 1998), the model performs somewhat better at representing the time evolution of the main pressure index relative to the North Atlantic.

Composite fields of anomalous heat loss difference between NAO+ and NAO- states from the observations and HadAM3 show similar spatial patterns with reduced (enhanced) heat loss off the south-east coast of the United States (in the Labrador Sea and region to the south of Iceland). In each case, these patterns are set mainly by anomalously weak (strong) latent heat loss arising from atmospheric circulation anomalies which give rise to moister air and weaker winds (drier air and stronger winds) over the regions concerned. The anomalous sea surface temperature fields are quite different for the model and observations which indicates that they do not play a significant role in establishing the heat flux anomalies associated with the NAO. It should be noted that the idealized experiments of Rodwell et al. (1999), which suggest that the NAO arises from anomalies in the SST field, give rise to a pattern of latent heat loss which is essentially opposite in sign to that found in the current analysis. In their analysis they obtain enhanced latent heat loss over the southern pole of the dipole and reduced heat loss over the northern pole, the reason being that the SST anomalies are maintained throughout their experiment without adjustment for losses to the atmosphere.

Turning now to the causal relationship between atmosphere and ocean anomalies, this has been investigated by means of a lag correlation analysis of the leading EOF modes of the sea level

pressure, net heat flux and sea surface temperature. As the model is forced with a prescribed SST field it is only possible to investigate lagged relationships where the atmosphere is responding to the ocean rather than vice versa although there is of course no such limitation on the observational dataset. Evidence is found for several coupled modes where the atmosphere leads the ocean on timescales of 1 to 3 months including that between the first EOF of pressure and the second EOF of SST noted by Kent et al. (1999). In contrast there is little indication that the atmospheric modes are being driven by anomalous SST patterns in either the model or observations.

Further, the results of the lagged analysis of the SOC dataset presented in Section 4.2 suggest that the SST does not play a significant role in forcing the NAO, at lead times of up to six months relative to the NAO maximum state. No evidence was found for a statistically significant pattern in the SST at lead times within this interval. This conclusion stands in contrast to the recent work of Czaja and Frankignoul (1999) who found, from a Singular Value Decomposition (SVD) of COADS based SST and heat flux fields and NMC pressures, that a zonal dipole in SST between the northeast Atlantic and the region east of Newfoundland preceded an NAO like pressure pattern by 3-4 months. Czaja and Frankignoul (1999) note that their SST dipole pattern is quite different from the more familiar tripole posited by Rodwell et al. (1999) as being a factor in establishing the NAO.

The role of SST anomalies in forcing the NAO clearly remains open to debate. The results of the present study strongly suggest that the SST does not play a significant role in establishing the NAO at seasonal to interannual timescales. In contrast, the two recent studies cited above (Czaja and Frankignoul, 1999 ; Rodwell et al., 1999) claim that anomalies in the SST field are important, while advocating significantly different patterns for the spatial structure of these anomalies. The disagreement between the conclusion of Czaja and Frankignoul (1999) and the results presented here may reflect differences in analysis technique. They find an SST dipole, obtained by SVD, that is associated with an 'NAO like pressure mode' but they stop short of establishing a connection between that mode and the observed temporal record of the NAO. However, the analysis of the SOC dataset presented in Section 4b. is a composite one based on the observed record of NAO extrema and thus the patterns found may be formally identified with the NAO rather than an NAO like phenomenon.

To conclude we note that the relatively short time period covered by the SOC dataset only permits analysis of variability at timescales up to interannual. On these timescales SST anomalies appear to be relatively unimportant in determining the atmospheric response. However, they may of course become important at interdecadal timescales and this would be consistent with the idea that interdecadal variability in the North Atlantic primarily represents a feedback from the ocean to the atmosphere (Kushnir, 1994).

ACKNOWLEDGEMENTS

The work described in this report has been funded as the second half of a commissioned research project for the Hadley Centre, UK Meteorological Office. It has benefited from discussions with Elizabeth Kent, Peter Taylor, Chris Gordon, Mark Rodwell and Claire Cooper. The first half of this project, which considered various issues related to variability in the SOC flux dataset, was conducted by Elizabeth Kent. The research that I have subsequently carried out was greatly facilitated by use of several computer programs written by her and it has been informed by the results of the earlier analysis, reported in Kent et al. (1999). The selected SOC EOF fields presented here are a subset of those published in Kent et al. (1999). The programs used for the EOF calculations were developed by Peter Challenor and Elizabeth Kent. Values for the Hurrell NAO index were obtained from http://goldhill.cgd.ucar.edu/cas/climind/nao_winter.html.

REFERENCES

Bjerknes, J., 1964: Atlantic air-sea interaction. *Advances in Geophysics*, **10**, Academic Press, 1-82.

Cayan, D. R., 1992: Latent and sensible heat flux anomalies over the Northern Oceans : Driving the sea surface temperature. *J. Phys. Oceanogr.*, **22**(8), 859 - 881.

Czaja, A. and C. Frankignoul, 1999: Influence of the North Atlantic SST on the atmospheric circulation. *Geophys. Res. Lett.*, **26**(19), 2969 - 2972.

Dickson, R., J. Lazier, J. Meincke and P. Rhines, 1996: Long-term coordinated changes in the convective activity of the North Atlantic. *NATO ASI series*, Vol. 44: *Decadal Climate Variability : Dynamics and Predictability*, D. A. J. Willebrand, Ed., Springer-Verlag, 211 - 262.

Dickson, R., T. J. Osborn, J. W. Hurrell, J. Meincke, J. Blindheim, B. Adlandsvik, T. Vinje, G. Alekseev and W. Maslowski, 2000: The Arctic Ocean response to the North Atlantic Oscillation. *J. Climate*, submitted.

Hurrell, J. W., 1995: Transient eddy forcing of the rotational flow during northern winter. *J. Atmos. Sci.*, 52, 2286 - 2301.

Hurrell, J. W. and H. van Loon, 1997: Decadal variations in climate associated with the North Atlantic Oscillation. *Climatic Change*, 36, 301 - 326.

Josey, S. A., E. C. Kent and P. K. Taylor, 1998: The Southampton Oceanography Centre (SOC) Ocean - Atmosphere Heat, Momentum and Freshwater Flux Atlas. *Southampton Oceanography Centre Report No. 6*, Southampton, UK, , 30 pp. & figs.

Josey, S. A., E. C. Kent and P. K. Taylor, 1999: New insights into the ocean heat budget closure problem from analysis of the SOC air-sea flux climatology. *J. Climate*, 12(9), 2856 - 2880.

Kent, E. C., P. K. Taylor and P. G. Challenor, 1999: Variability in the SOC Climatology from a combination of empirical orthogonal function and cluster analyses. *Hadley Centre Contract Report*, 30 pp. + figs + 2 Appendix Volumes.

Kushnir, Y., 1994: Interdecadal variations in North Atlantic sea surface temperature and associated atmospheric conditions. *J. Clim.*, 7(1), 141 - 157.

North, G. R., T. L. Bell, R. F. Cahalan and F. J. Moeng, 1982: Sampling errors in the estimation of Empirical Orthogonal Functions. *Mon. Wea. Rev.*, 110, 699 - 706.

Pope, V. D., M. L. Gallani, P. R. Rowntree and R. A. Stratton, 1999: The impact of new physical parameterizations in the Hadley Centre climate model. *Climate Dynamics*, submitted.

Rayner, N. A., E. B. Horton, D. E. Parker, C. K. Folland and R. B. Hackett, 1996: Version 2.2 of the Global sea-Ice and Sea Surface Temperature dataset , 1903 - 1994. *Hadley Centre Climate Research Technical Note No. 74*, 21pp. +figs.

Rodwell, M. J., D. P. Rowell and C. K. Folland, 1999: Oceanic forcing of the wintertime North Atlantic Oscillation and European climate. *Nature*, 398, 320 - 323.

Rogers, J. C., 1990: Patterns of low-frequency monthly sea level pressure variability (1899-1986) and associated wave cyclone frequencies. *J. Clim.*, 3(12), 1364 - 1379.

Trenberth, K. E. and K. E. Hurrell, 1994: Decadal atmosphere - ocean variations in the Pacific. *Climate Dynamics*, 9, 303 - 319.

von Storch, H. and F. W. Zwiers, 1999: *Statistical analysis in climate research*, Cambridge University Press, Cambridge, pp. 494.

Wallace, J. M. and D. S. Gutzler, 1981: Teleconnections in the geopotential height field during the Northern Hemisphere winter. *Mon. Wea. Rev.*, 109, 784 - 812.

Zhang, Y., J. M. Wallace and D. S. Battisti, 1997: ENSO-like interdecadal variability : 1900-93. *J. Clim.*, 10, 1004 - 1020.

TABLES

	SOC	HadAM3
Tahiti Pole	178ºE - 77ºW 21ºS - 21ºN	178.125ºE - 76.875ºW 21.25ºS - 21.25ºN
Darwin Pole	77ºW - 178ºE 21ºS - 21ºN	76.875ºW - 178.125ºE 21.25ºS - 21.25ºN

Table 1. Latitude / longitude ranges for the poles used to define the Southern Oscillation Index.

	SOC	HadAM3
Azores High	32ºW - 9ºE 34ºN - 41ºN	31.875 ºW - 9.375ºE 33.75ºN - 41.25ºN
Iceland Low	24ºW - 9ºE 61ºN - 66ºN	24.375 ºW - 9.375ºE 61.25ºN - 66.25ºN

Table 2a. Latitude / longitude ranges for the boxes used to define the North Atlantic Oscillation Index.

	SOC	HadAM3	TH
North Pacific Index	30 - 65º N, 160º E - 140º W	28.75 - 66.25º N, 159.375º E - 140.625º W	30 - 65º N, 160º E - 140º W

Table 2b. Latitude / longitude ranges for the boxes used to define the North Pacific Index.

HadAM3 NAO+	HadAM3 NAO-	SOC NAO+	SOC NAO-
2/80 (2.2)	1/80 (-2.7)	12/82 (3.1)*	1/80 (-3.4)
12/82 (2.4)	3/80 (-4.3)	1/83 (3.0)	3/81 (-1.9)*
3/83 (2.2)	12/81 (-2.1)	1/84 (3.9)*	12/81 (-2.0)*
12/83 (2.0)	1/82 (-3.8)	2/84 (1.7)*	1/82 (-2.8)
2/84 (1.9)	2/82 (-6.0)	1/86 (2.3)*	2/83 (-2.7)
12/84 (3.0)	1/83 (-3.6)	3/86 (3.0)	3/84 (-3.8)
1/85 (4.3)	2/83 (-5.1)	12/86 (2.6)*	1/85 (-4.6)
12/87 (2.1)	12/85 (-3.2)	1/89 (2.0)*	2/85 (-2.9)*
2/89 (4.2)	1/86 (-1.7)	2/89 (3.9)	2/86 (-5.3)
3/89 (2.6)	12/91 (-2.4)	3/89 (2.3)	1/87 (-6.0)
2/90 (3.6)	2/93 (-2.7)	1/90 (3.4)	2/87 (-1.6)*
2/91 (2.5)	12/93 (-2.4)	2/90 (4.4)	12/87 (-3.4)
3/91 (2.1)	1/94 (-3.7)	2/92 (2.5)*	12/89 (-4.6)*
1/92 (2.6)	2/94 (-4.0)	3/92 (2.3)*	3/91 (-2.1)*
	2/95 (-6.7)	1/93 (2.8)	1/92 (-2.5)
	3/95 (-2.4)	12/93 (3.3)*	12/95 (-5.8)
	12/95 (-3.9)	1/94 (2.1)	
		3/94 (3.6)	
		12/94 (2.2)	
		1/95 (1.5)	
		2/95 (2.6)	

Table 3. Months used to form the NAO composite anomaly fields for HadAM3 and SOC. Index values for each are given in parentheses, values marked with an asterisk indicates those months in the period 1980-93 not included in the Kent et al. (1999) composite analysis.

Mode	SST	SLP
EOF1	0.96	0.24
EOF2	0.95	0.11
EOF3	0.95	0.11
EOF4	0.76	0.02
EOF5	0.77	0.14
EOF6	0.81	-0.11

Table 4a. Values for the correlation coefficient (r) for corresponding SOC and HadAM3 North Atlantic EOF time series.

Mode	SST	SLP
EOF1	0.97	0.27
EOF2	0.96	0.14
EOF3	0.96	0.06
EOF4	0.91	0.01
EOF5	0.87	0.06
EOF6	0.64	0.03

Table 4b. Values for the correlation coefficient (r) for corresponding SOC and HadAM3 North Pacific EOF time series.

Full Name	Figure Label	Full Name	Figure Label
Surface pressure	P	Convective cloud amount	CCL
Wind speed at 10 m	WS	Precipitation	RR
Wind stress magnitude	ST	Net shortwave flux	SW
Wind stress - eastward component	E	Net longwave flux	LW
Wind stress - northward component	N	Latent heat flux	LAT
Sea surface temperature	SST	Sensible heat flux	SEN
Air temperature at 1.5 m	AT	Net heat flux	TOT
Humidity at 1.5 m	HUM	Cloud amount from longwave radiation	LWC

Table 5. Variables included in the cluster analysis of the HadAM3 fields together with labels employed for figure.

	r_{max} (SLP/Qnet)	r_{max} (SLP/SST)	r_{max} (Qnet/SST)
Group 1 : SLP1 / Qnet1 / SST2	-0.65 (0)	0.44 (1)	0.42 (1)
Group 2 : SLP2 / Qnet2 / SST1	0.41 (0)	0.35 (1)	0.27 (3)
Group 3 : SLP3 / Qnet2 / SST3	-0.52 (0)	0.31 (1)	-0.28 (1)

Table 6. Peak values, r_{max}, of the correlation coefficients, between pairs of SOC EOF modes for each group identified in Section 3.4. Values in parentheses indicate the lag in months, defined for the second member of each pair relative to the first, at which the peak occurs.

	r^2 (SOC)	r^2 (HadAM3)
SOI - NAO	0.07	0.29
NPI - NAO	0.00	0.45
SOI - NPI	0.25	0.66

Table 7. Level of correlation (as measured by r^2) between SOC and HadAM3 winter mean NAO, NPI and SOI time series.

FIGURE CAPTIONS

Figure 1) Time series of the normalised Southern Oscillation Index for 1980-1995 in the SOC and HadAM3 datasets.

Figure 2a) Time series of the normalised North Atlantic Oscillation Index for 1980-1995 in the SOC and HadAM3 datasets. Winter (December-March) months are shaded black rather than grey. b.)Time series of the normalised winter mean North Atlantic Oscillation Index for 1980-1995 for SOC, HadAM3 and Hurrell.

Figure 3a) Time series of the anomalous North Pacific Index for 1980-1995 in the SOC and HadAM3 datasets, units mb. Winter (December-March) months are shaded black rather than grey. b.)Time series of the anomalous winter mean North Pacific Index for 1980-1995 for SOC, HadAM3 and Trenberth and Hurrell.

Figure 4) Global variation of the correlation coefficient (r) between HadAM3 and SOC anomaly time series for coincident grid cells, determined for a version of the SOC dataset that has been averaged onto the HadAM3 grid a.) SLP; b.) Latent heat; c.) Sensible heat; d.) Shortwave; e.) Longwave; f.) Net Heat; g.) SST.

Figure 5) Difference in composite anomaly plots for NAO+ and NAO- states obtained by selecting winter months with NAO index magnitude > 1.5 within the period 1980-1995 : a.) SOC Pressure ; b.) HadAM3 Pressure; c.) SOC Air Temperature; d.) HadAM3 Air Temperature ; e.) SOC Specific Humidity; f.) HadAM3 Specific Humidity; g.) SOC SST ; h.) HadAM3 SST. Note HadAM3 fields have been scaled by a factor $\sqrt{6}$, excepting SST.

Figure 6) Difference in composite anomaly plots between NAO+ and NAO- states obtained by selecting winter months with NAO index magnitude > 1.5 within the period 1980-1995 : a.) SOC Net Heat Flux ; b.) HadAM3 Net Heat Flux ; c.) SOC Latent Heat Flux; d.) HadAM3 Latent Heat Flux ; e.) SOC Sensible Heat Flux; f.) HadAM3 Sensible Heat Flux; g.) SOC Longwave Flux ; h.) HadAM3 Longwave Flux ; i.) SOC Shortwave Flux ; j.) HadAM3 Shortwave Flux ; k.) SOC 10m Wind Speed ; l.) SOC sea surface humidity - 10m humidity ; m.) SOC sea surface temperature - 10m temperature. Note HadAM3 fields have been scaled by a factor $\sqrt{6}$.

Figure 7) Leading six SST EOFs (units deg C) for the North Atlantic determined for the period 1980-1993 with the seasonal cycle removed for a-f.) HadAM3 and g-l.) SOC ; m.) shows the time series for each EOF pair, SOC (black), HadAM3 (grey). The percentage of variance explained by each EOF and whether it is distinct are included in the title information for each plot. Note that the SOC EOF plots shown in Figs. 7 - 11 are modified versions of plots that have already appeared in Kent et al. (1999).

Figure 8) Leading six pressure EOFs (units mb) for the North Atlantic determined for the period 1980-1993 with the seasonal cycle removed for a-f.) HadAM3 and g-l.) SOC ; m.) shows the time series for each EOF pair, SOC (black), HadAM3 (grey). Note HadAM3 fields have been scaled by a factor $\sqrt{6}$

Figure 9) Leading six net heat flux EOFs (units Wm^{-2})for the North Atlantic determined for the period 1980-1993 with the seasonal cycle removed for a-f.) HadAM3 and g-l.) SOC ; m.) shows the time series for each EOF pair, SOC (black), HadAM3 (grey). Note HadAM3 fields have been scaled by a factor $\sqrt{6}$

Figure 10) Leading six latent heat flux EOFs (units Wm^{-2}) for the North Atlantic determined for the period 1980-1993 with the seasonal cycle removed for a-f.) HadAM3 and g-l.) SOC ; m.) shows the time series for each EOF pair, SOC (black), HadAM3 (grey). Note HadAM3 fields have been scaled by a factor $\sqrt{6}$

Figure 11) Leading six shortwave flux EOFs (units Wm^{-2}) for the North Atlantic determined for the period 1980-1993 with the seasonal cycle removed for a-f.) HadAM3 and g-l.) SOC ; m.) shows the time series for each EOF pair, SOC (black), HadAM3 (grey).

Figure 12) Cluster analysis of HadAM3 North Atlantic EOFs, for details of labeling see Table 5.

Figure 13) Leading six SST EOFs (units deg C) for the North Pacific determined for the period 1980-1993 with the seasonal cycle removed for a-f.) HadAM3 and g-l.) SOC ; m.) shows the time series for each EOF pair, SOC (black), HadAM3 (grey). The percentage of variance explained by each EOF and whether it is distinct are included in the title information for each plot. Note that the SOC EOF plots shown in Figs. 7 - 11 are modified versions of plots that have already appeared in Kent et al. (1999).

Figure 14) Leading six pressure EOFs (units mb) for the North Pacific determined for the period 1980-1993 with the seasonal cycle removed for a-f.) HadAM3 and g-l.) SOC ; m.) shows the time series for each EOF pair, SOC (black), HadAM3 (grey). Note HadAM3 fields have been scaled by a factor $\sqrt{6}$ and that SOC EOF1 has been multiplied by -1 for ease of comparison with HadAM3 EOF1.

Figure 15) Leading six net heat flux EOFs (units Wm^{-2})for the North Pacific determined for the period 1980-1993 with the seasonal cycle removed for a-f.) HadAM3 and g-l.) SOC ; m.) shows the time series for each EOF pair, SOC (black), HadAM3 (grey). SOC EOF2 has been multiplied by -1 for ease of comparison.

Figure 16) Leading six latent heat flux EOFs (units Wm^{-2}) for the North Pacific determined for the period 1980-1993 with the seasonal cycle removed for a-f.) HadAM3 and g-l.) SOC ; m.) shows the time series for each EOF pair, SOC (black), HadAM3 (grey). HadAM3 EOF2 and SOC EOF1 have been multiplied by -1 for ease of comparison.

Figure 17) Leading six shortwave flux EOFs (units Wm^{-2}) for the North Pacific determined for the period 1980-1993 with the seasonal cycle removed for a-f.) HadAM3 and g-l.) SOC ; m.)

shows the time series for each EOF pair, SOC (black), HadAM3 (grey). SOC EOF2 has been multiplied by -1 for ease of comparison.

Figure 18) Cluster analysis of HadAM3 North Pacific EOFs, for details of labeling see Table 5.

Figure 19) Leading six net heat flux EOFs (units Wm^{-2}) for the Global Ocean determined for the period 1980-1993 with the seasonal cycle removed from HadAM3.

Figure 20) Lagged correlation plots for selected EOF pairs. The time axis gives the number of months by which the second member of the pair lags the first i.e. negative values imply SST leading. SOC (x symbol), HadAM3 (+ symbol).

Figure 21) Lagged correlation plots for EOF pairs in Group 1 (a-c), Group 2 (d-f) and Group 3 (g-i). The time axis gives the number of months by which the second member of the pair lags the first e.g. negative values imply SST leading. SOC (x symbol), HadAM3 (+ symbol). A schematic of the relationships between the groups is shown in Fig.21j.

Figure 22) Composite anomalies at various leads/ lags with respect to NAO+ index maximum. Only anomalies that are significant at 5% level shown. Lag intervals are in units of months, negative values imply a lead interval: a.) SLP, lead 1month to lag 1month, b.) SST, lead 0 to 2 months, c.) SST, lag 1 to 6 months, d.) Qnet, lead 0 to 2 months, e.) Qnet, lag 1 to 6 months, f.) SST & Qnet, lag 11-12 months.

Figure 23) Time series of NAO (solid), NPI (dash-dot) and SOI (dashed) winter (Nov-Mar) indices in SOC and HadAM3

Figure 24) Difference in global sea level pressure composite anomaly plots for NAO+ and NAO- states obtained by selecting winter months with NAO index magnitude > 1.5 within the period 1980-1995 a.)SOC ; b.) HadAM3.

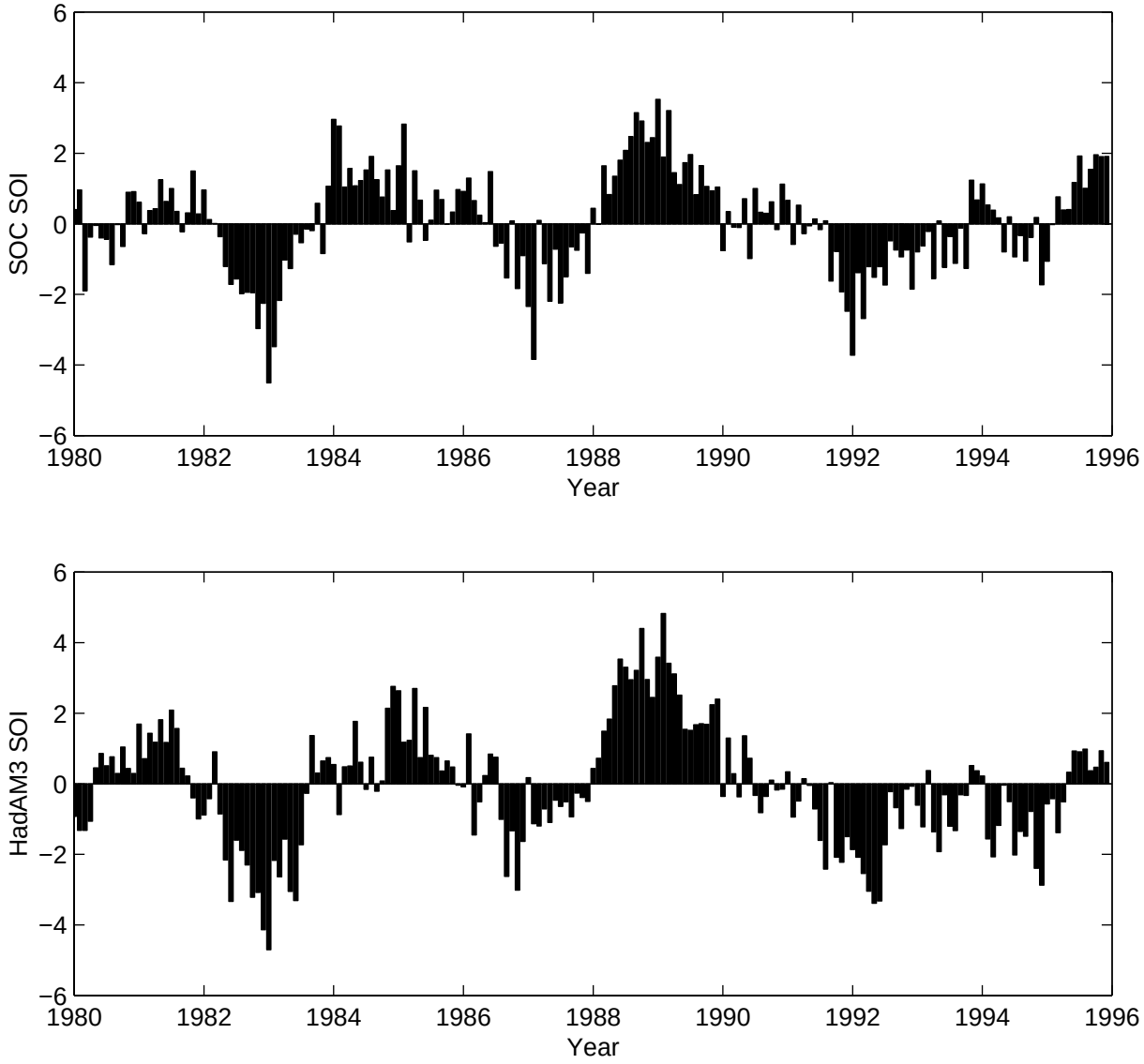

Figure 1. Time Series of the Southern Oscillation Index in SOC and HadAM3

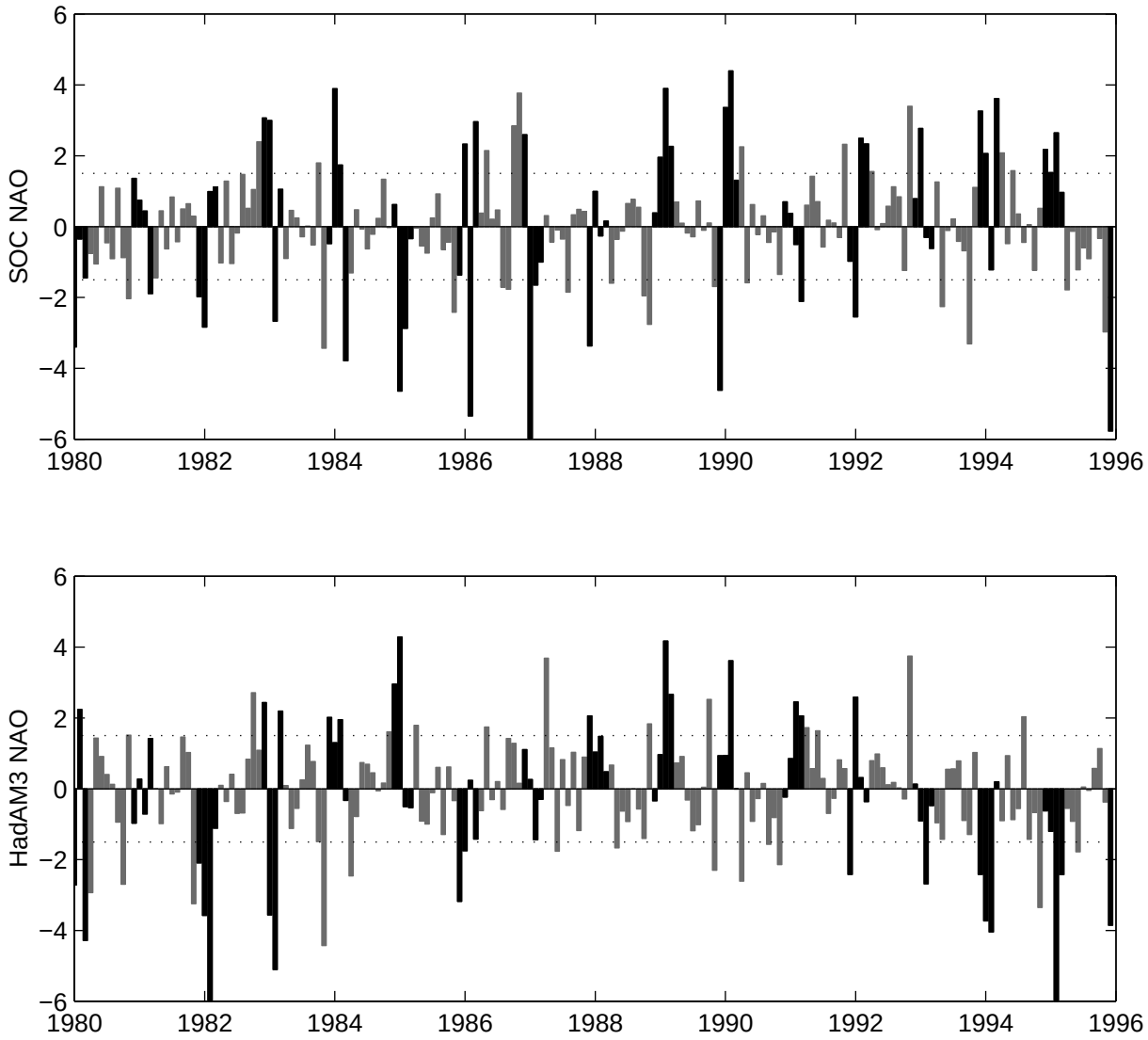

Figure 2a. Time Series of the normalised North Atlantic Oscillation Index in SOC and HadAM3. Winter(DJFM) values shaded black, other months grey. Dotted lines are at index values of +/−1.5.

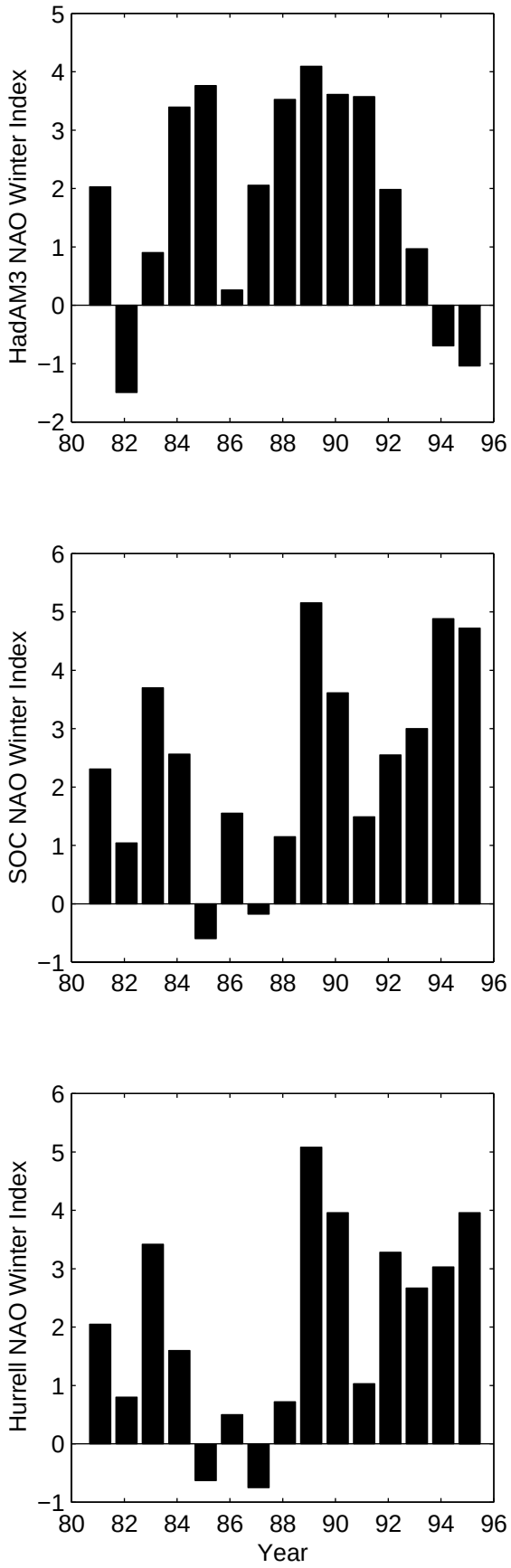

Figure 2b. Winter mean normalised North Atlantic Oscillation Index for HadAM3, SOC and Hurrell.

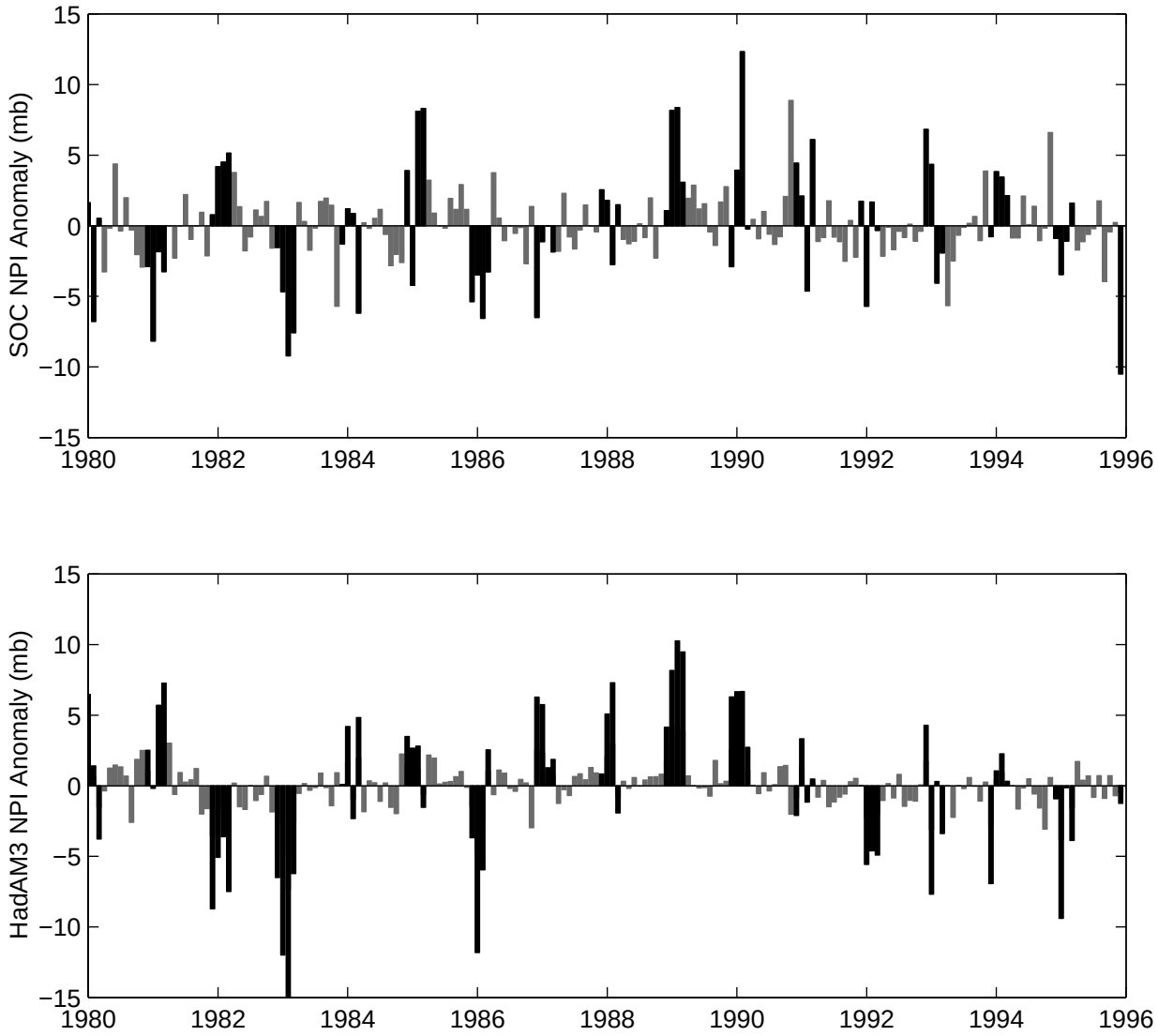

Figure 3a. Time Series of the Anomalous North Pacific Index in SOC and HadAM3. Winter(DJFM) values shaded black, other months grey.

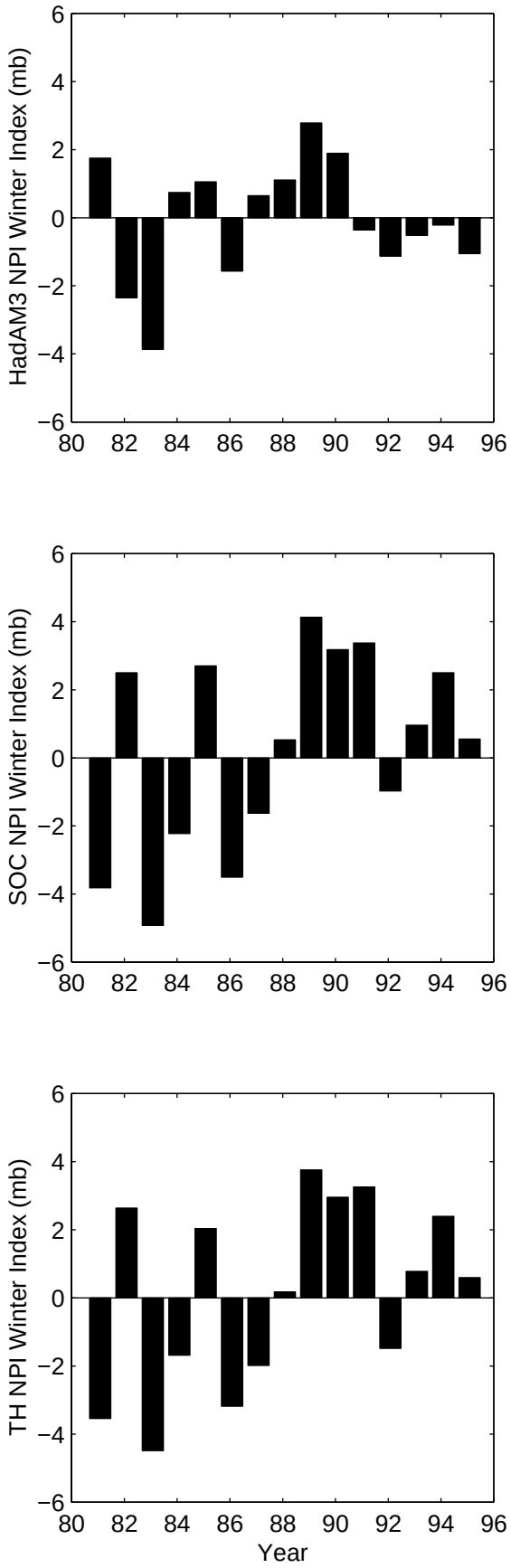

Figure 3b. Winter mean North Pacific Index for HadAM3, SOC and TH.

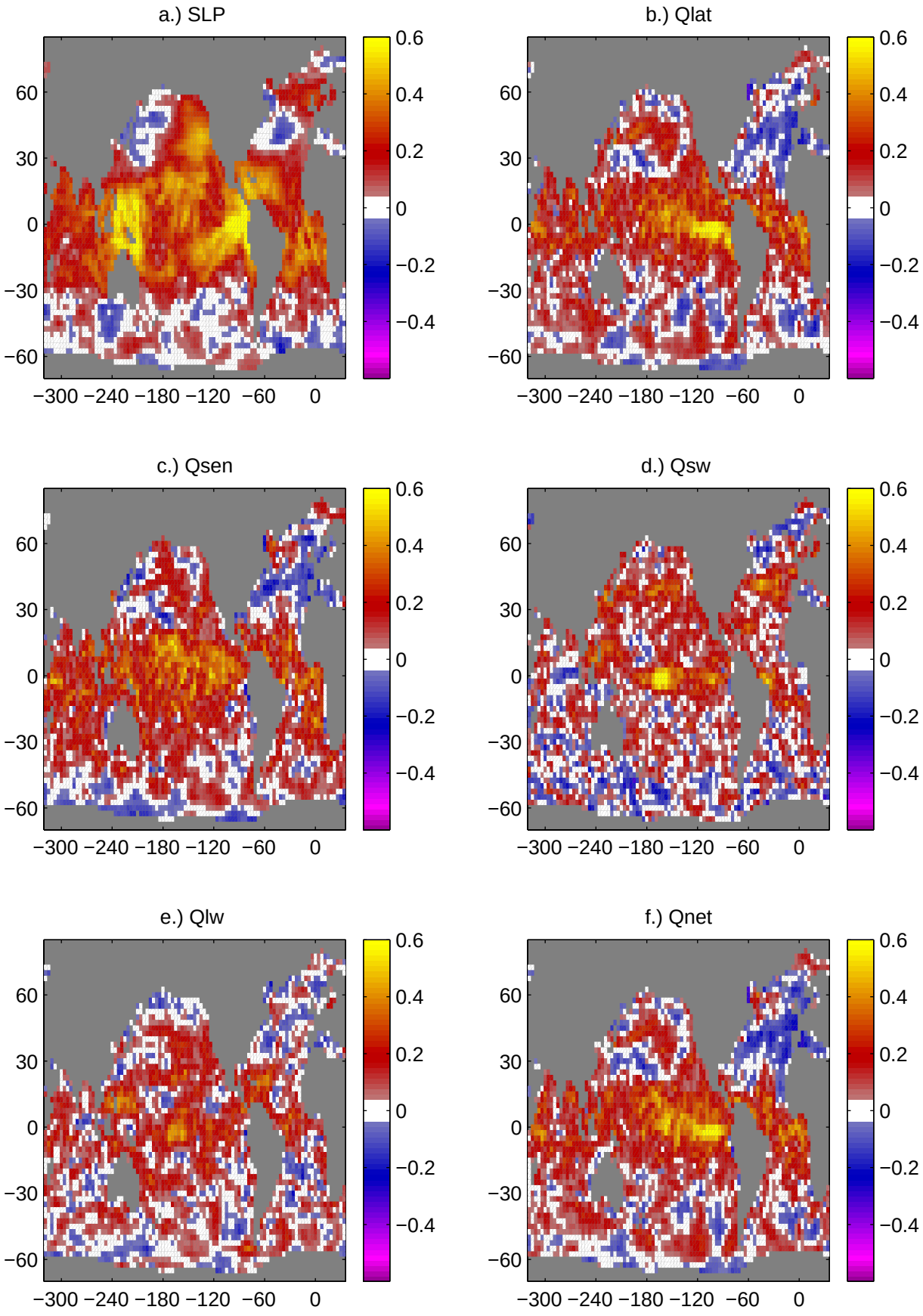

Figure 4a−f.) Correlation coefficient fields for grid point comparisons of HadAM3 and SOC anomaly time series.

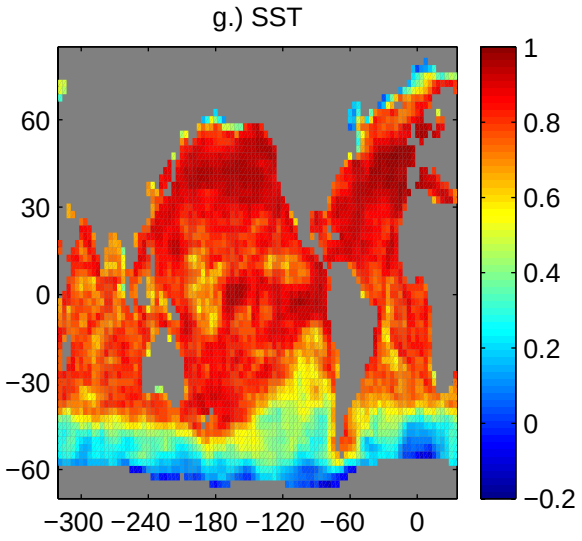

Figure 4g.) Correlation coefficient field for grid point comparison of HadAM3 and SOC SST anomaly time series.

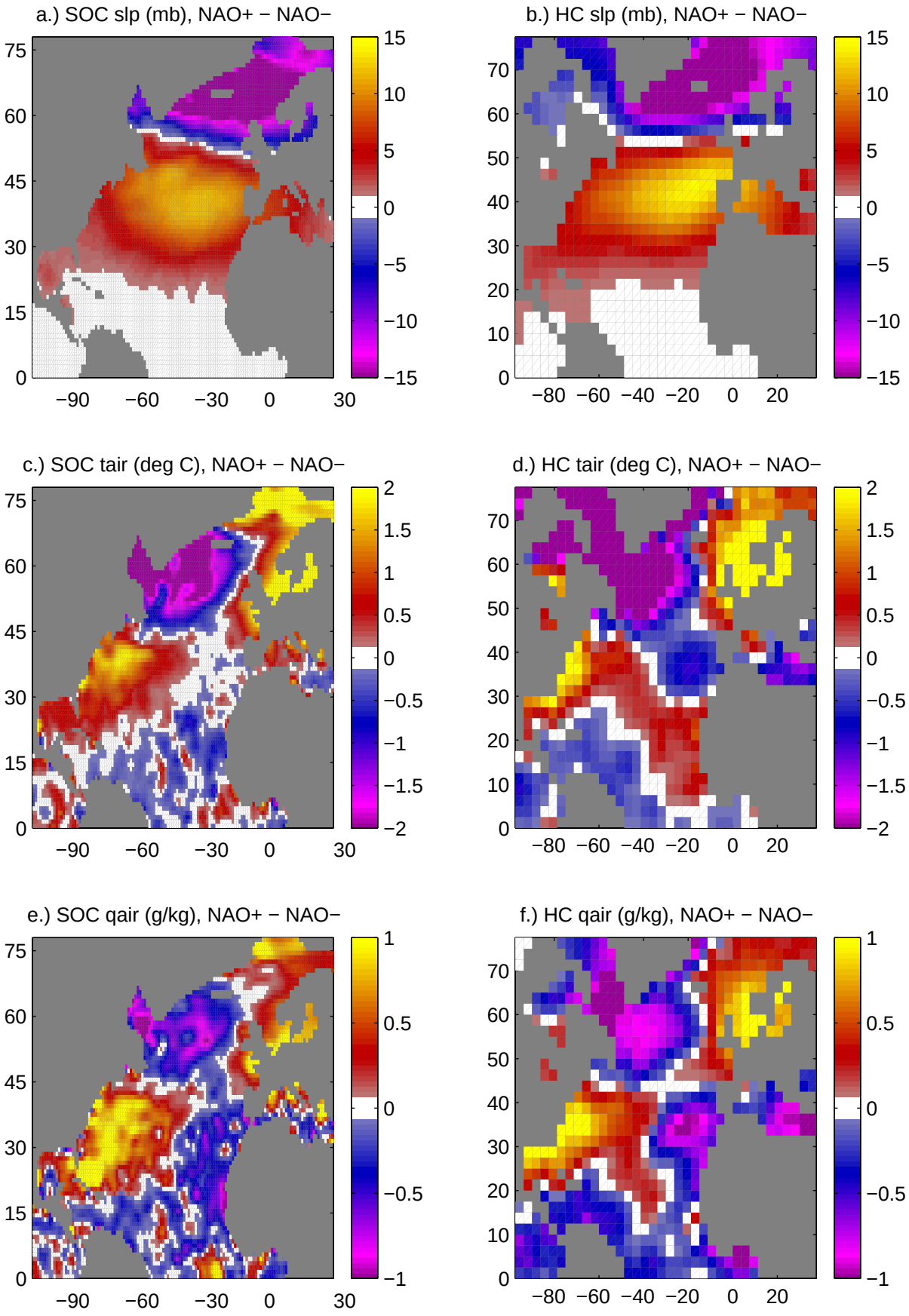

Fig.5 Difference in met field composite anomaly plots for NAO+ and NAO− states.

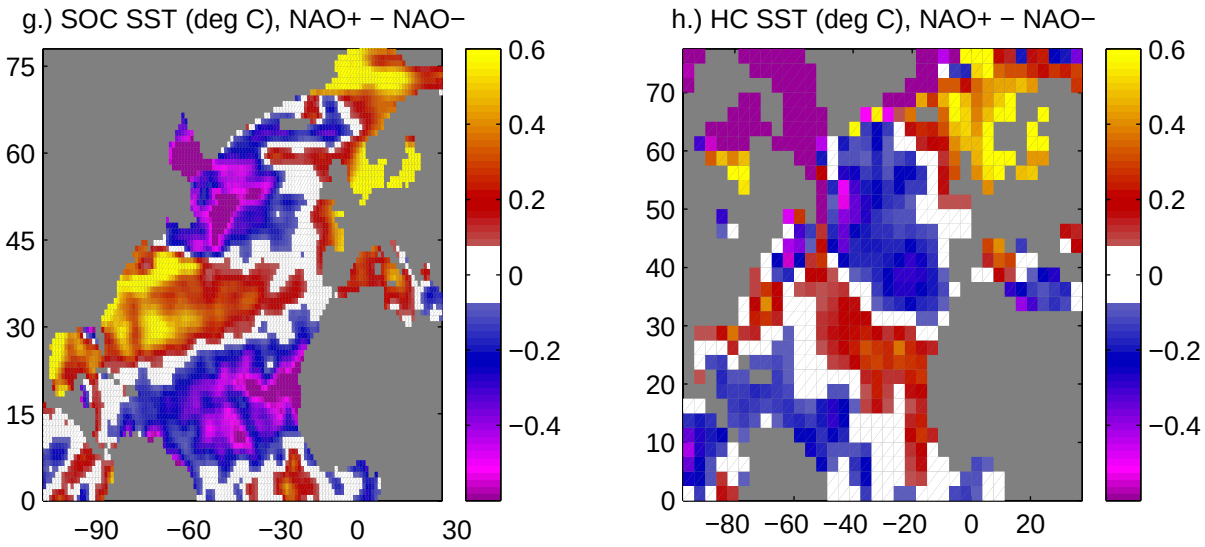

Fig.5 Difference in met field composite anomaly plots for NAO+ and NAO− states.

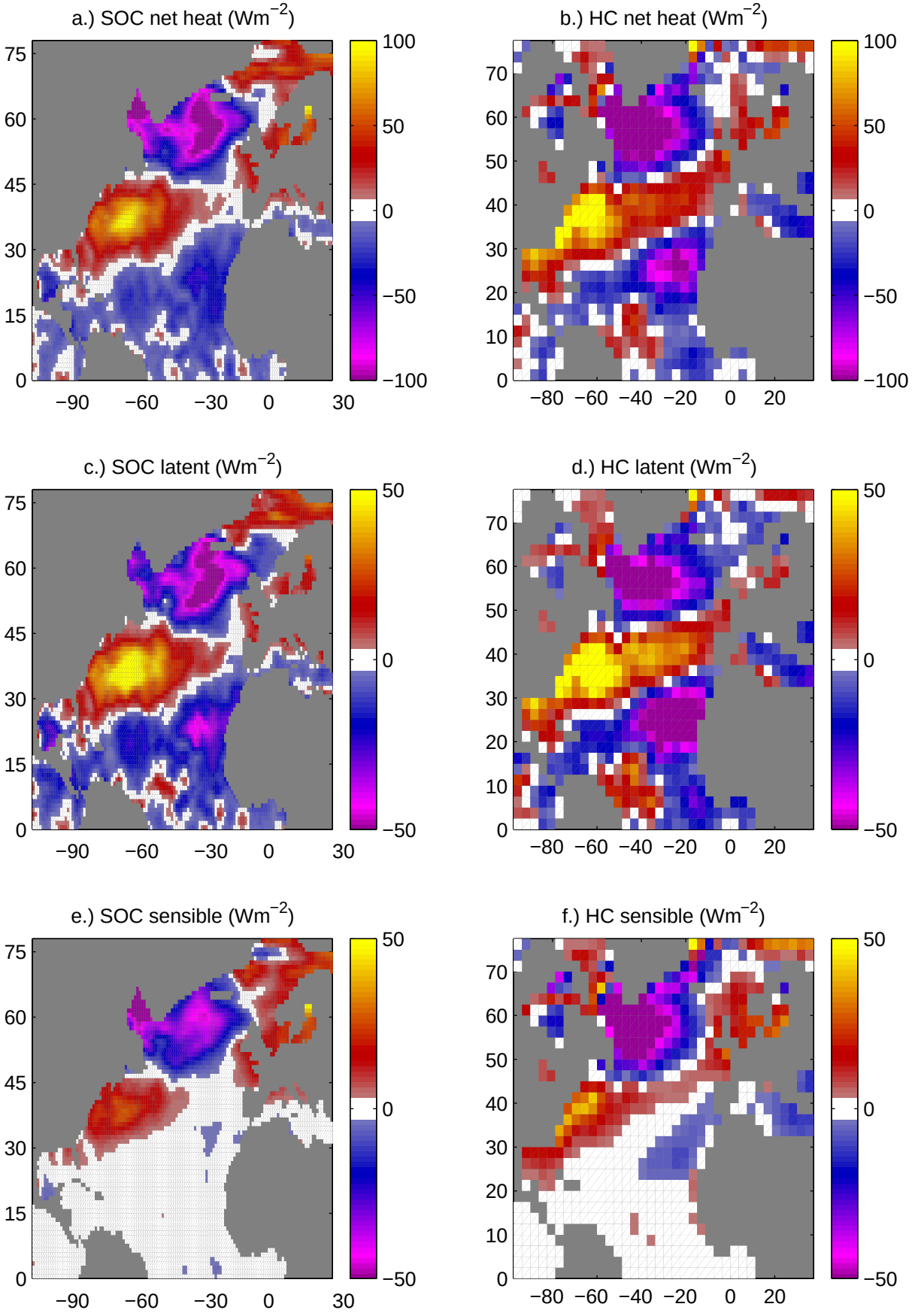

Fig.6 Difference in flux field composite anomaly plots between NAO+ and NAO− states.

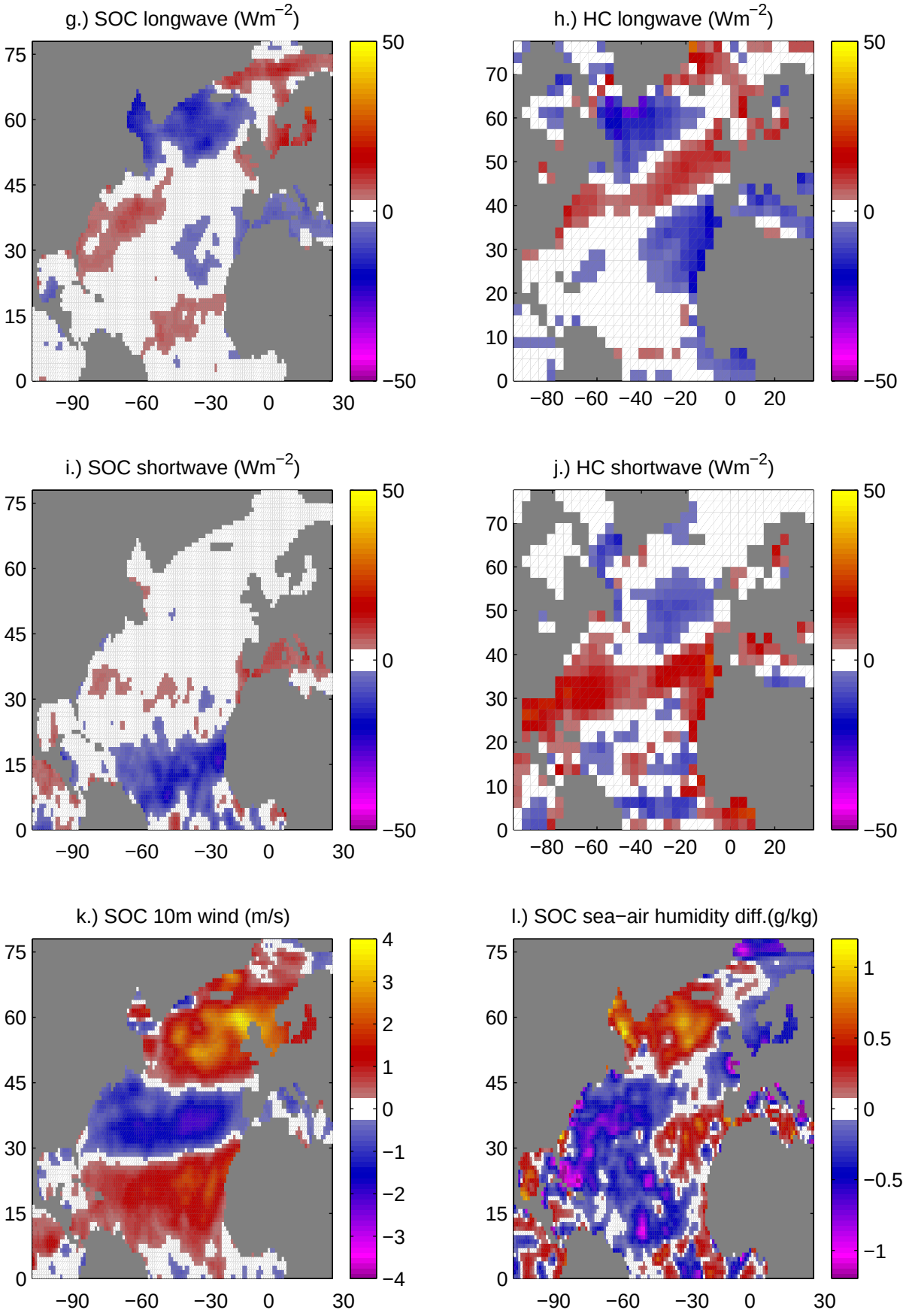

Fig.6 Difference in flux field composite anomaly plots for NAO+ and NAO− states.

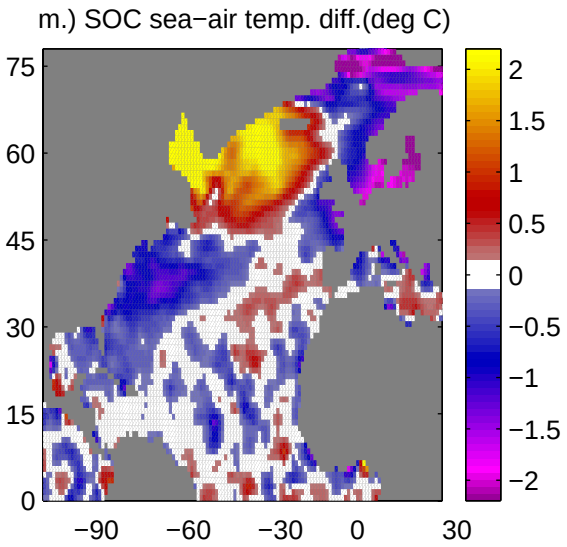

Fig.6 Difference in composite anomaly plots for NAO+ and NAO− states.

Fig.7a HC SST - eof1 , 15.71 % , dist

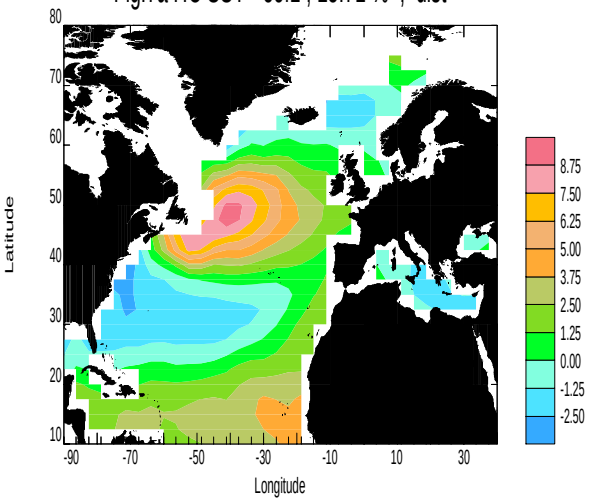

Fig.7b HC SST - eof2 , 12.43 % , dist

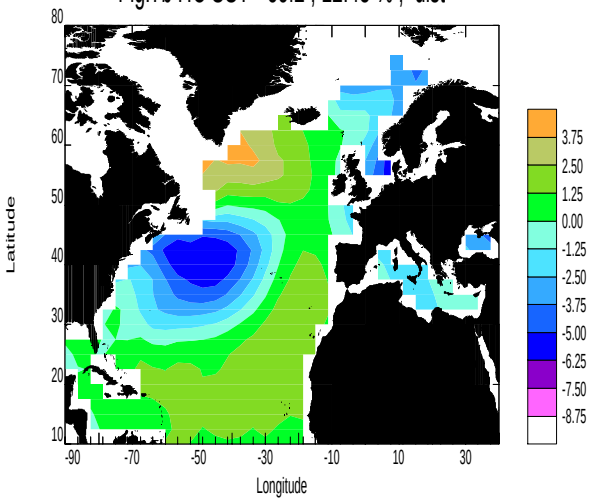

Fig.7c HC SST - eof3 , 10.49 % , dist

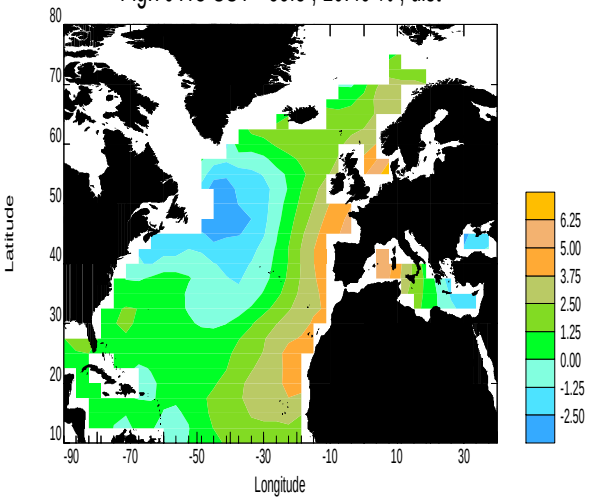

Fig.7d HC SST - eof4 , 6.89 % , dist

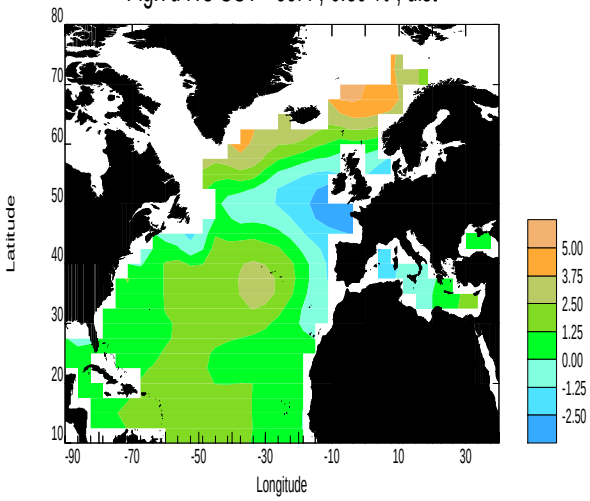

Fig.7e HC SST - eof5 , 6.40 % , dist

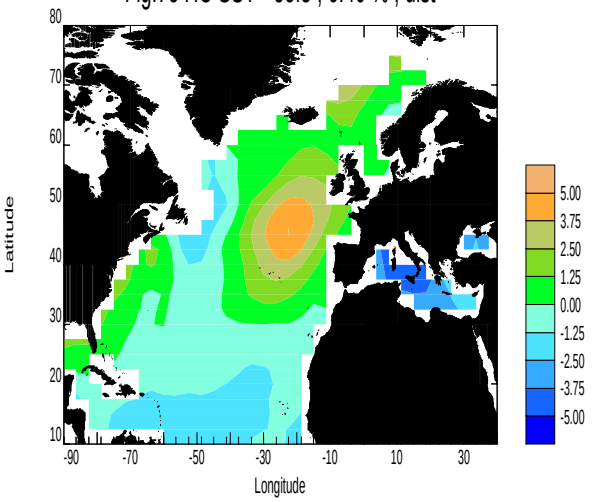

Fig.7f HC SST - eof6 , 4.55 % , dist

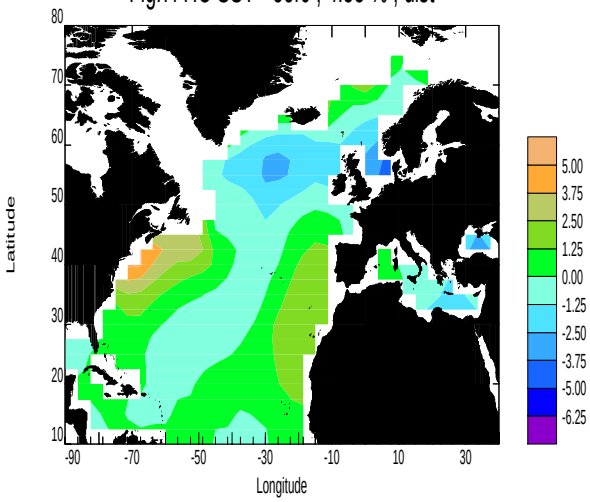

Fig.7g SOC SST - eof1 , 14.25 % , dist

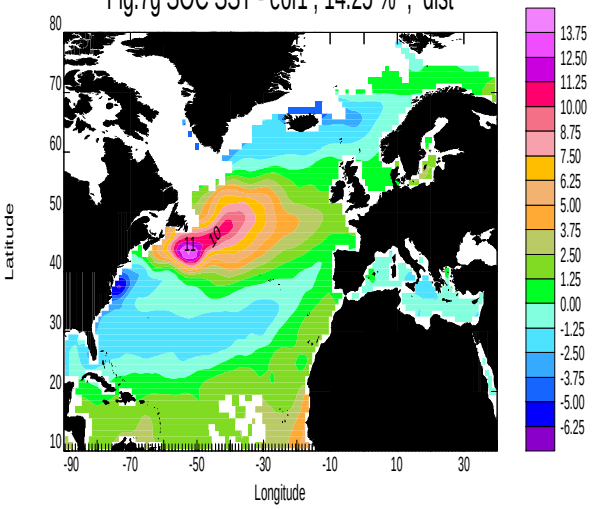

Fig.7h SOC SST - eof2 , 11.59 % , dist

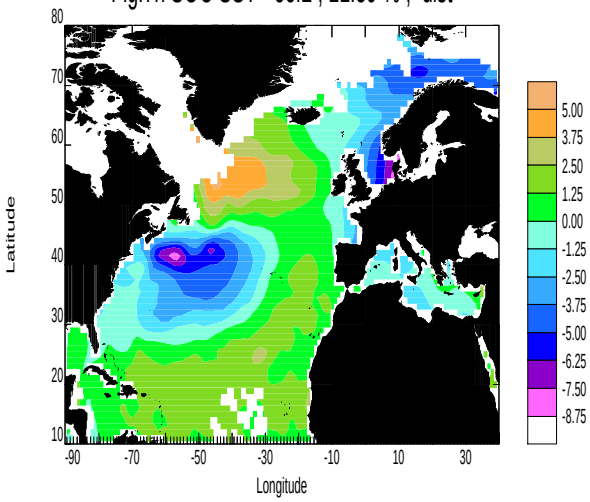

Fig.7i SOC SST - eof3 , 8.28 % , dist

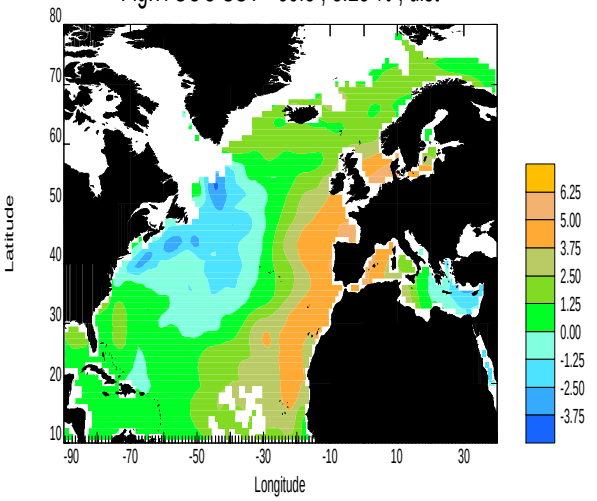

Fig.7j SOC SST - eof4 , 5.62 % , dist

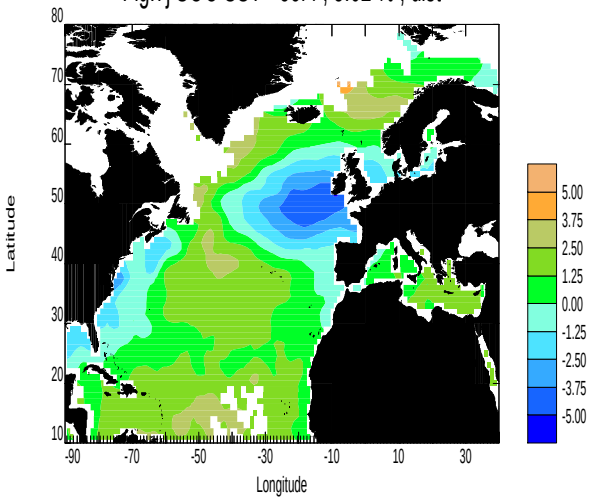

Fig.7k SOC SST - eof5 , 5.29 % , dist

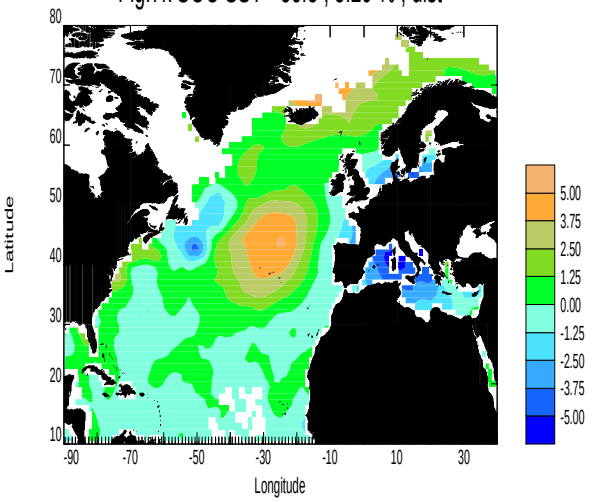

Fig.7l SOC SST - eof6 , 3.91 % , dist

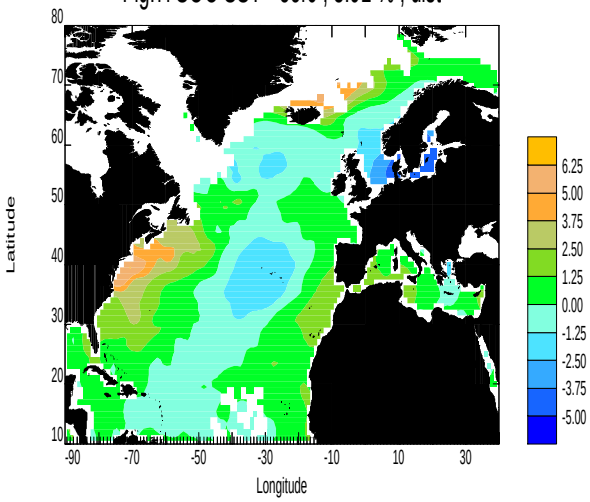

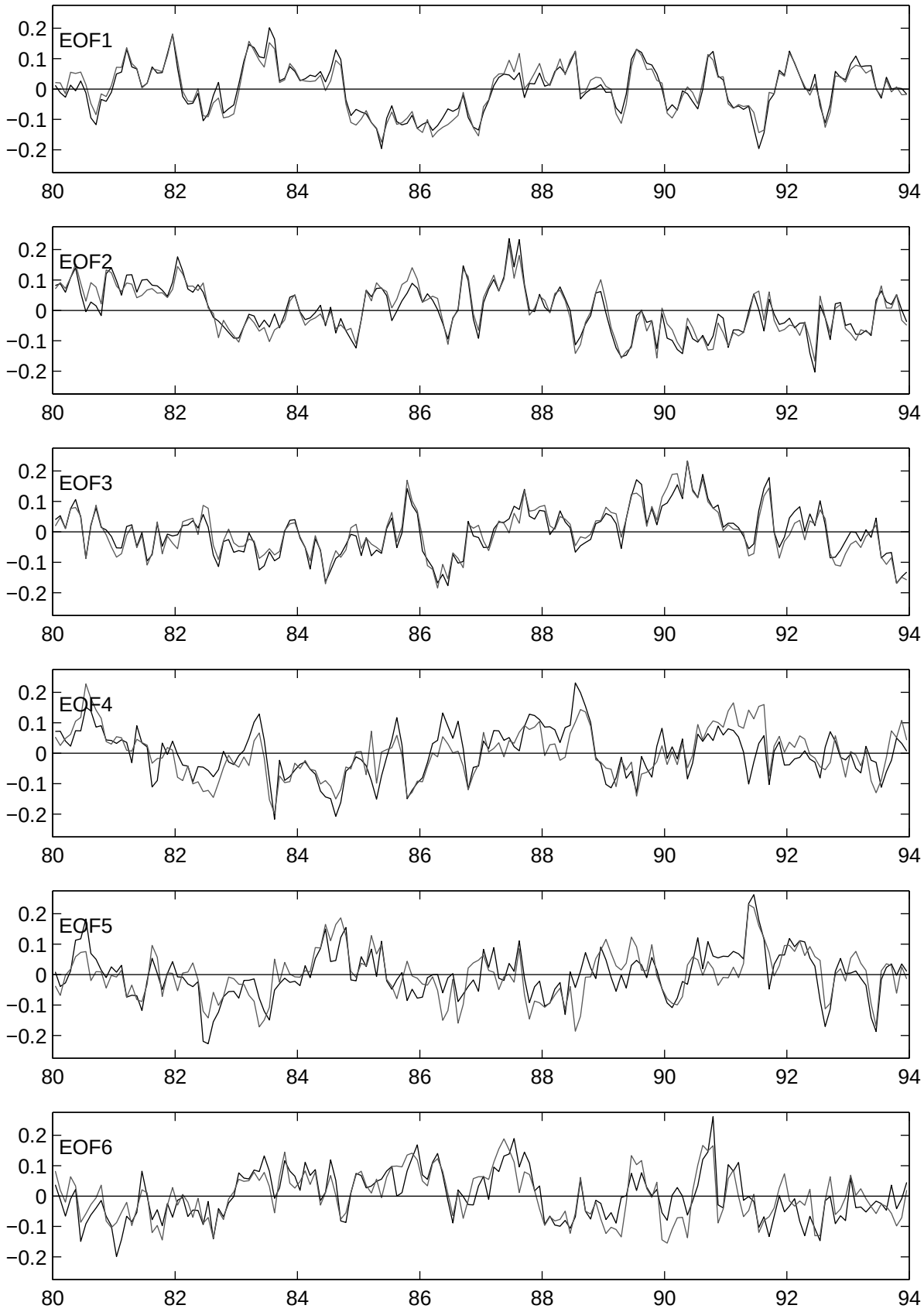

Fig. 7m Time series of SST EOFs 1 to 6. SOC−black, HC−grey.

Fig.8a HC SLP - eof1 , 35.87 % , dist

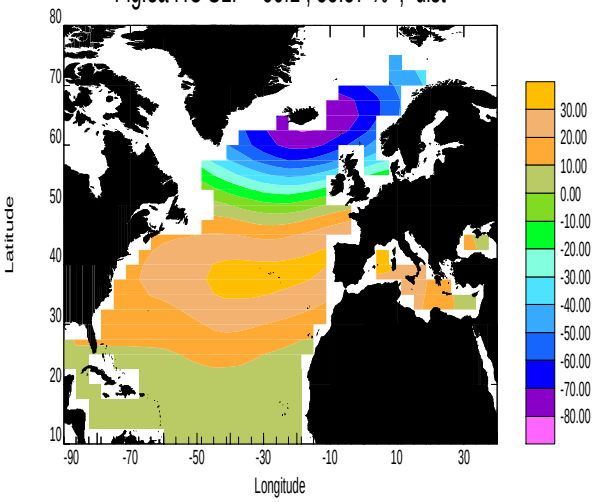

Fig.8b HC SLP - eof2 , 25.04 % , dist

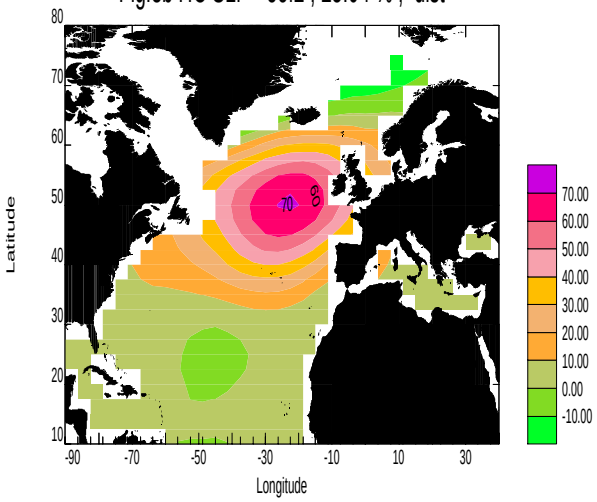

Fig.8c HC SLP - eof3 , 8.62 % , dist

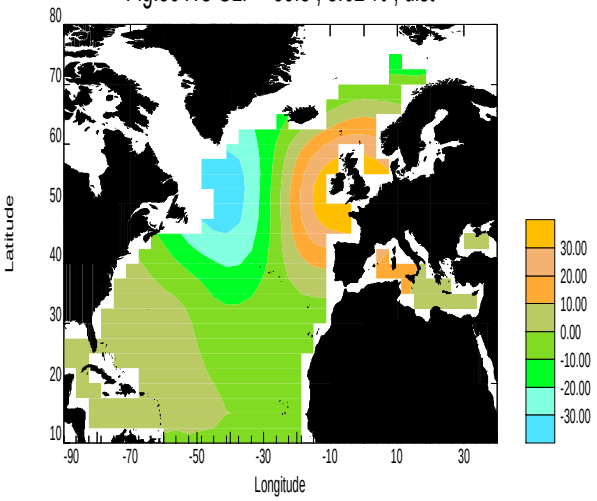

Fig.8d HC SLP - eof4 , 7.78 % , dist

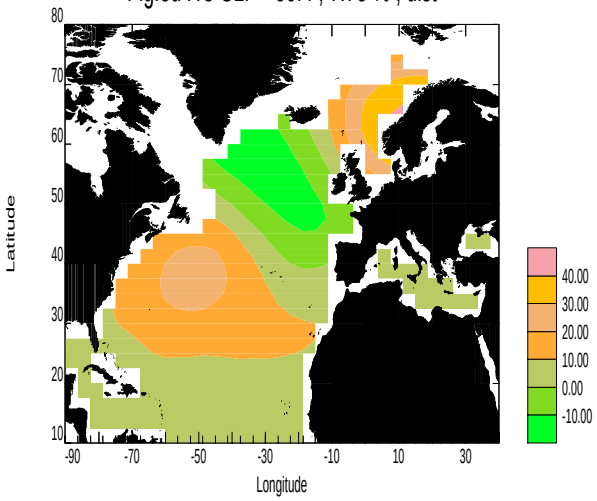

Fig.8e HC SLP - eof5 , 4.91 % , dist

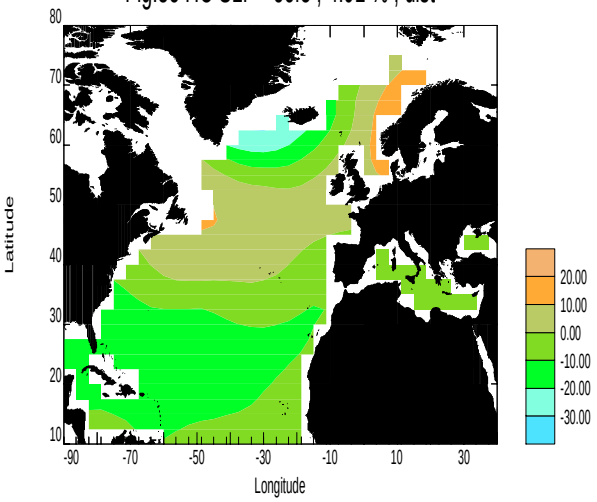

Fig.8f HC SLP - eof6 , 3.95 % , dist

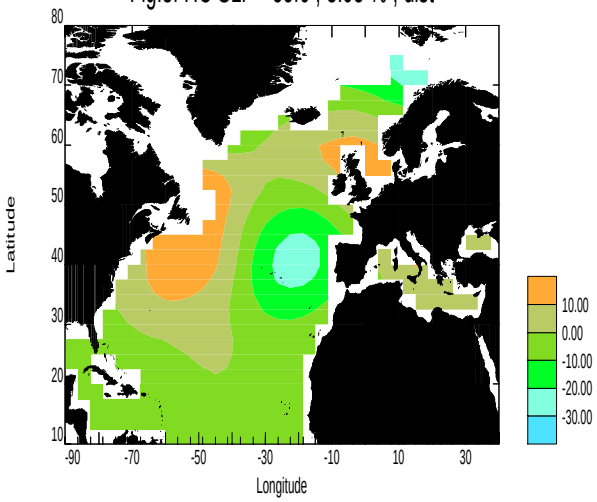

Fig.8g SOC SLP - eof1 , 36.22 % , dist

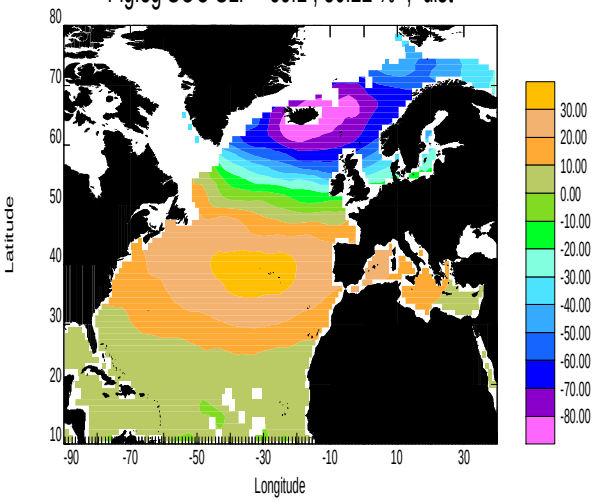

Fig.8h SOC SLP - eof2 , 20.30 % , dist

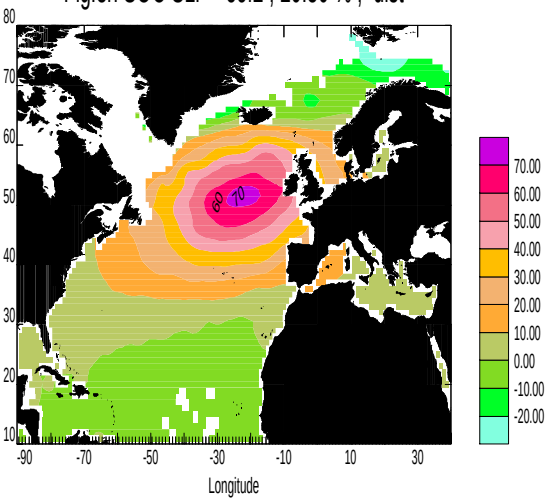

Fig.8i SOC SLP - eof3 , 9.90 % , dist

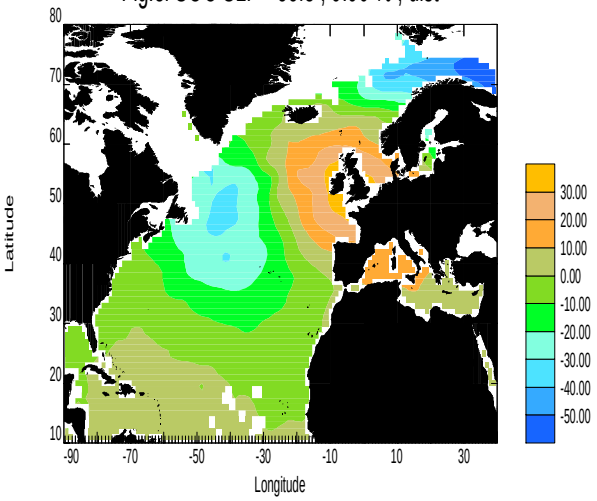

Fig.8j SOC SLP - eof4 , 6.71 % , dist

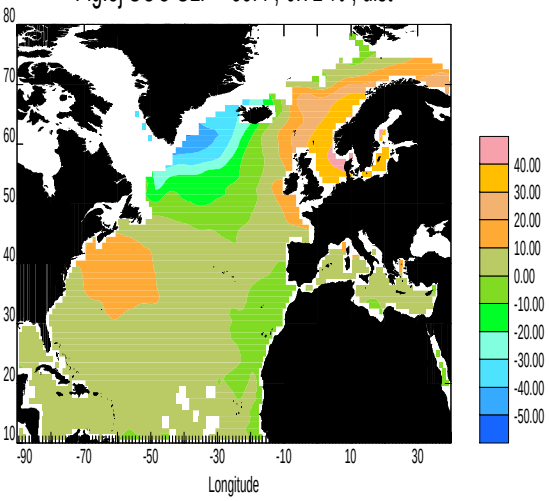

Fig.8k SOC SLP - eof5 , 3.30 % , dist

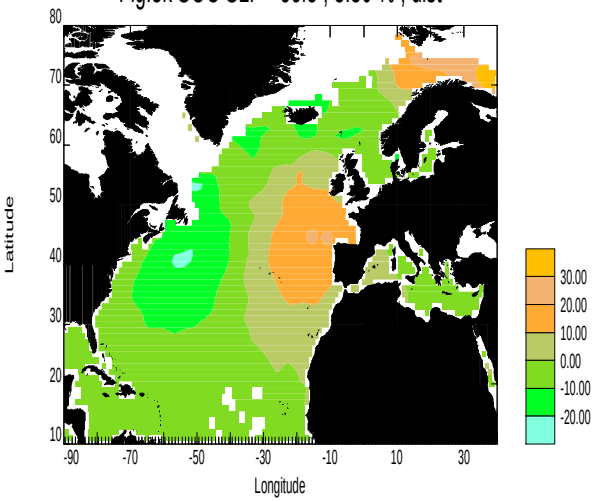

Fig.8l SOC SLP - eof6 , 2.55 % , dist

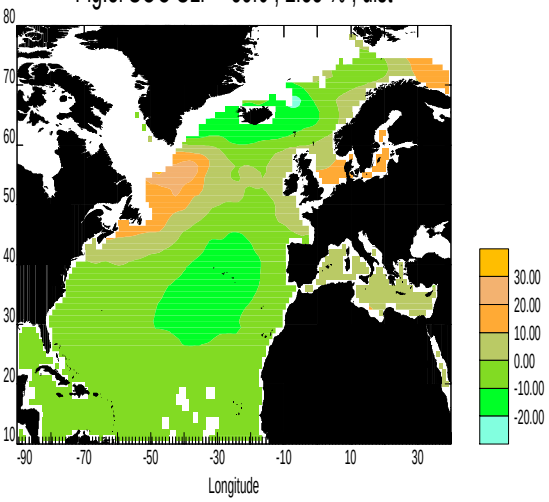

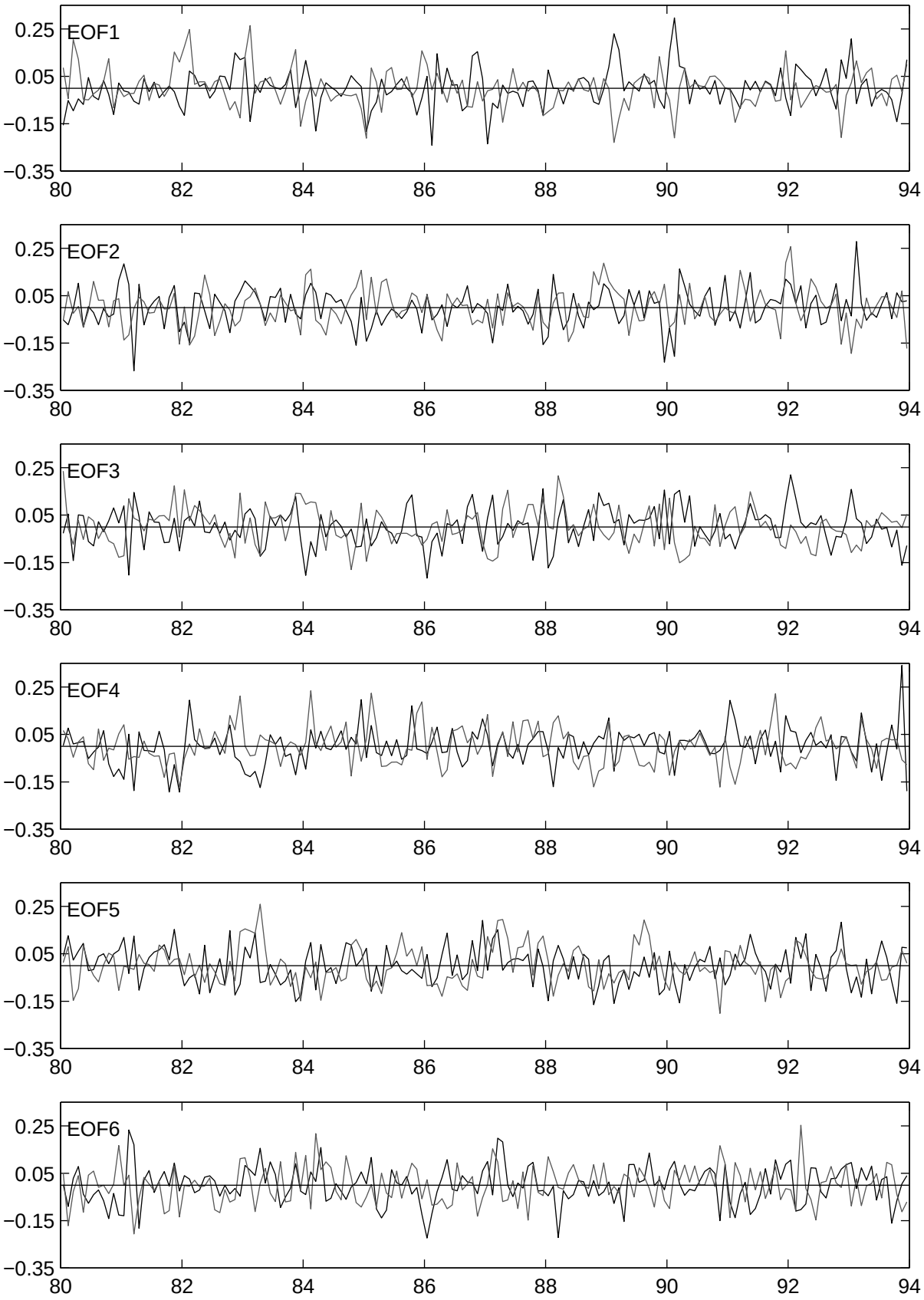

Fig. 8m Time series of SLP EOFs 1 to 6. SOC−black, HC−grey.

Fig.9a HC Qnet - eof1 , 13.96 % , dist

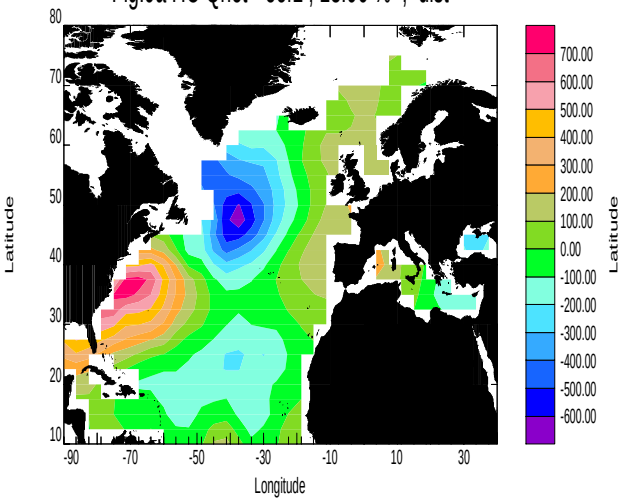

Fig.9b HC Qnet - eof2 , 11.85 % , dist

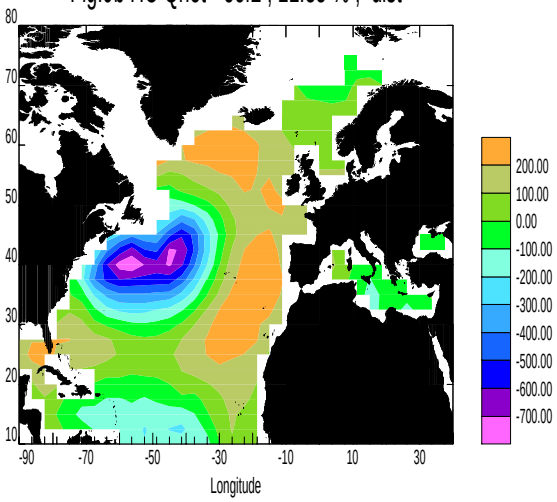

Fig.9c HC Qnet - eof3 , 6.59 % , dist

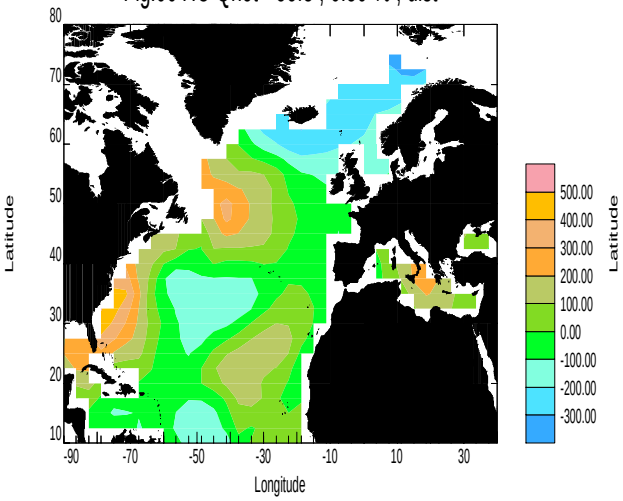

Fig.9d HC Qnet - eof4 , 5.70 % , dist

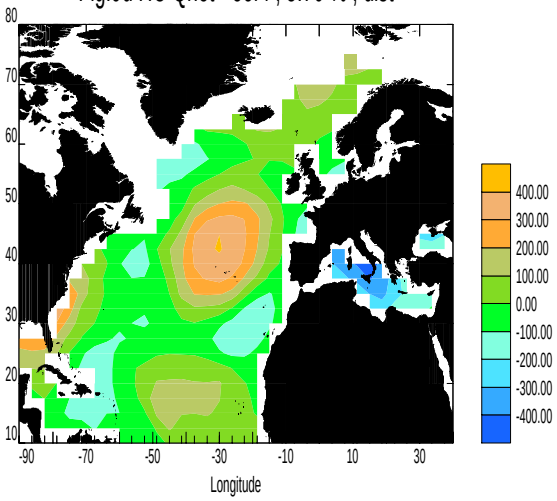

Fig.9e HC Qnet - eof5 , 4.80 % , dist

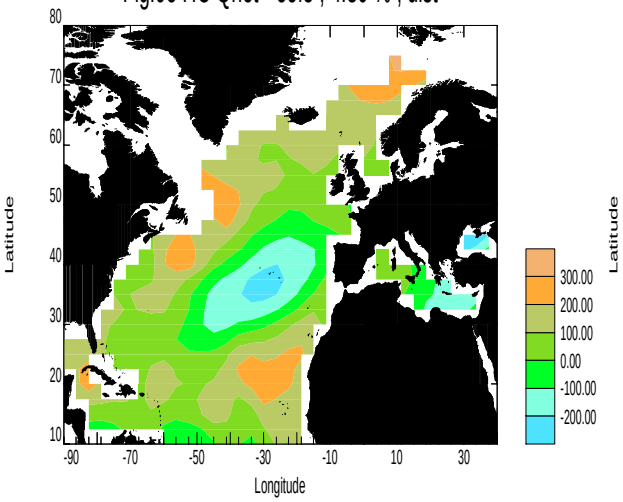

Fig.9f HC Qnet - eof6 , 4.40 % , dist

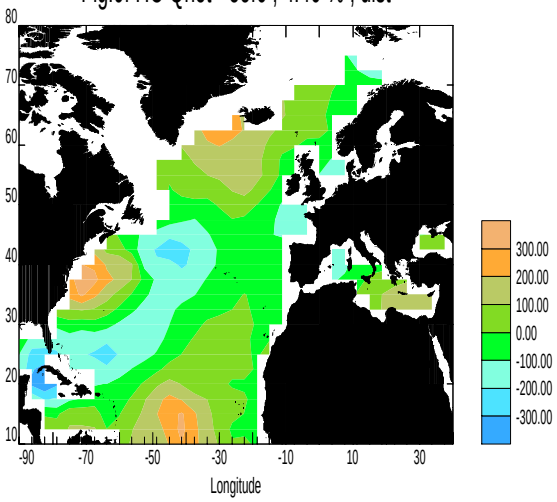

Fig.9g SOC Qnet - eof1 , 16.14 % , dist

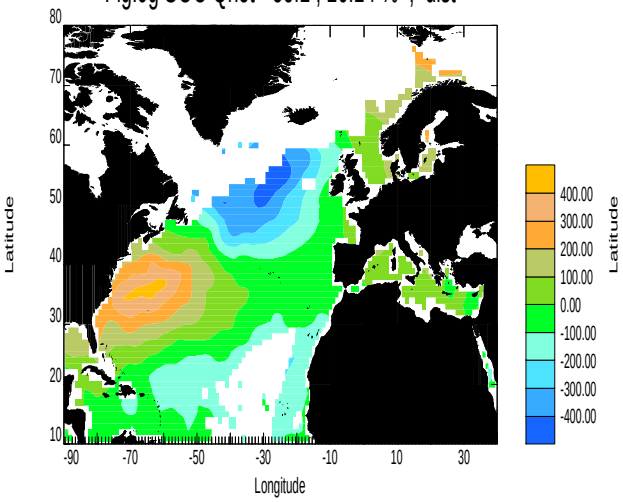

Fig.9h SOC Qnet - eof2 , 10.70 % , dist

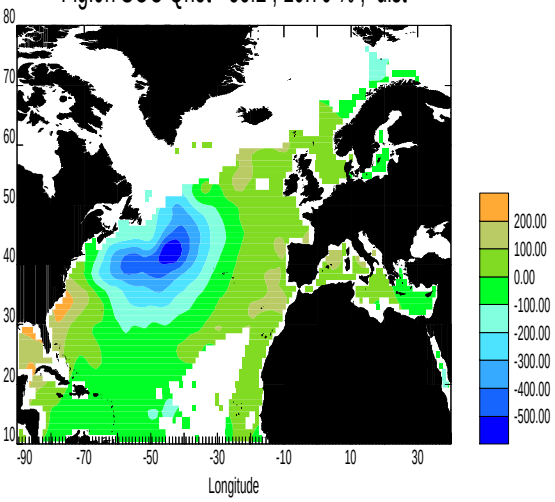

Fig.9i SOC Qnet - eof3 , 5.47 % , dist

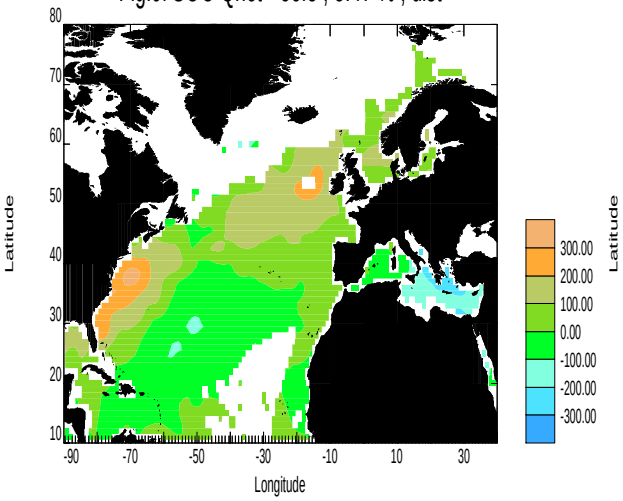

Fig.9j SOC Qnet - eof4 , 4.78 % , dist

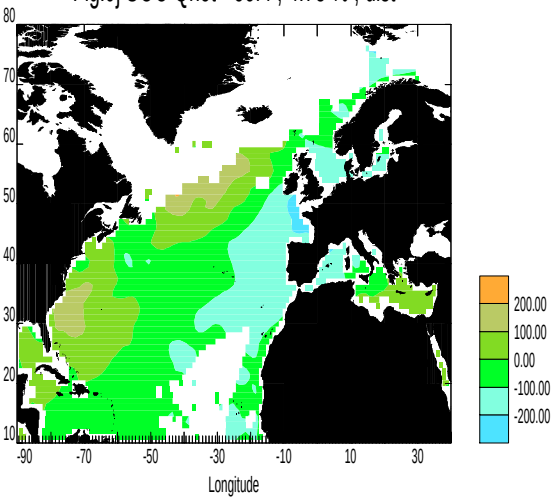

Fig.9k SOC Qnet - eof5 , 4.35 % , dist

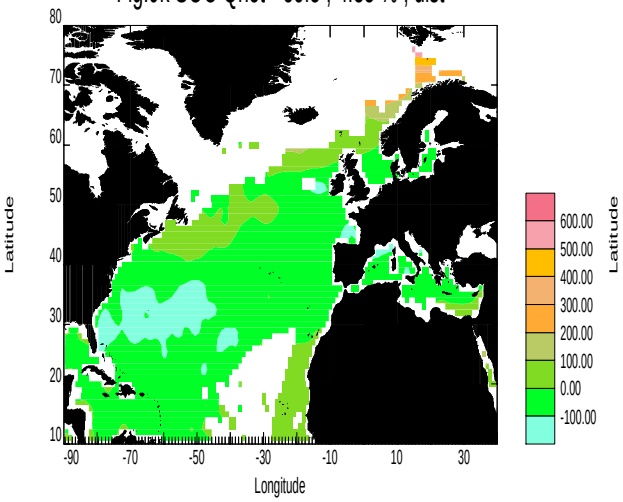

Fig.9l SOC Qnet - eof6 , 3.72 % , dist

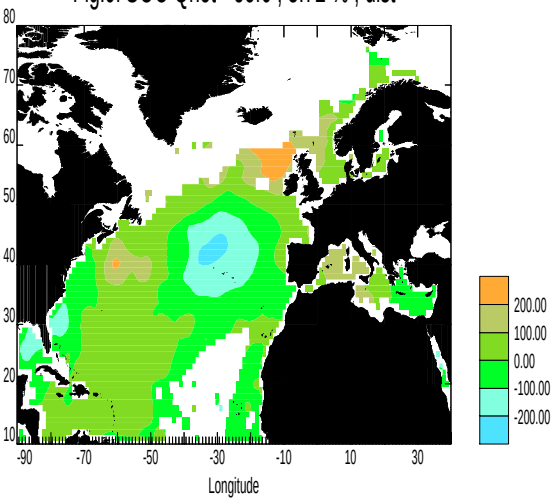

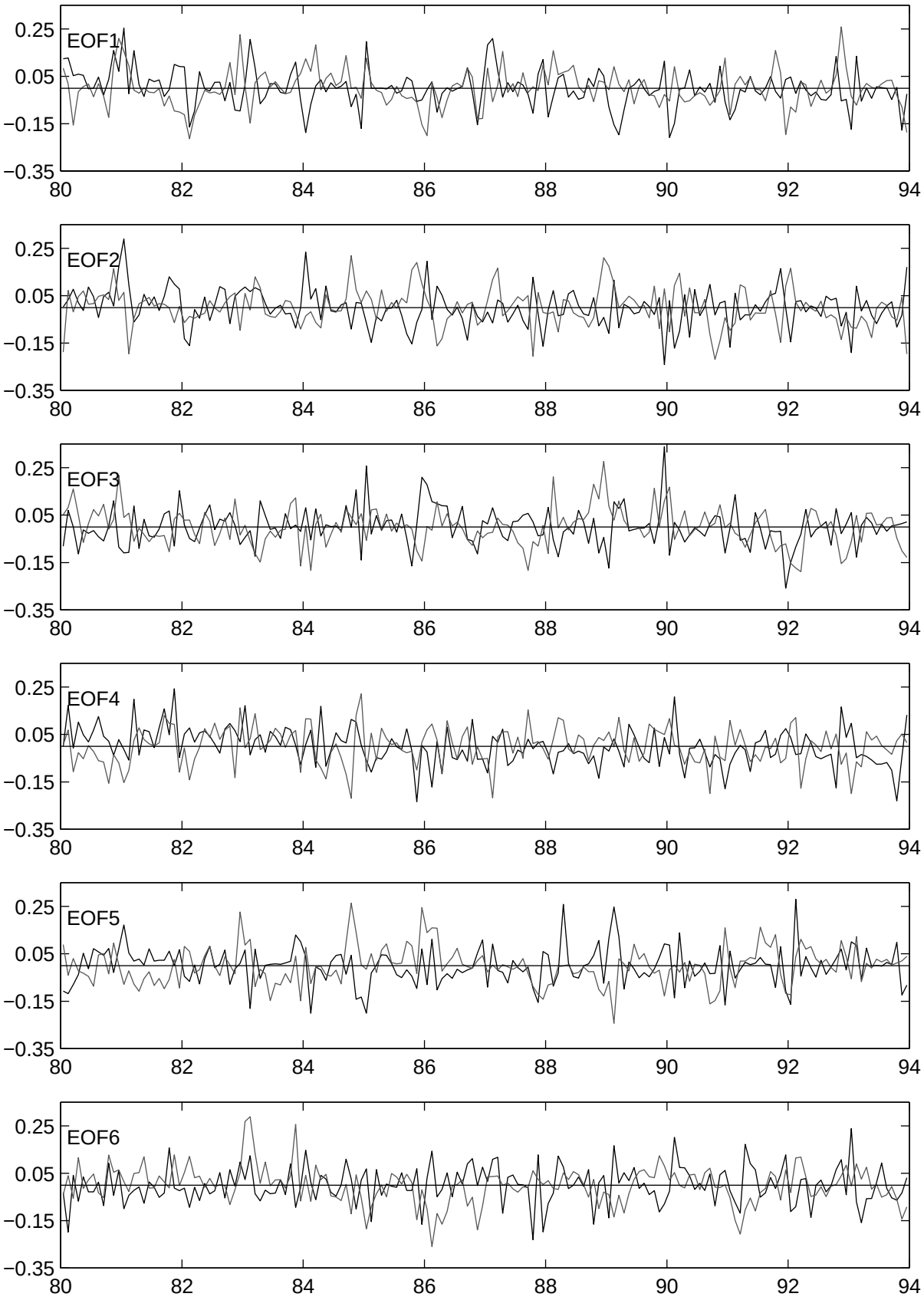

Fig. 9m Time series of Qnet EOFs 1 to 6. SOC−black, HC−grey.

Fig.10a HC Qlat - eof1 , 12.51 % , ndist

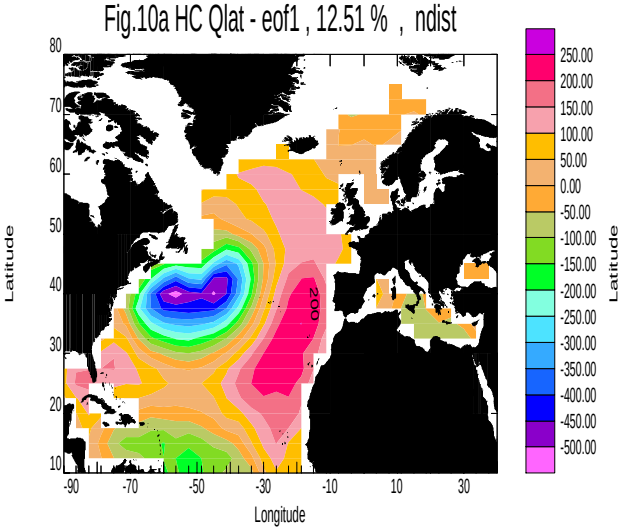

Fig.10b HC Qlat - eof2 , 12.31 % , dist

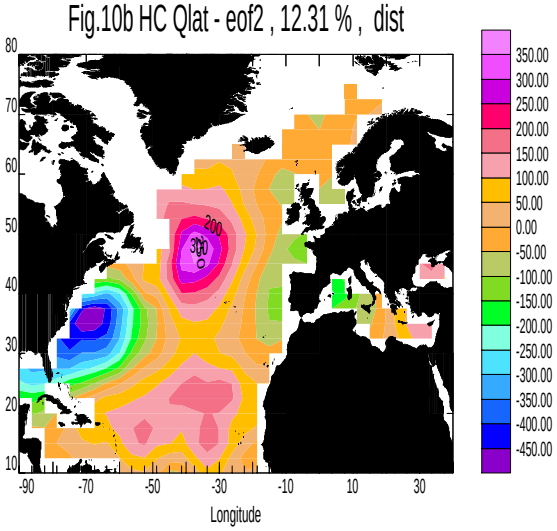

Fig.10c HC Qlat - eof3 , 6.63 % , dist

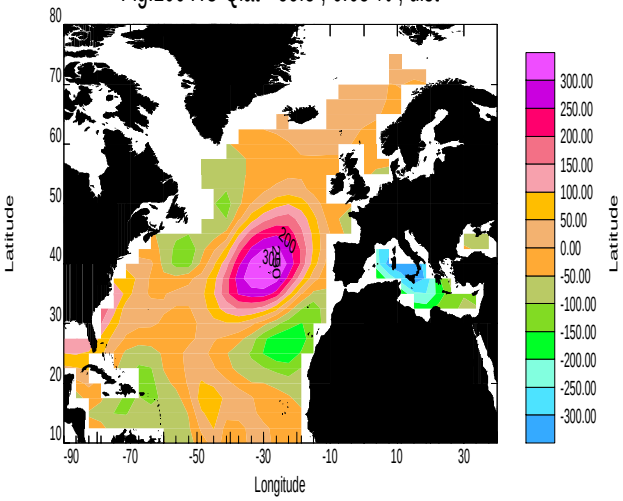

Fig.10d HC Qlat - eof4 , 5.82 % , dist

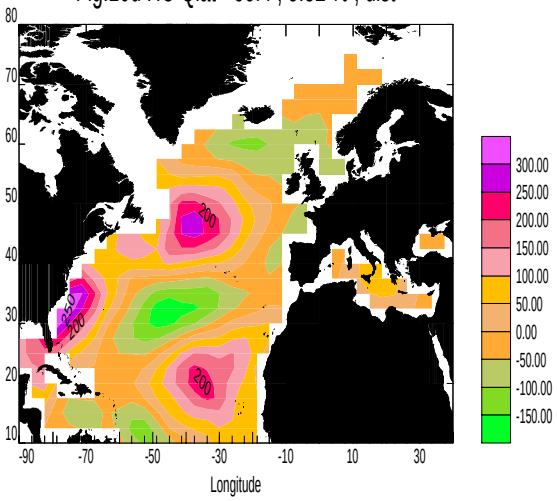

Fig.10e HC Qlat - eof5 , 5.03 % , ndist

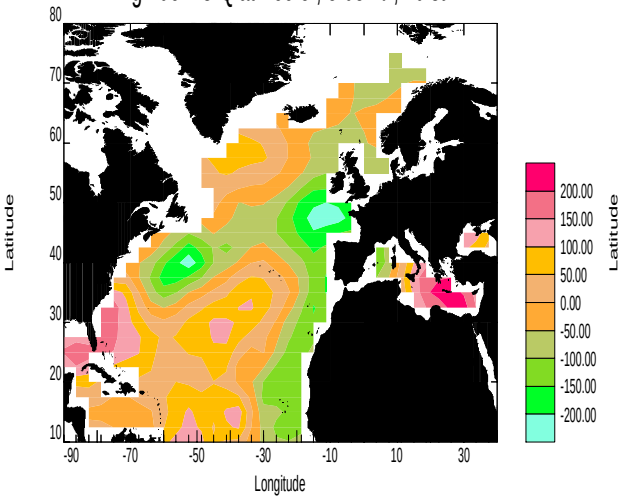

Fig.10f HC Qlat - eof6 , 4.76 % , dist

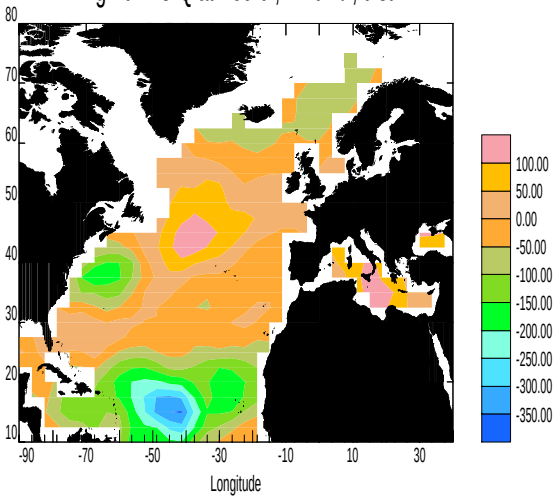

Fig.10g SOC Qlat - eof1 , 14.24 % , dist

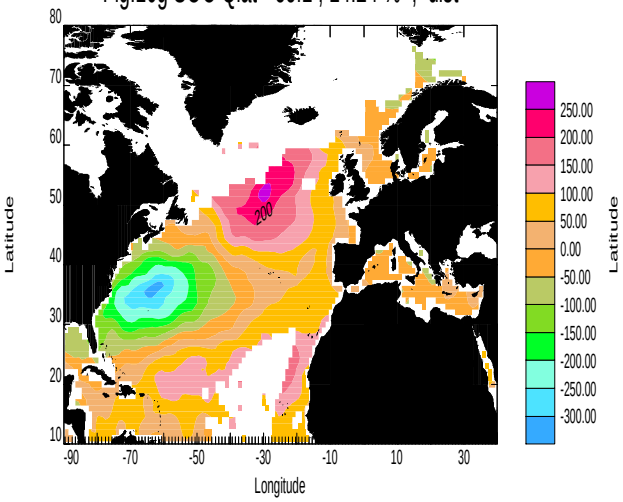

Fig.10h SOC Qlat - eof2 , 10.15 % , dist

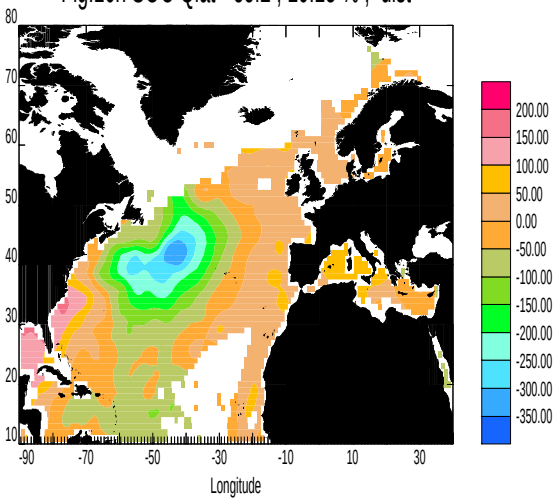

Fig.10i SOC Qlat - eof3 , 5.29 % , dist

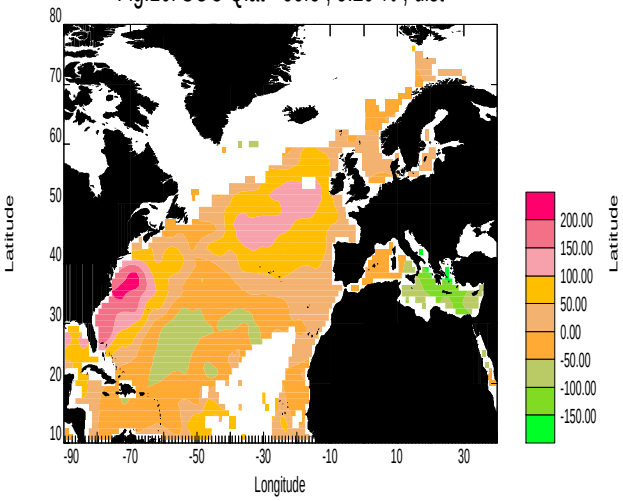

Fig.10j SOC Qlat - eof4 , 4.74 % , dist

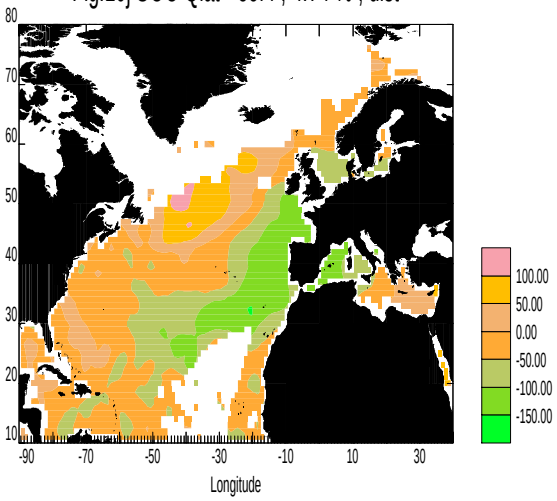

Fig.10k SOC Qlat - eof5 , 3.99 % , dist

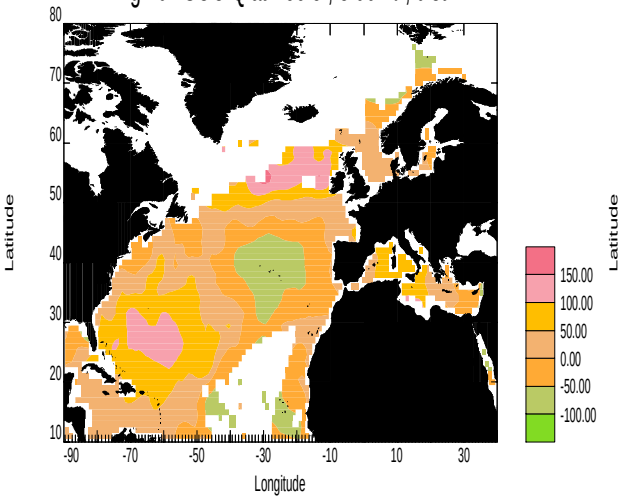

Fig.10l SOC Qlat - eof6 , 3.56 % , dist

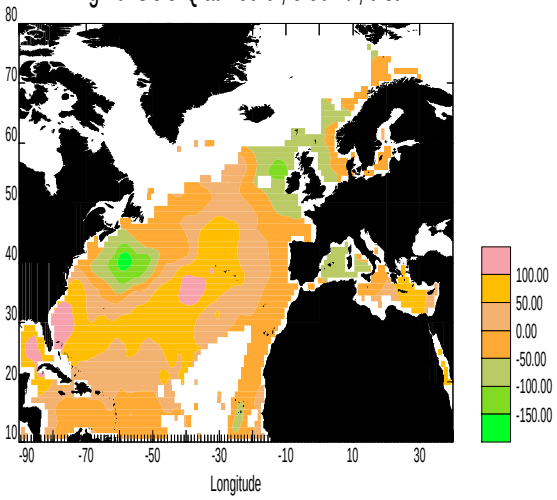

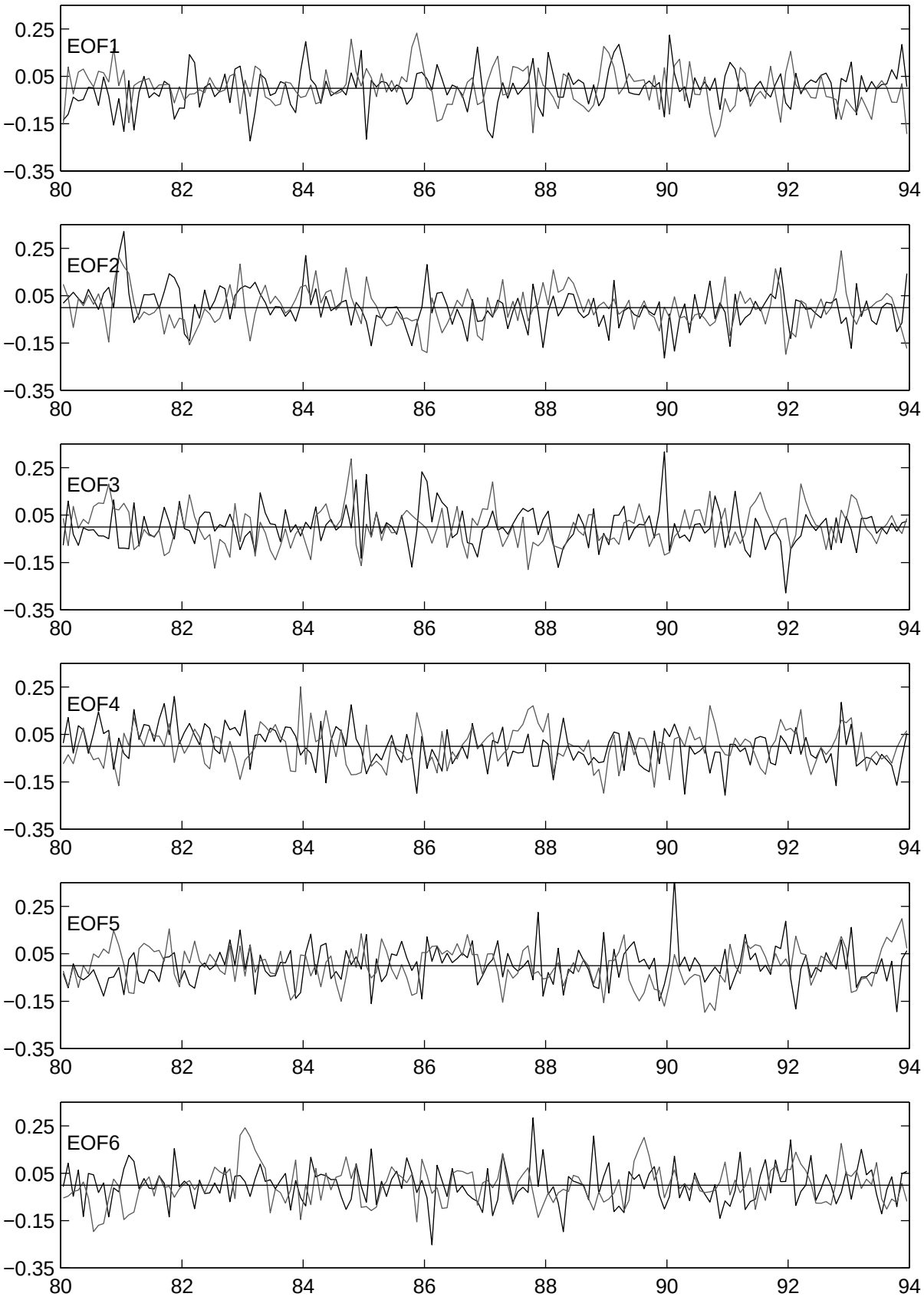

Fig.10m Time series of Qlat EOFs 1 to 6. SOC−black, HC−grey.

Fig.11a HC Qsw - eof1 , 10.79 % , dist

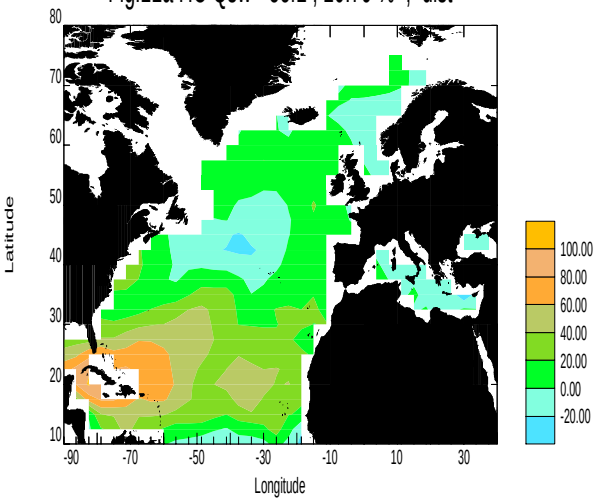

Fig.11b HC Qsw - eof2 , 6.03 % , dist

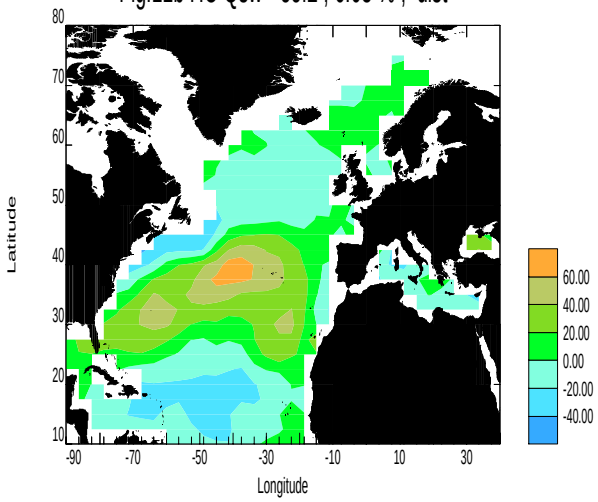

Fig.11c HC Qsw - eof3 , 5.42 % , ndist

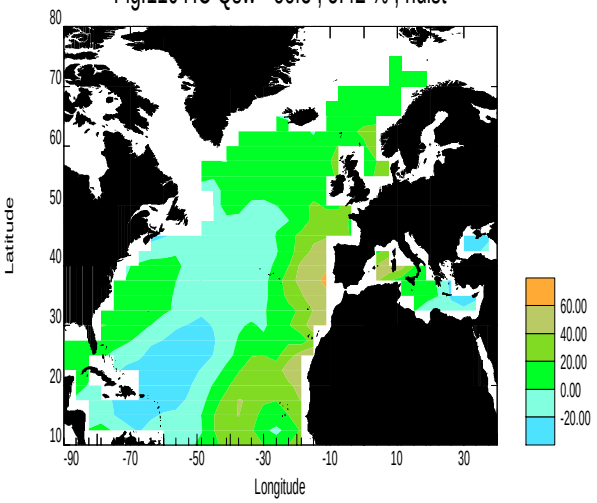

Fig.11d HC Qsw - eof4 , 5.18 % , dist

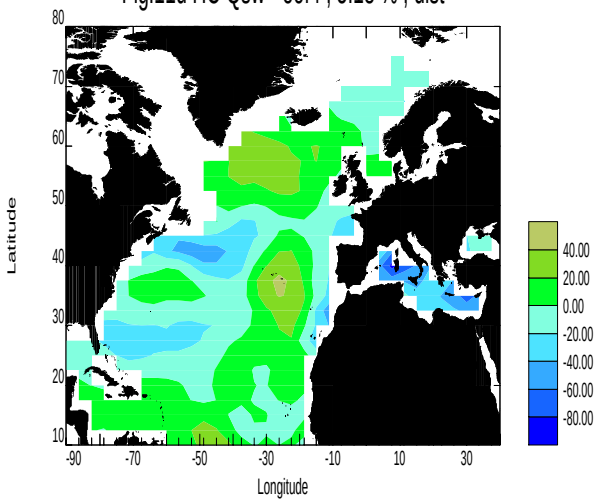

Fig.11e HC Qsw - eof5 , 4.58 % , dist

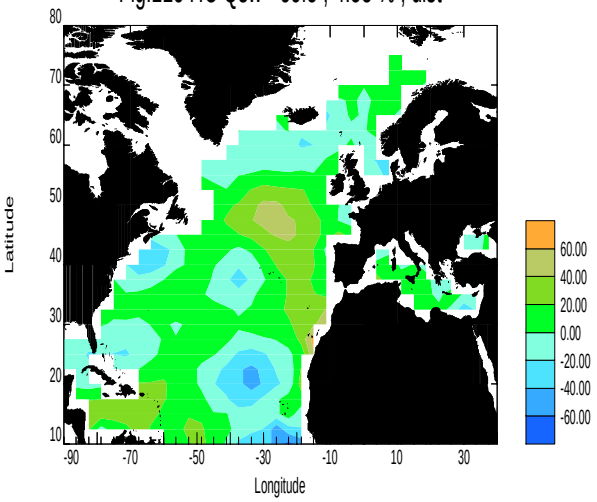

Fig.11f HC Qsw - eof6 , 3.82 % , ndist

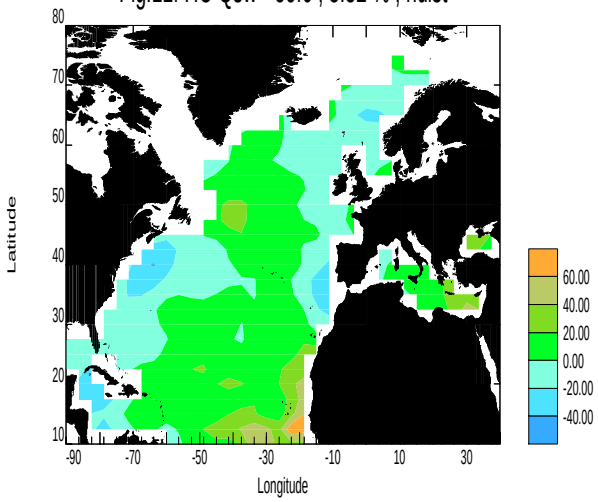

Fig.11g SOC Qsw - eof1 , 9.76 % , dist

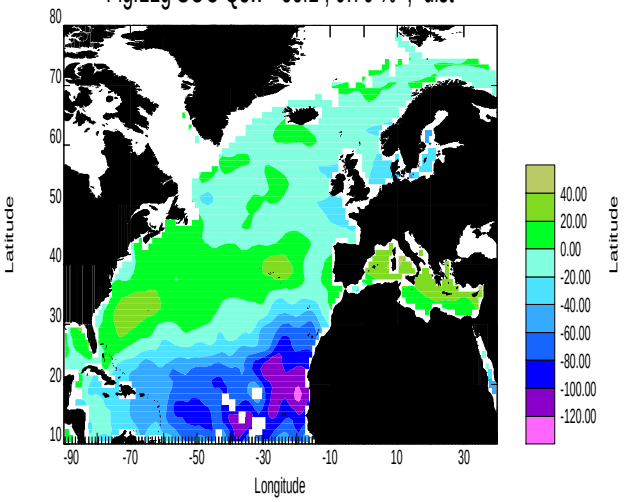

Fig.11h SOC Qsw - eof2 , 4.99 % , dist

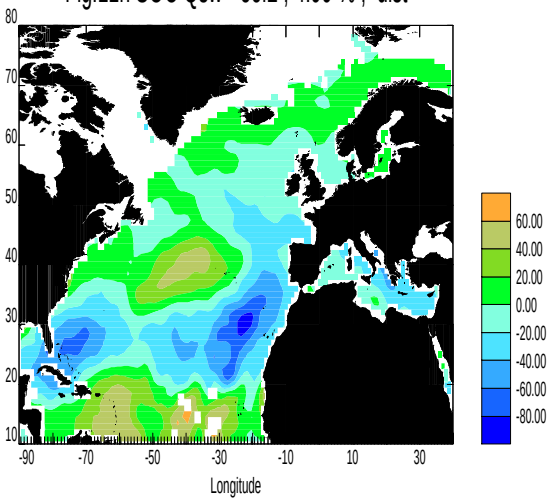

Fig.11i SOC Qsw - eof3 , 4.62 % , dist

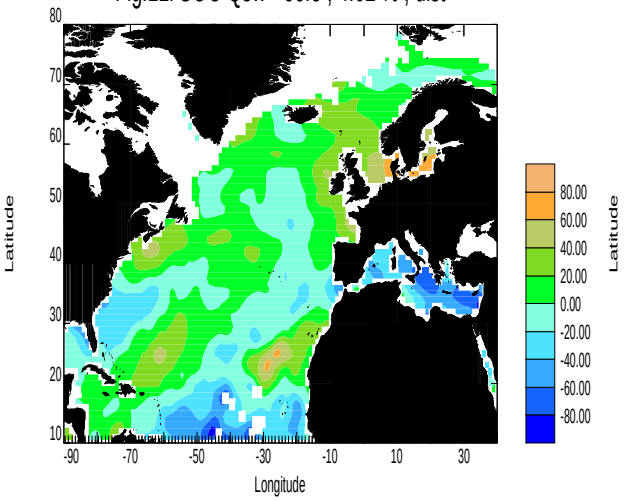

Fig.11j SOC Qsw - eof4 , 4.45 % , dist

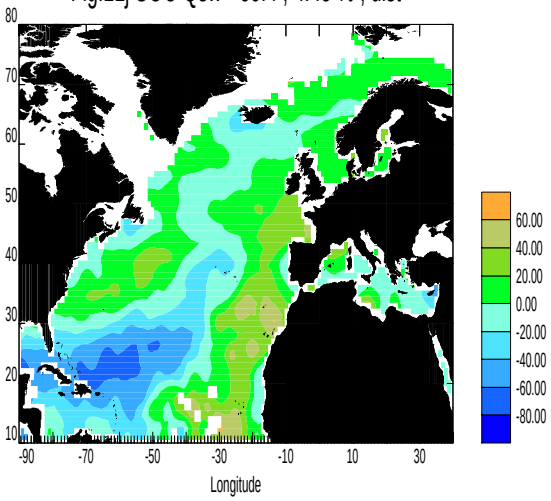

Fig.11k SOC Qsw - eof5 , 3.44 % , ndist

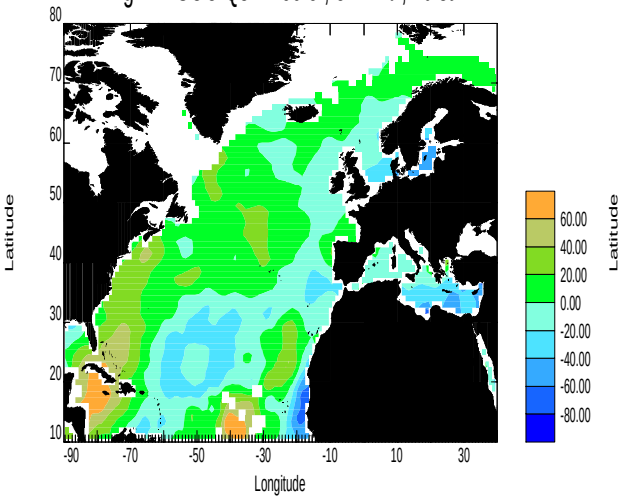

Fig.11l SOC Qsw - eof6 , 3.38 % , dist

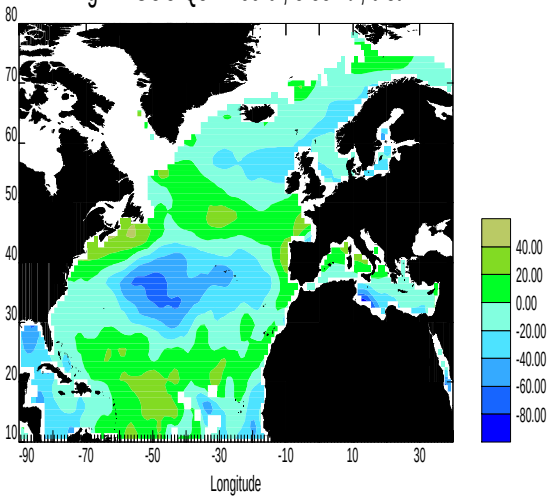

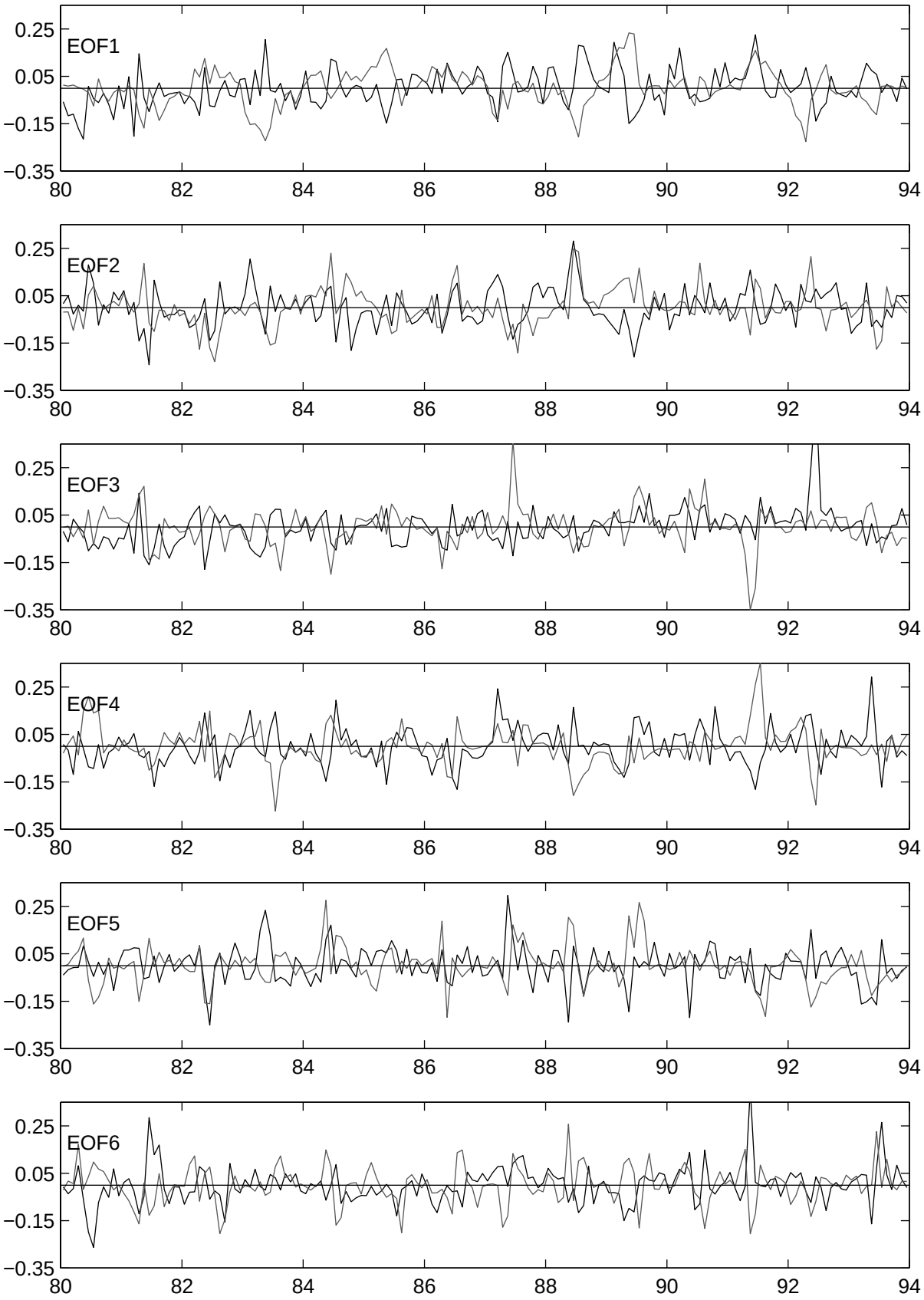

Fig.11m Time series of Qsw EOFs 1 to 6. SOC−black, HC−grey.

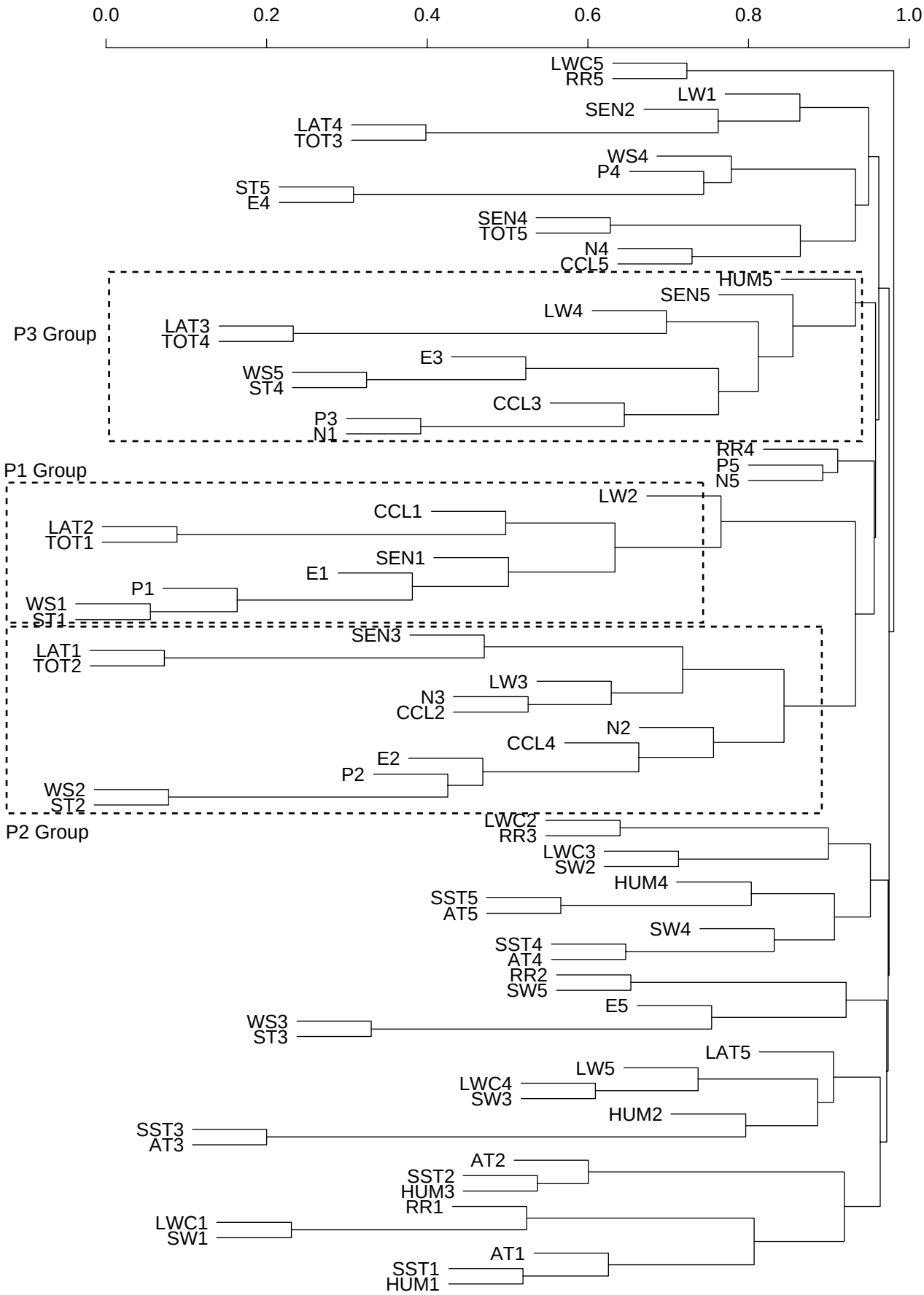

Fig. 12 Cluster analysis of HadAM3 North Atlantic EOFs.

Fig.13a HC SST - eof1 , 17.72 % , dist

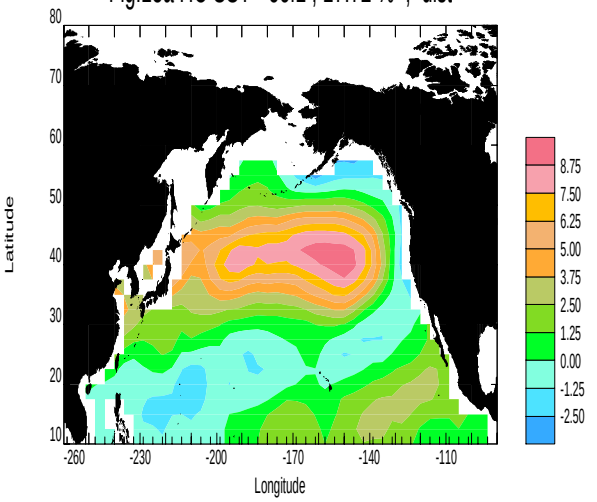

Fig.13b HC SST - eof2 , 11.87 % , dist

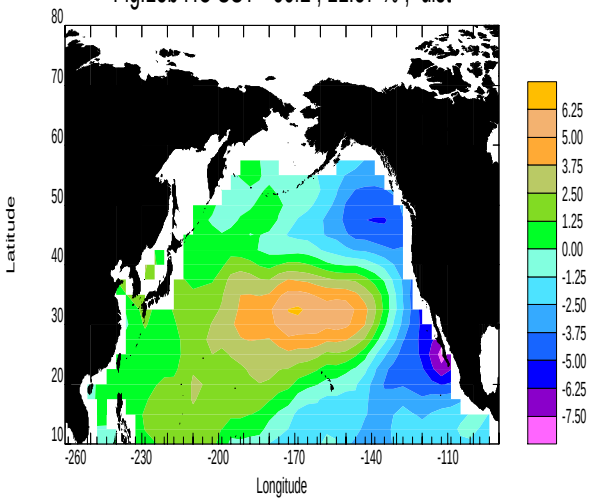

Fig.13c HC SST - eof3 , 9.25 % , dist

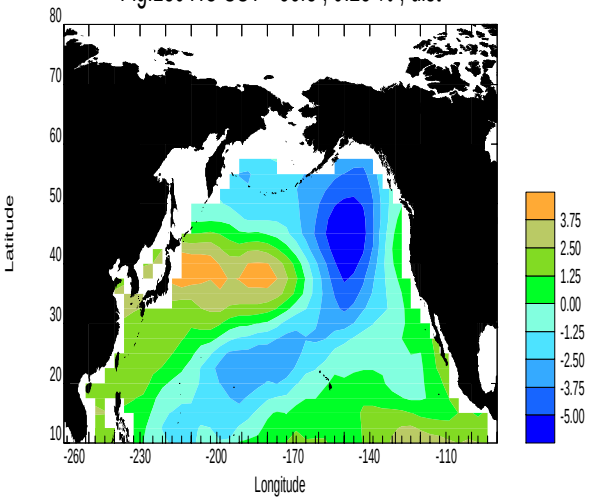

Fig.13d HC SST - eof4 , 7.24 % , dist

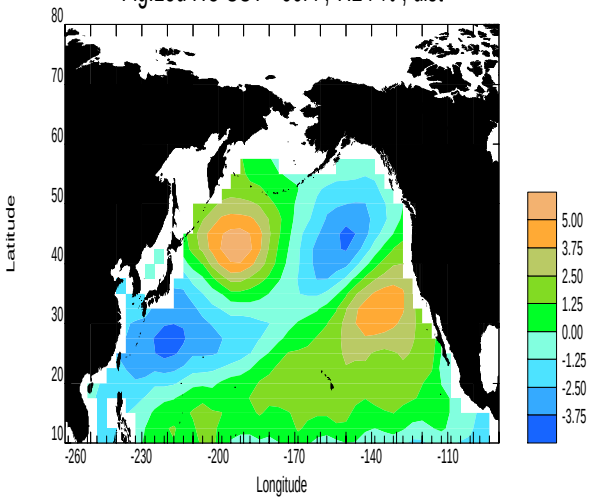

Fig.13e HC SST - eof5 , 5.40 % , dist

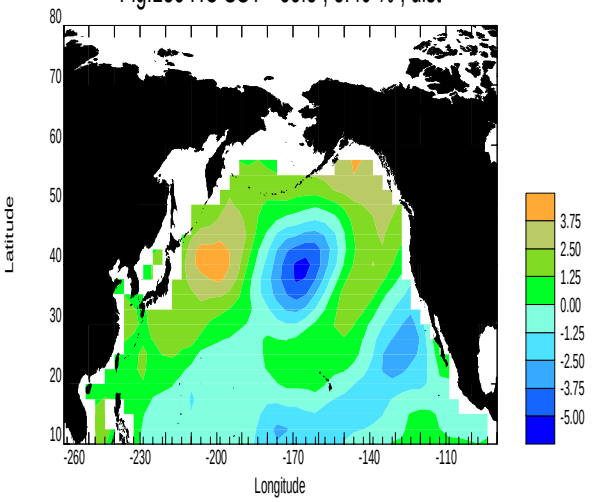

Fig.13f HC SST - eof6 , 4.59 % , dist

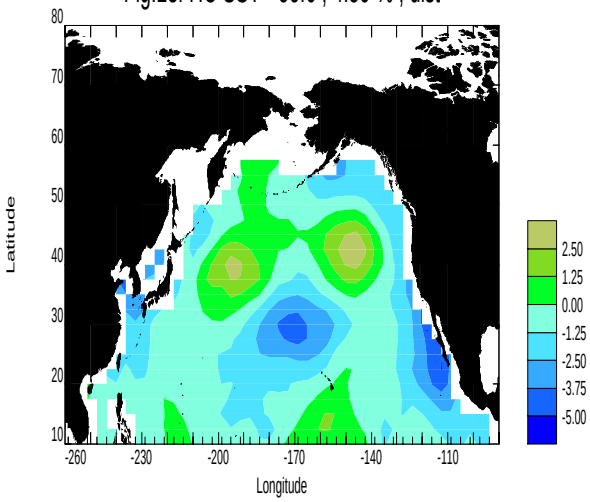

Fig.13g SOC SST - eof1 , 15.53 % , dist

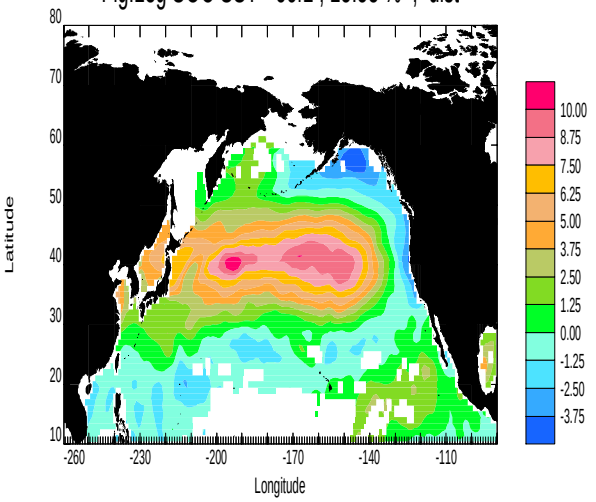

Fig.13h SOC SST - eof2 , 9.86 % , dist

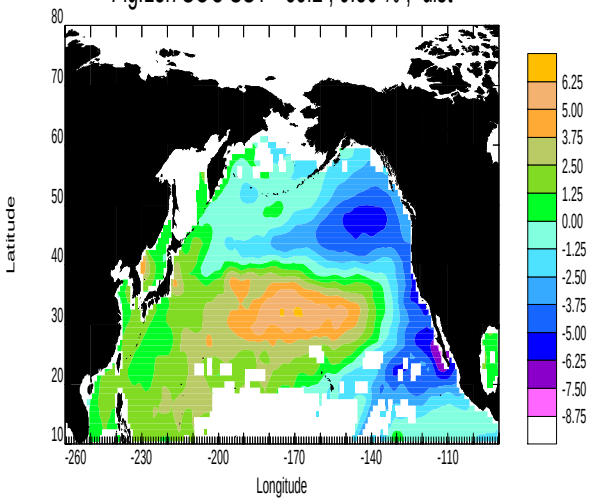

Fig.13i SOC SST - eof3 , 7.81 % , dist

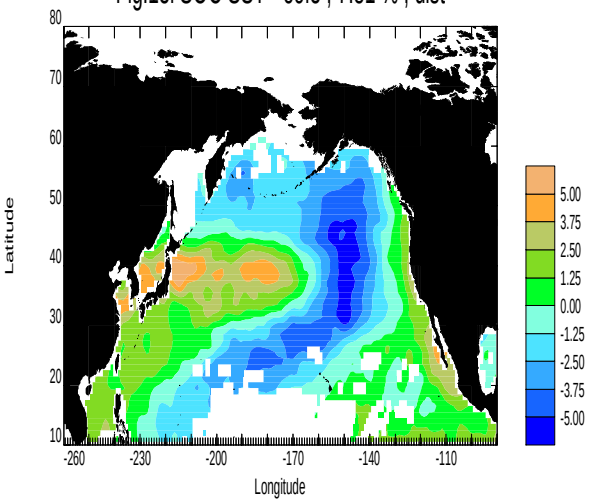

Fig.13j SOC SST - eof4 , 6.26 % , dist

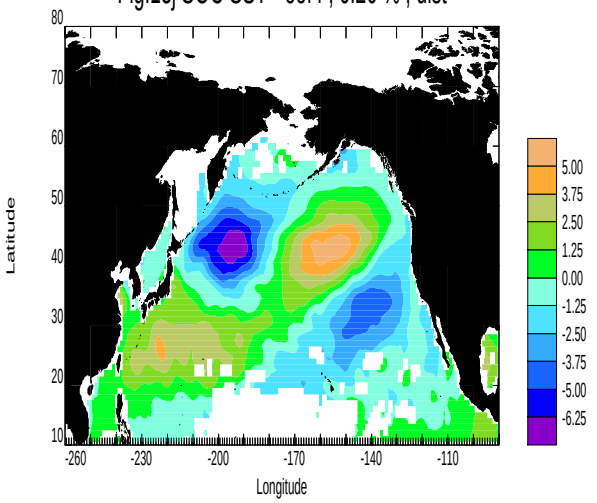

Fig.13k SOC SST - eof5 , 4.89 % , dist

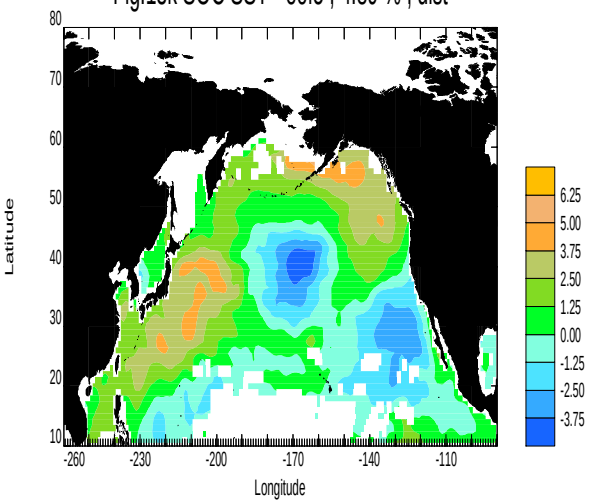

Fig.13l SOC SST - eof6 , 3.84 % , dist

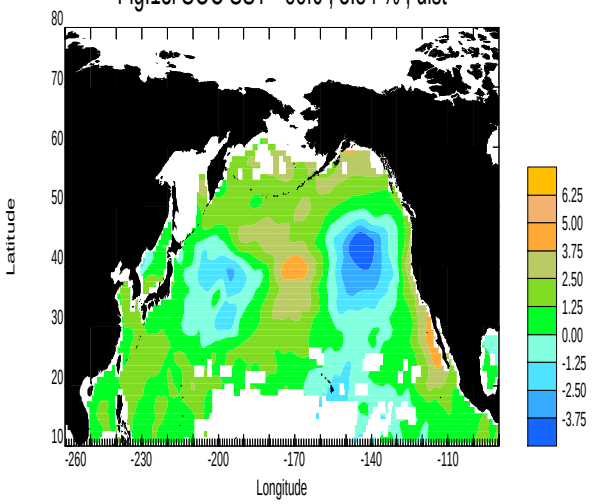

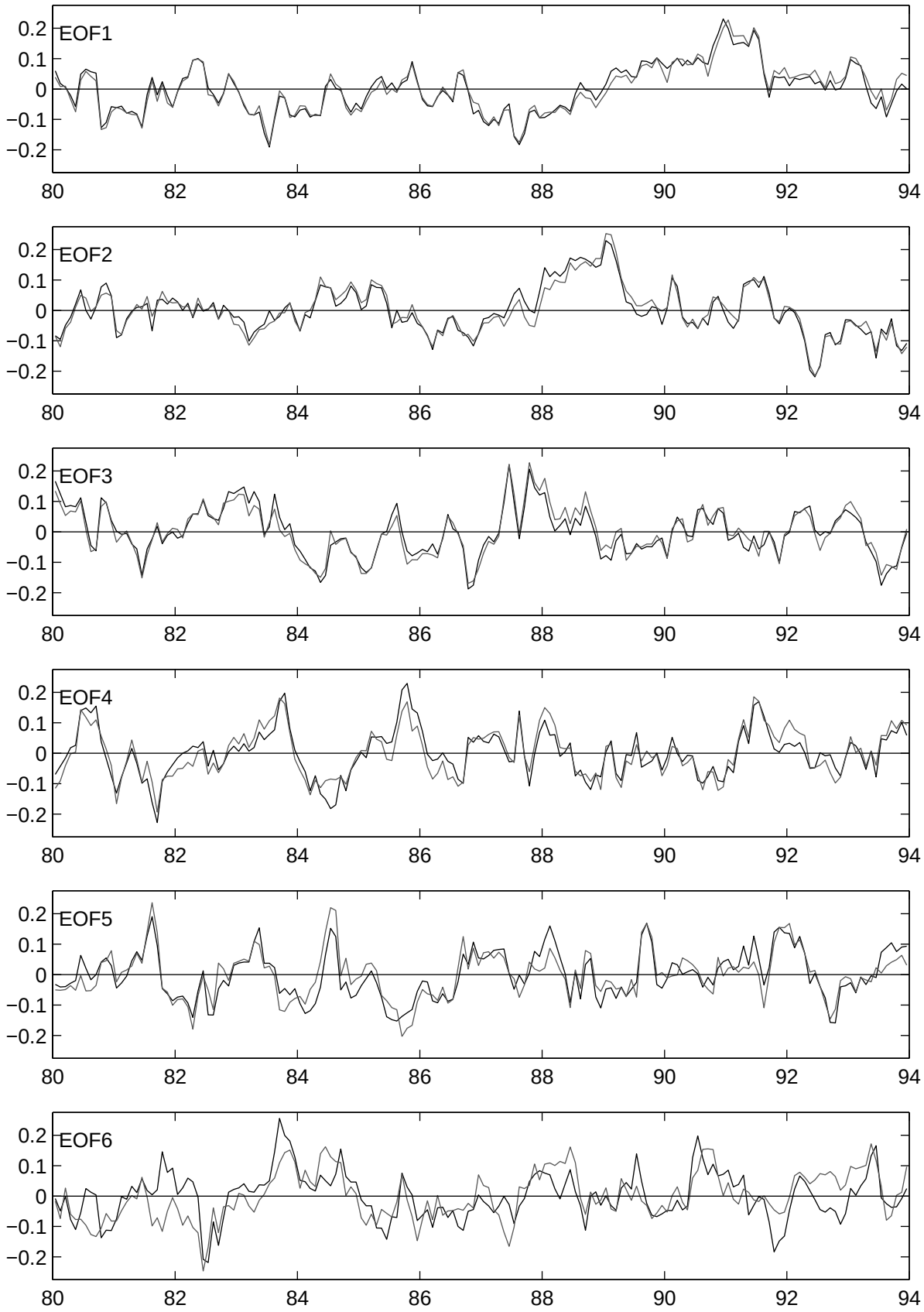

Fig. 13m Time series of North Pacific SST EOFs 1 to 6. SOC−black, HC−grey.

Fig.14a HC SLP - eof1 , 48.95 % , dist

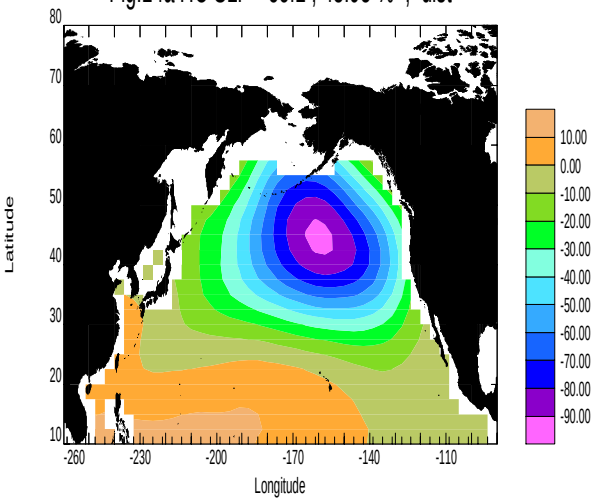

Fig.14b HC SLP - eof2 , 12.73 % , dist

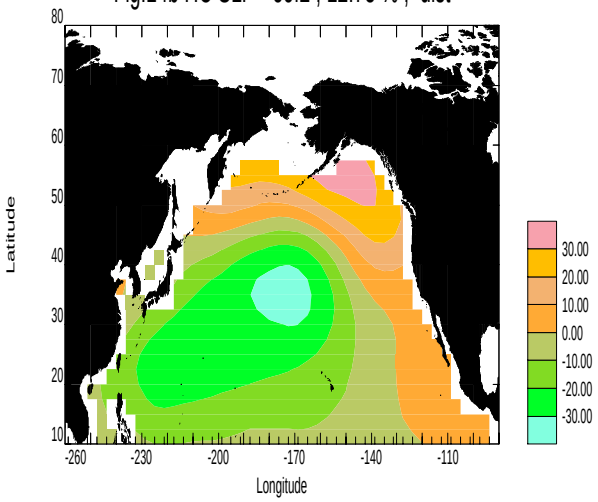

Fig.14c HC SLP - eof3 , 9.33 % , dist

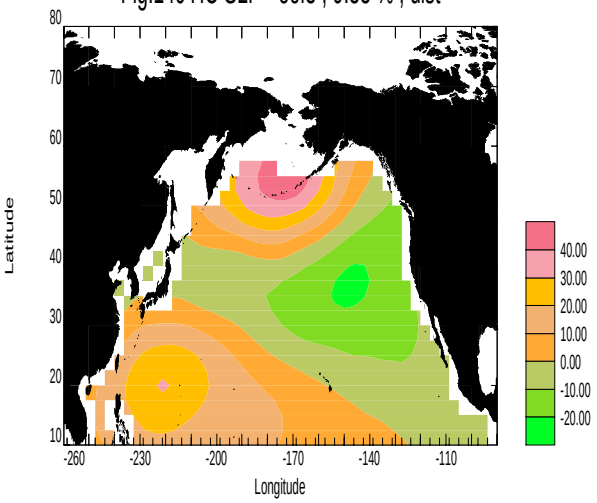

Fig.14d HC SLP - eof4 , 8.04 % , dist

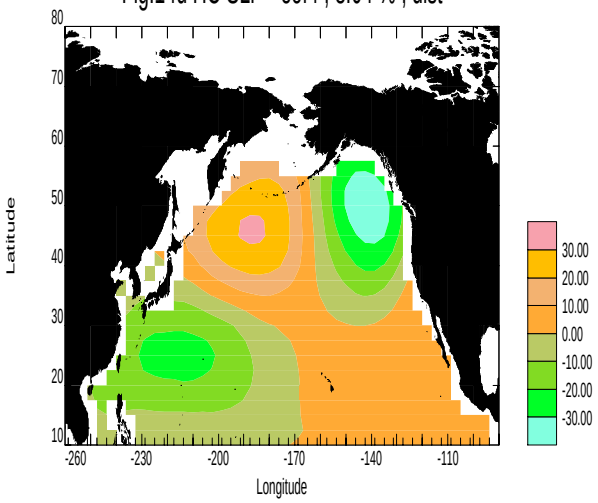

Fig.14e HC SLP - eof5 , 4.13 % , dist

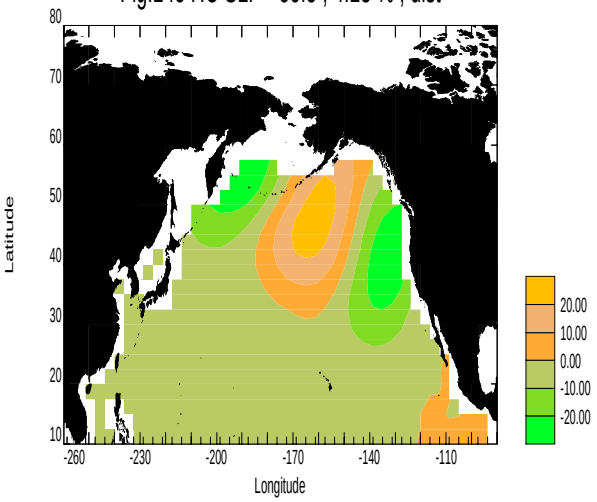

Fig.14f HC SLP - eof6 , 3.25 % , dist

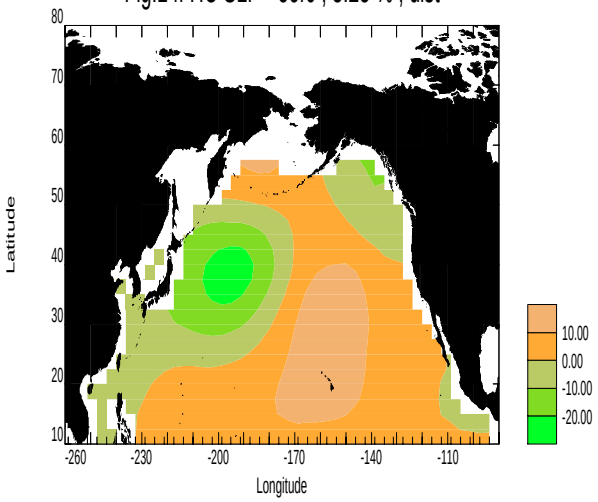

Fig.14g SOC SLP - eof1 , 42.88 % , dist

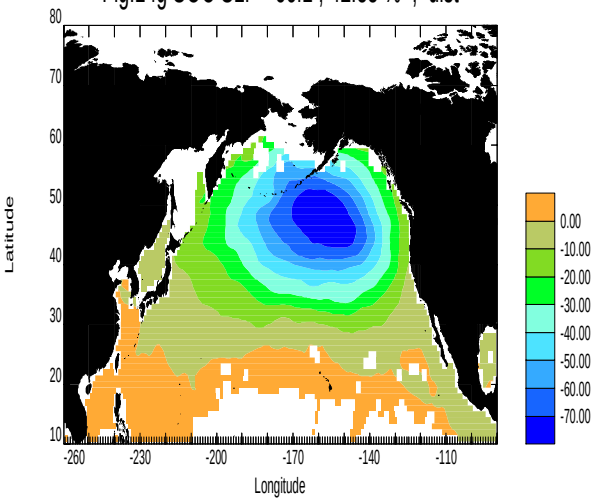

Fig.14h SOC SLP - eof2 , 15.42 % , dist

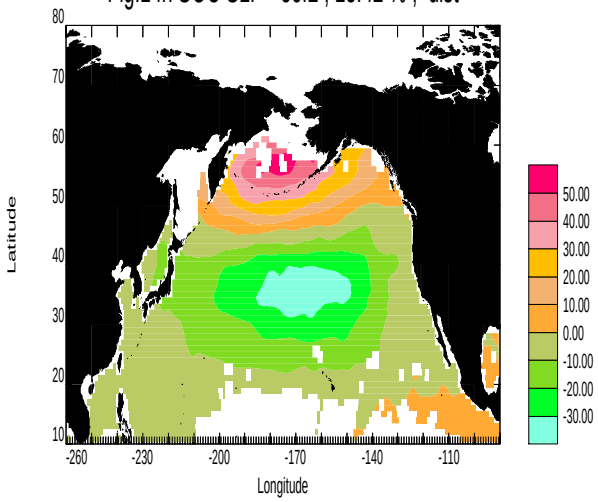

Fig.14i SOC SLP - eof3 , 9.98 % , dist

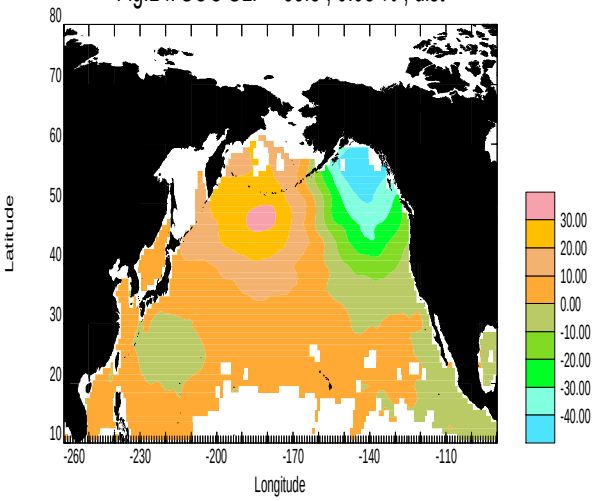

Fig.14j SOC SLP - eof4 , 5.36 % , dist

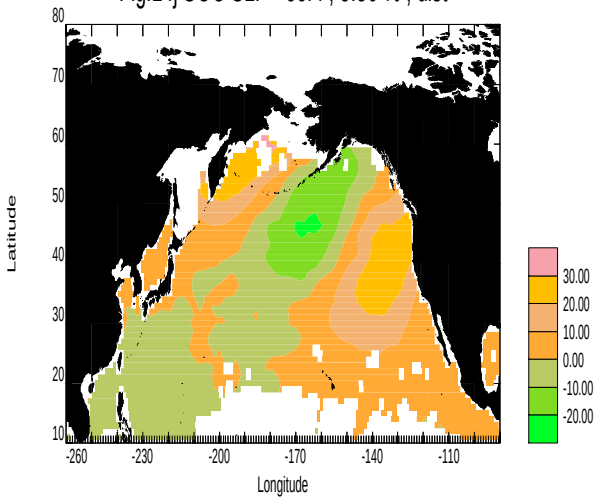

Fig.14k SOC SLP - eof5 , 3.77 % , dist

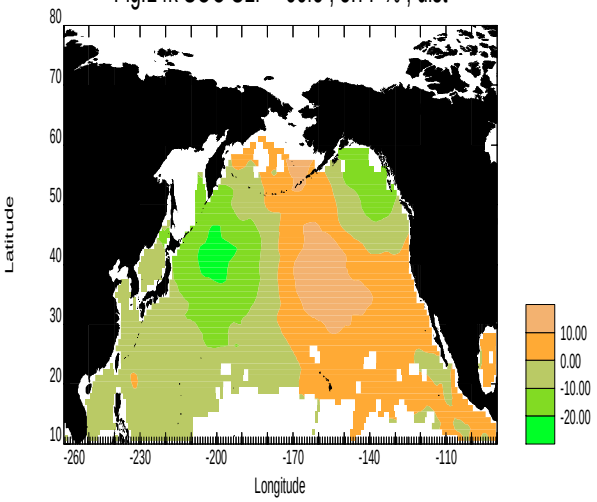

Fig.14l SOC SLP - eof6 , 2.03 % , dist

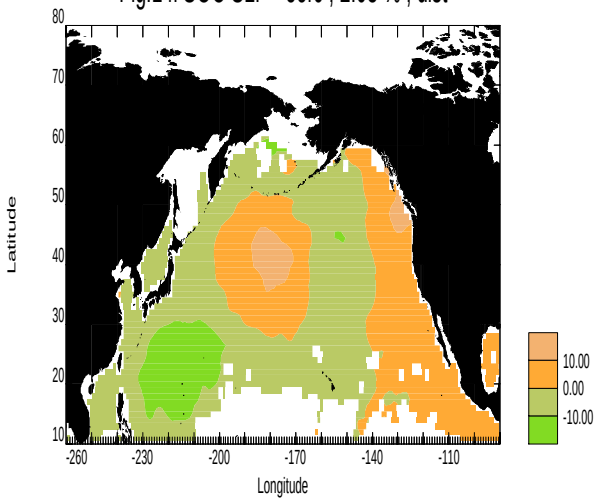

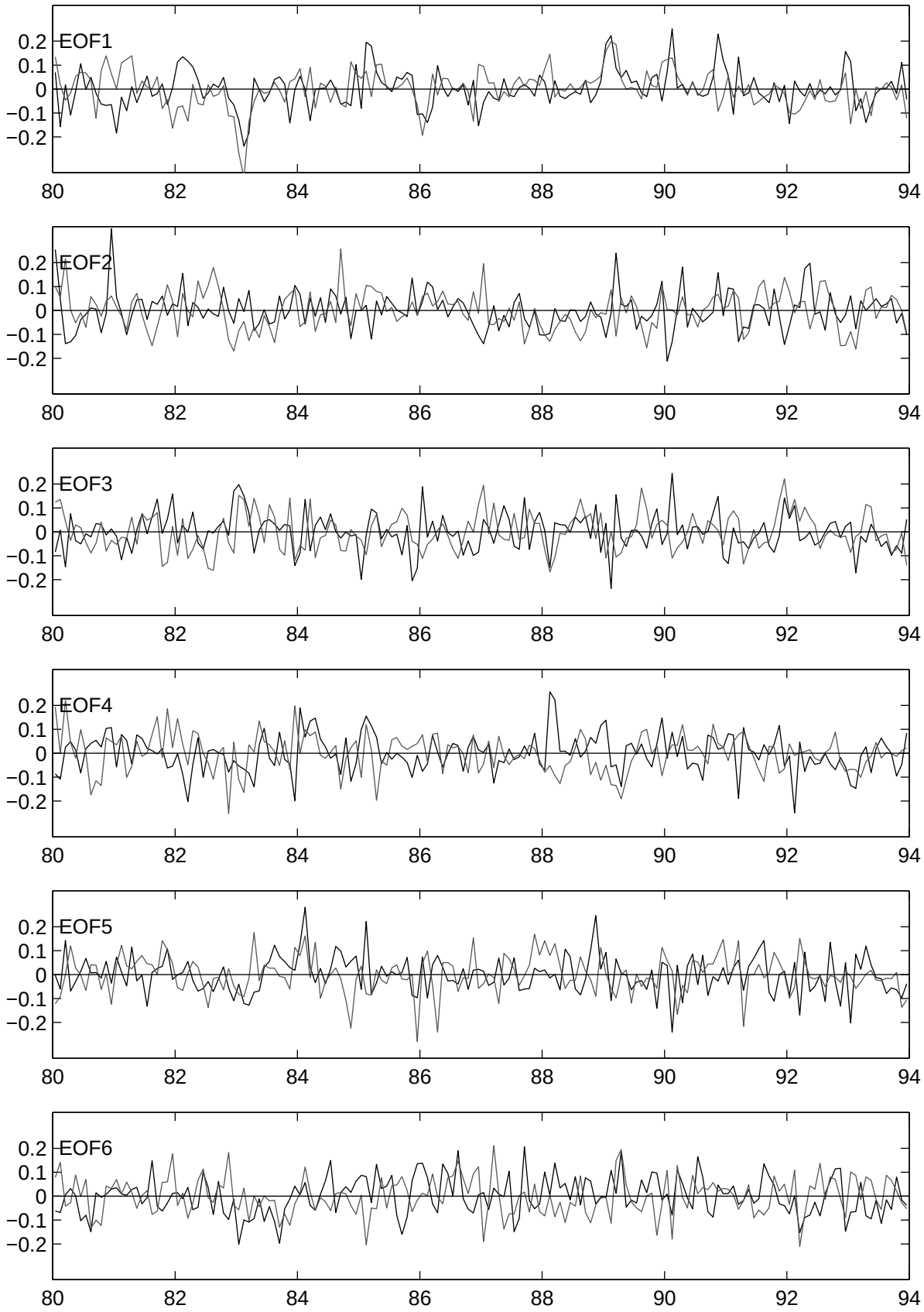

Fig. 14m Time series of North Pacific SLP EOFs 1 to 6. SOC−black, HC−grey.

Fig.15a HC Qnet - eof1 , 11.62 % , dist

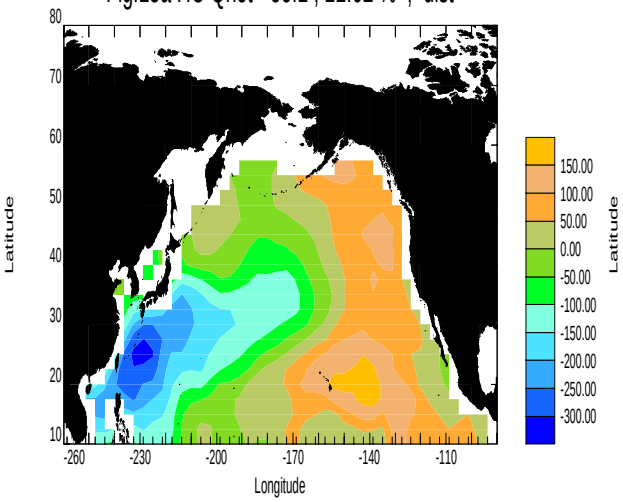

Fig.15b HC Qnet - eof2 , 9.03 % , dist

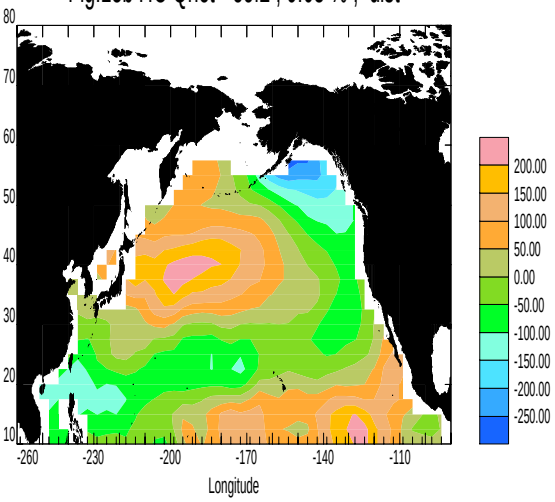

Fig.15c HC Qnet - eof3 , 7.71 % , dist

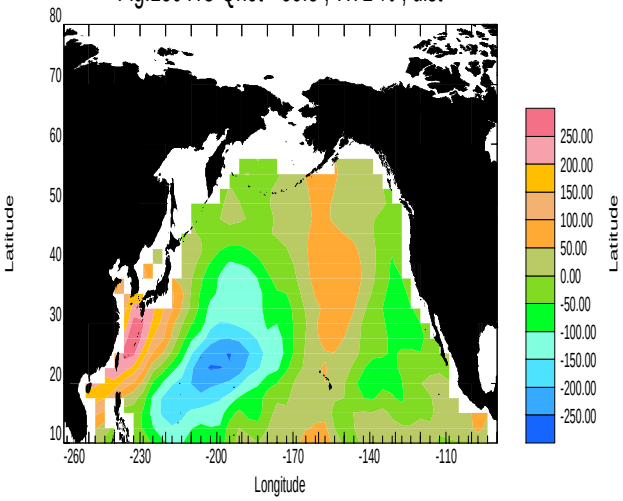

Fig.15d HC Qnet - eof4 , 5.92 % , ndist

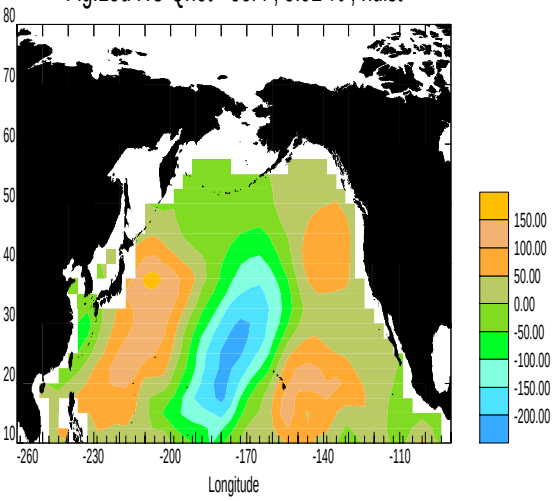

Fig.15e HC Qnet - eof5 , 5.65 % , dist

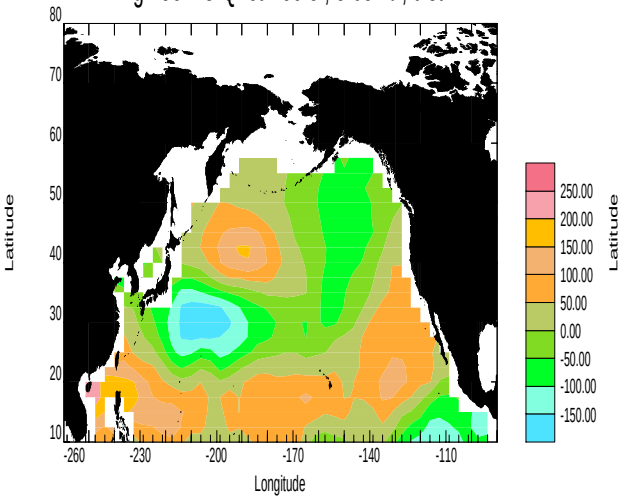

Fig.15f HC Qnet - eof6 , 4.28 % , dist

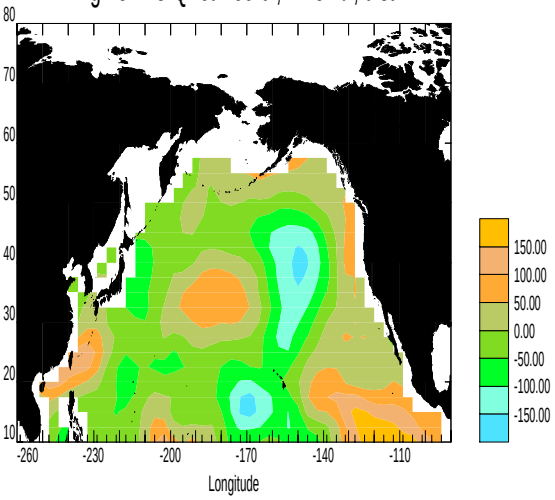

Fig.15g SOC Qnet - eof1 , 9.97 % , dist

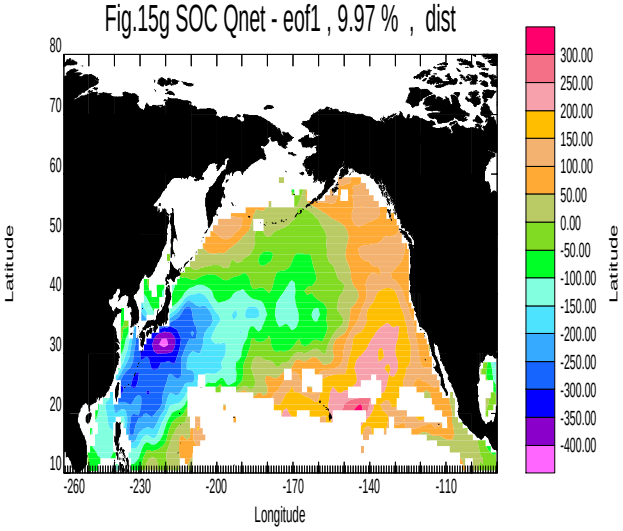

Fig.15h SOC Qnet - eof2 , 6.82 % , dist

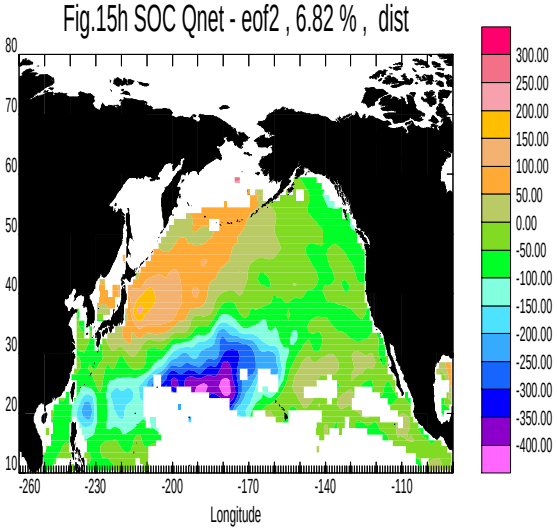

Fig.15i SOC Qnet - eof3 , 5.26 % , dist

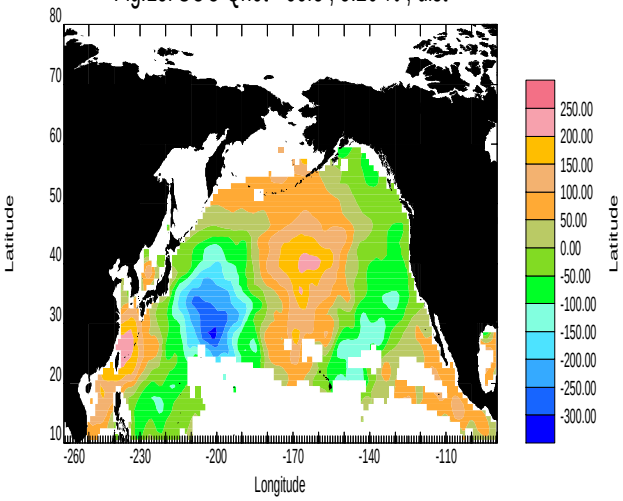

Fig.15j SOC Qnet - eof4 , 4.76 % , dist

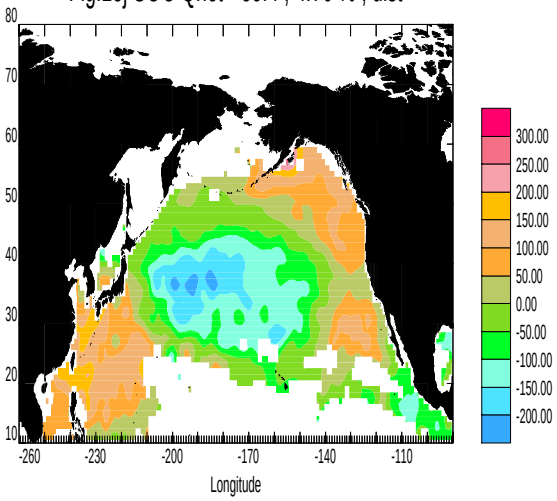

Fig.15k SOC Qnet - eof5 , 4.18 % , dist

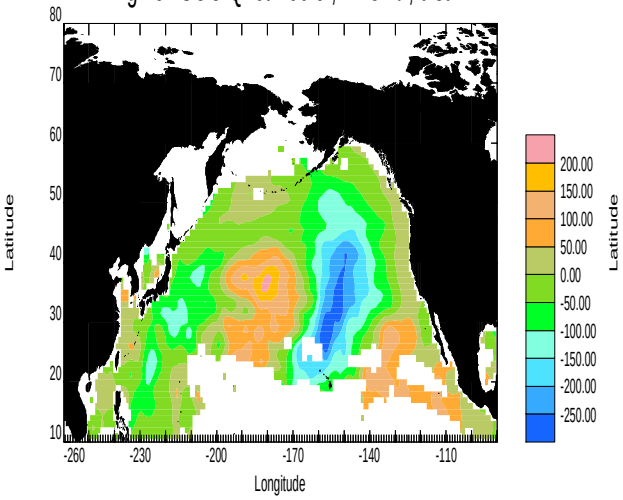

Fig.15l SOC Qnet - eof6 , 3.90 % , dist

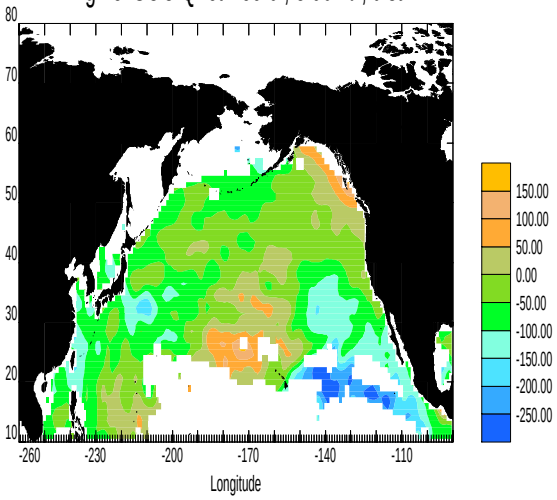

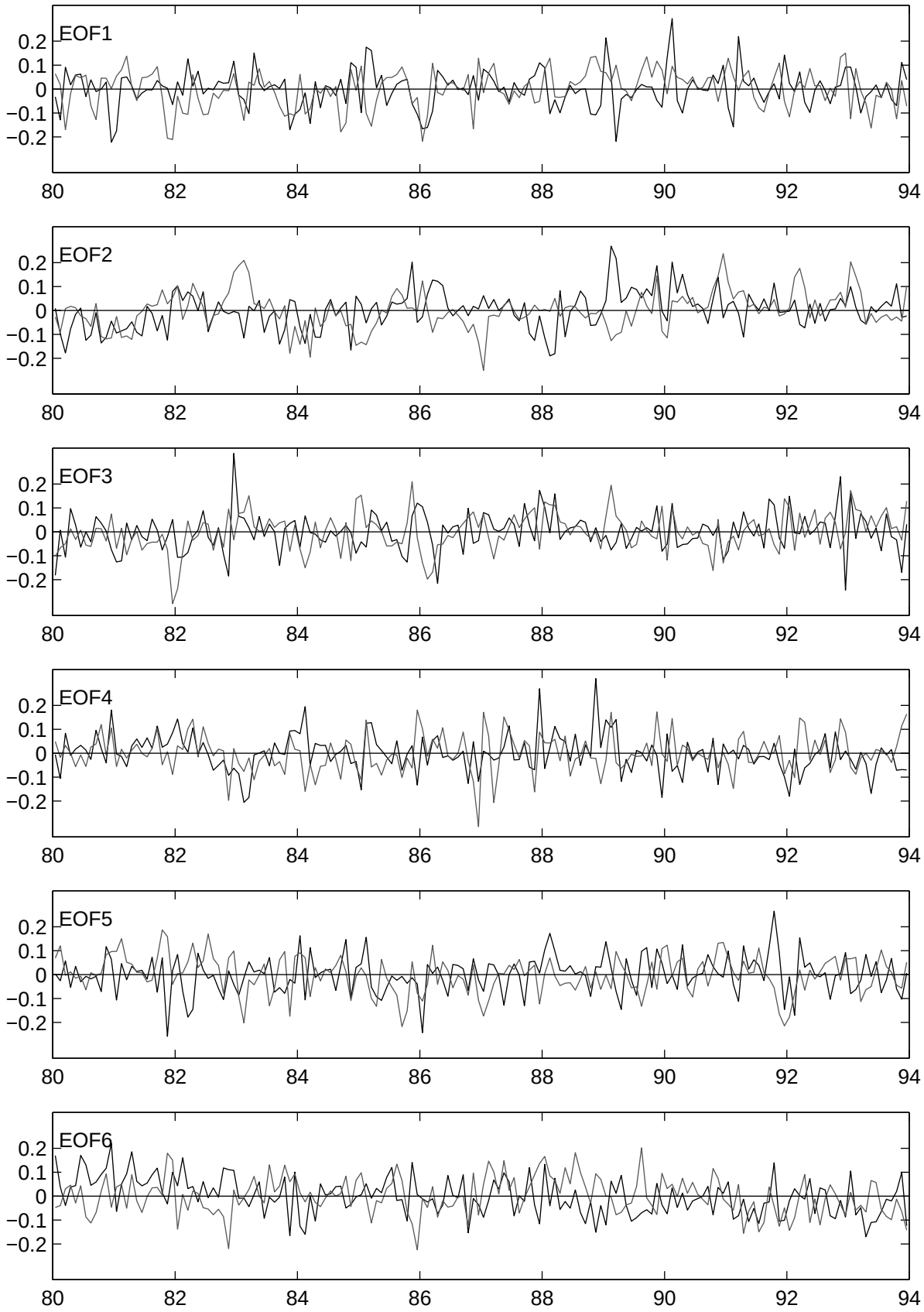

Fig. 15m Time series of North Pacific Qnet EOFs 1 to 6. SOC−black, HC−grey.

Fig.16a HC Qlat - eof1 , 11.02 % , dist

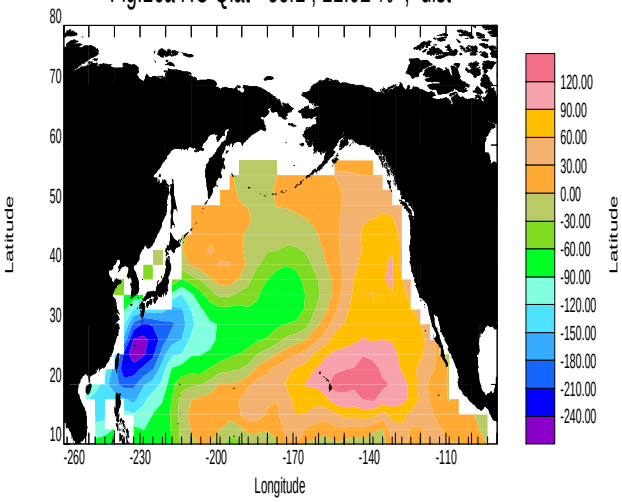

Fig.16b HC Qlat - eof2 , 8.42 % , dist

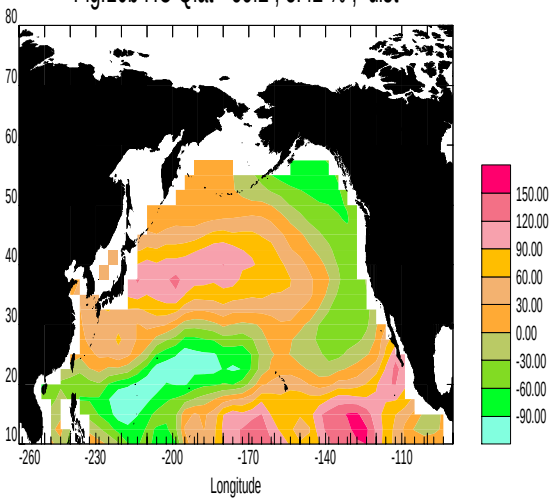

Fig.16c HC Qlat - eof3 , 7.76 % , dist

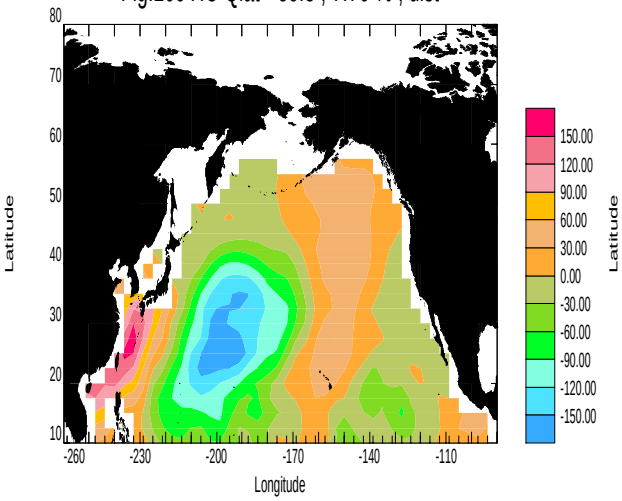

Fig.16d HC Qlat - eof4 , 6.50 % , dist

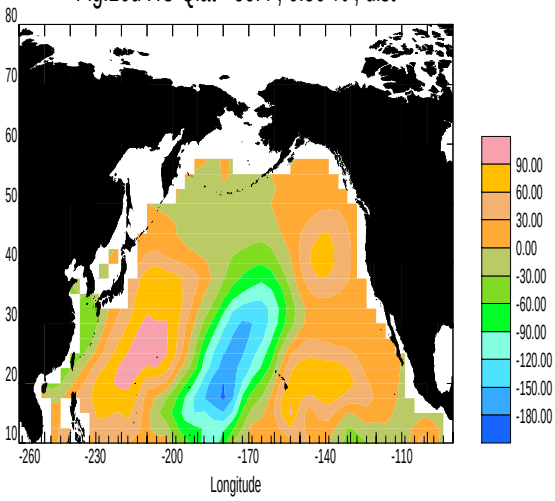

Fig.16e HC Qlat - eof5 , 5.64 % , dist

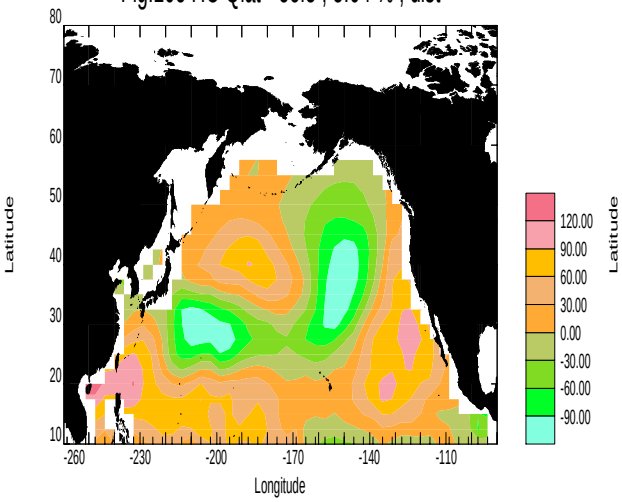

Fig.16f HC Qlat - eof6 , 4.13 % , dist

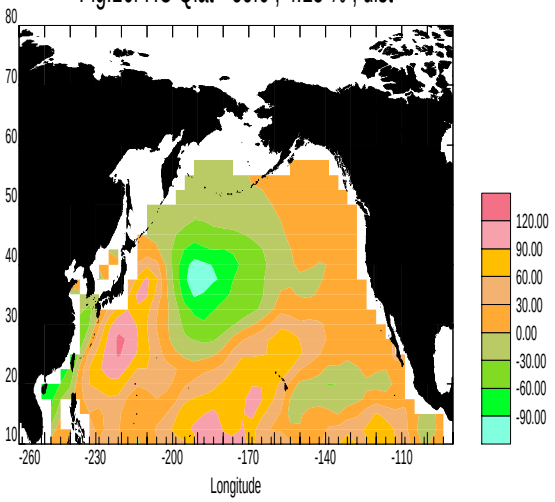

Fig.16g SOC Qlat - eof1 , 9.33 % , dist

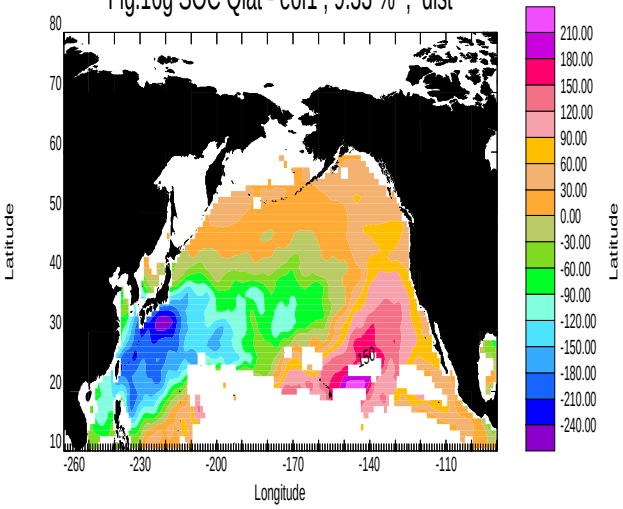

Fig.16h SOC Qlat - eof2 , 6.32 % , dist

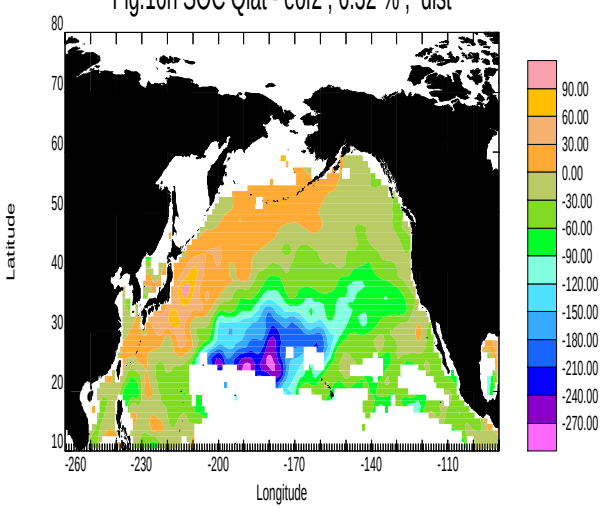

Fig.16i SOC Qlat - eof3 , 5.24 % , dist

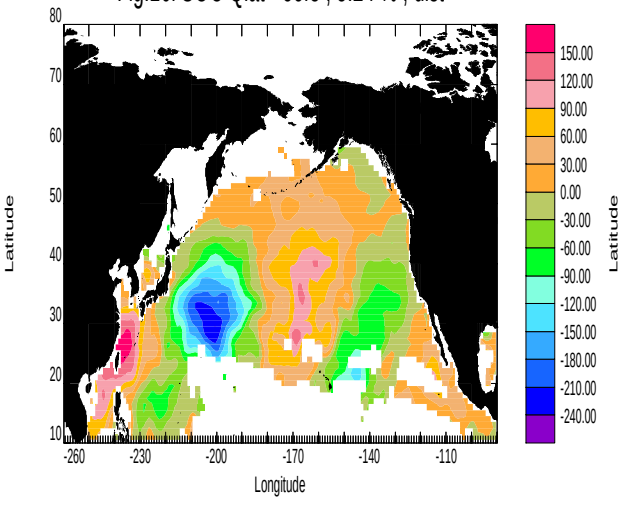

Fig.16j SOC Qlat - eof4 , 4.55 % , dist

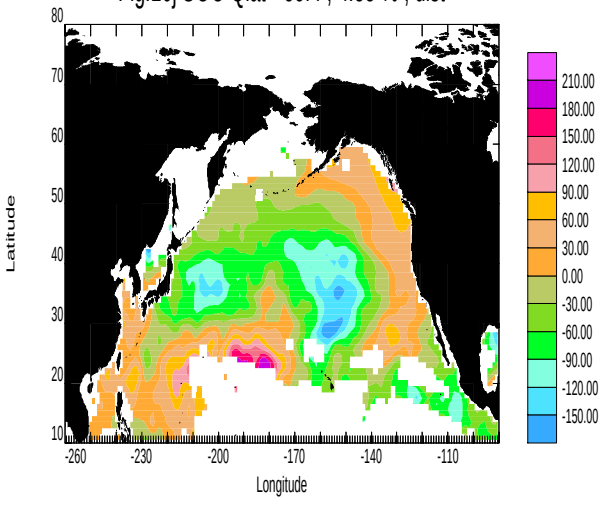

Fig.16k SOC Qlat - eof5 , 4.03 % , ndist

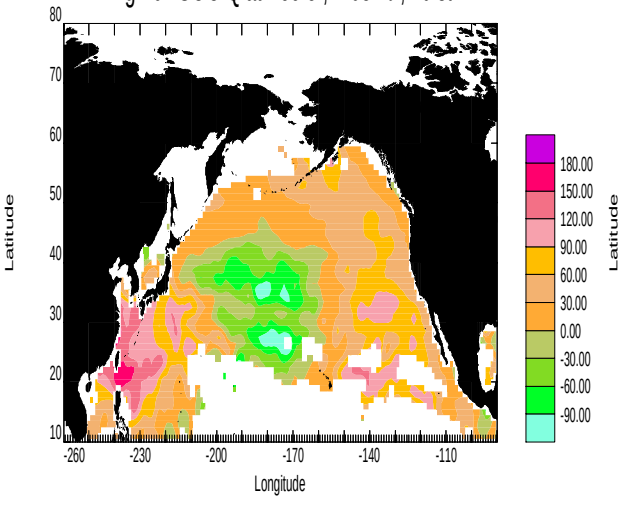

Fig.16l SOC Qlat - eof6 , 3.99 % , dist

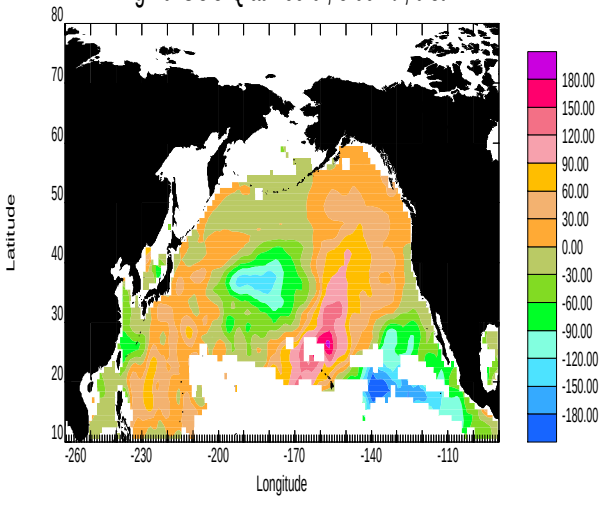

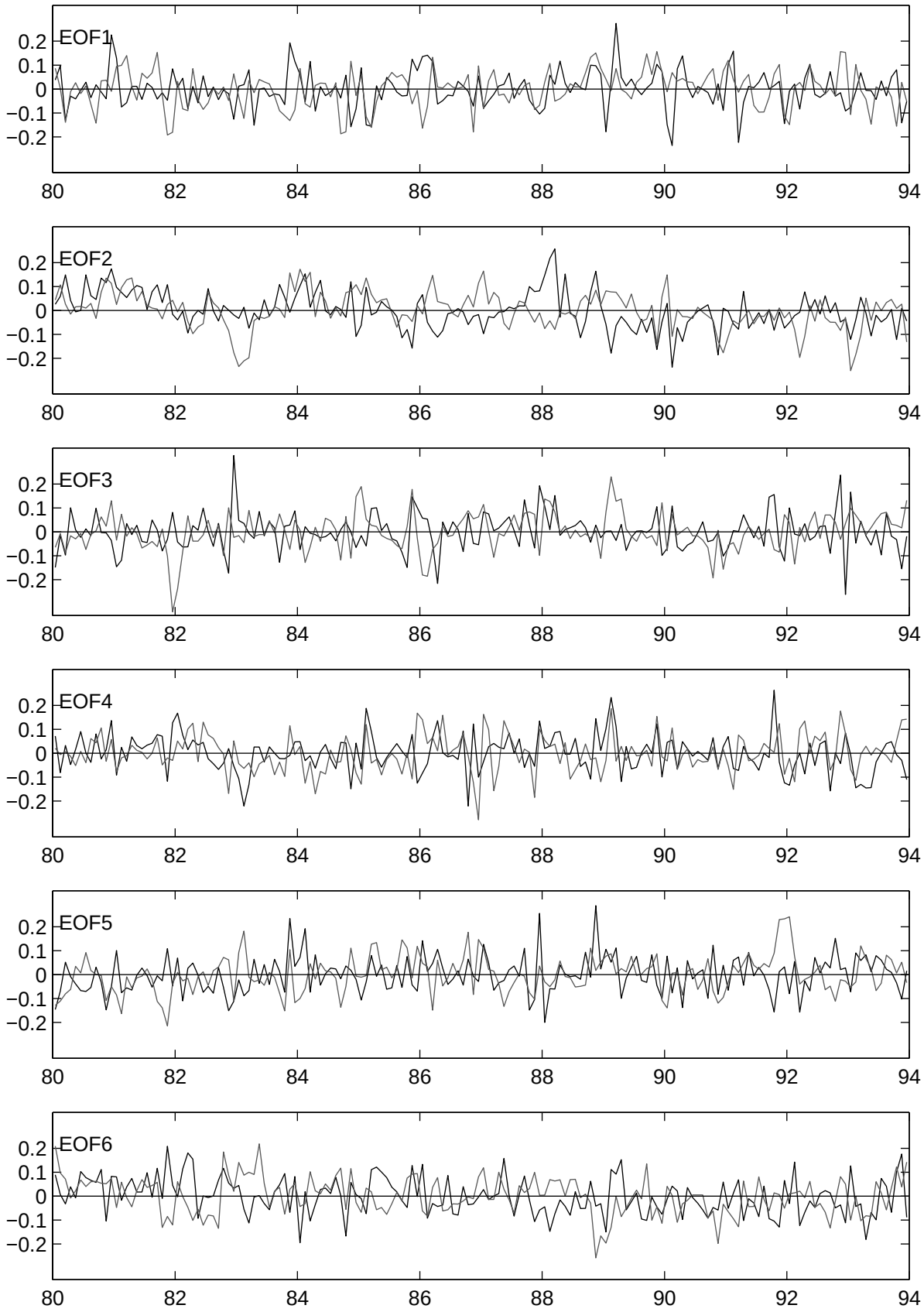

Fig. 16m Time series of North Pacific Qlat EOFs 1 to 6. SOC−black, HC−grey.

Fig.17a HC Qsw - eof1 , 16.82 % , dist

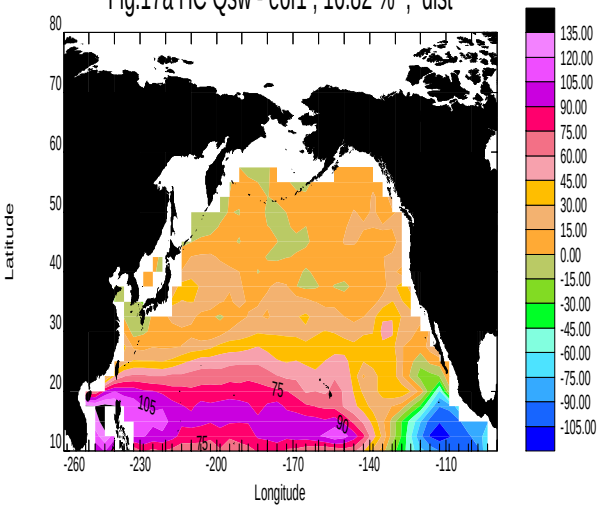

Fig.17b HC Qsw - eof2 , 10.31 % , dist

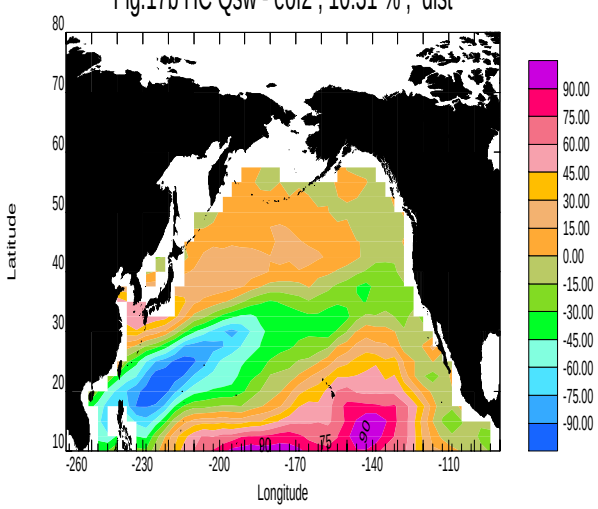

Fig.17c HC Qsw - eof3 , 6.65 % , dist

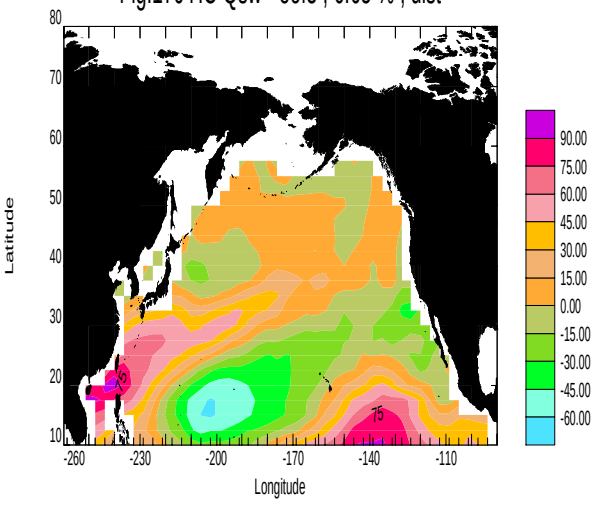

Fig.17d HC Qsw - eof4 , 5.69 % , dist

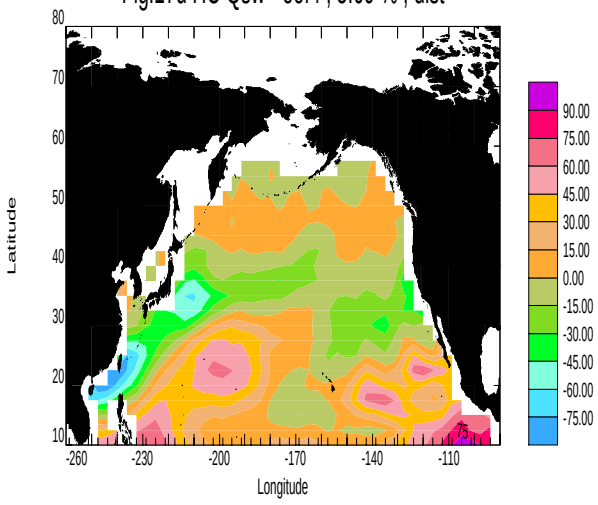

Fig.17e HC Qsw - eof5 , 3.79 % , ndist

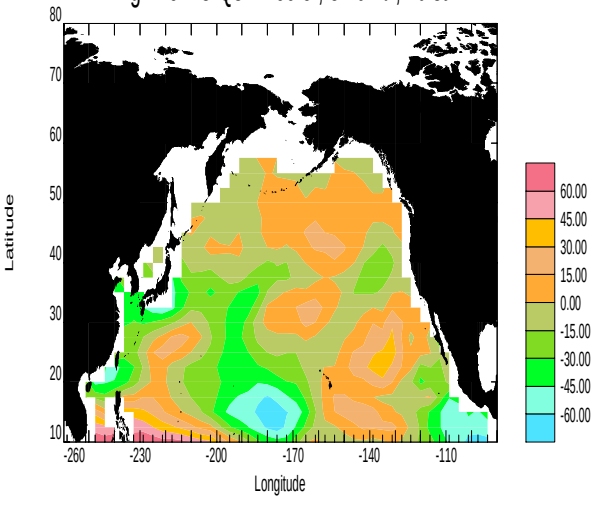

Fig.17f HC Qsw - eof6 , 3.65 % , ndist

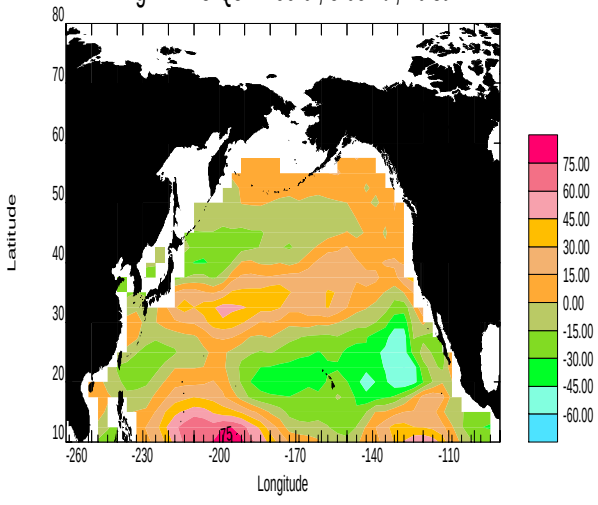

Fig.17g SOC Qsw - eof1 , 7.05 % , dist

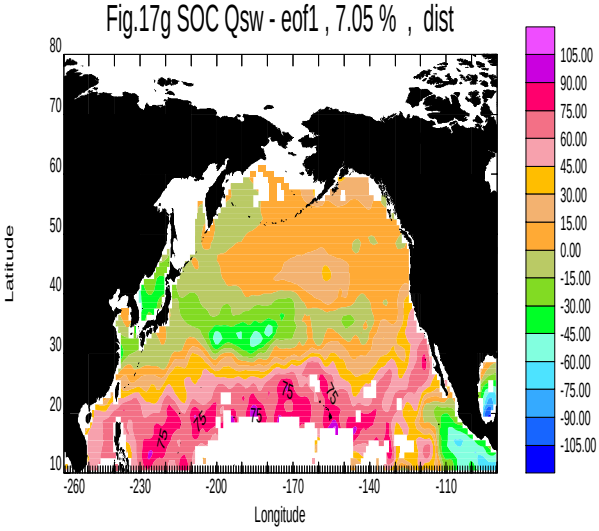

Fig.17h SOC Qsw - eof2 , 5.72 % , dist

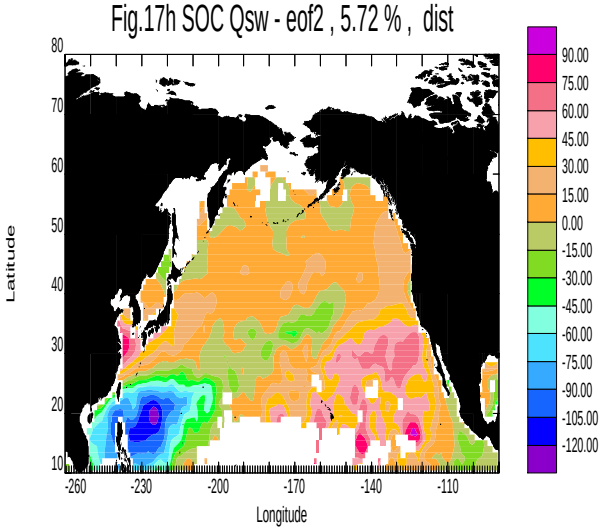

Fig.17i SOC Qsw - eof3 , 4.59 % , dist

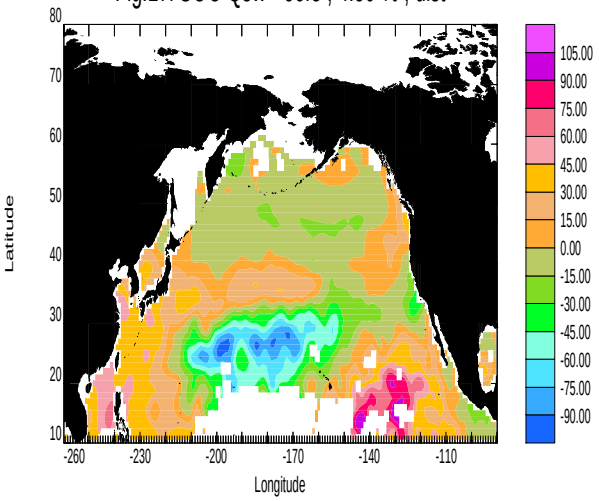

Fig.17j SOC Qsw - eof4 , 3.84 % , dist

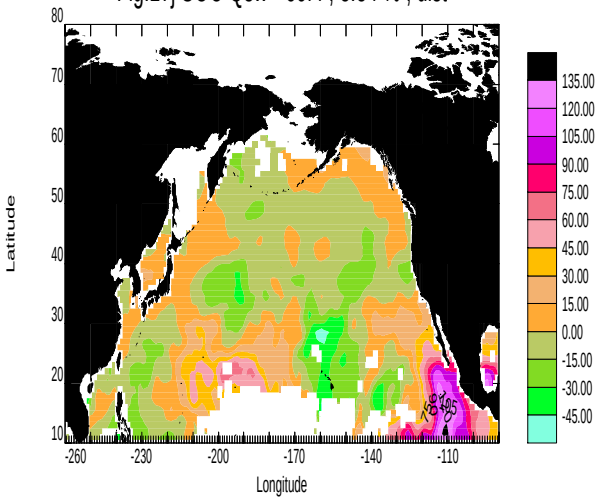

Fig.17k SOC Qsw - eof5 , 3.47 % , dist

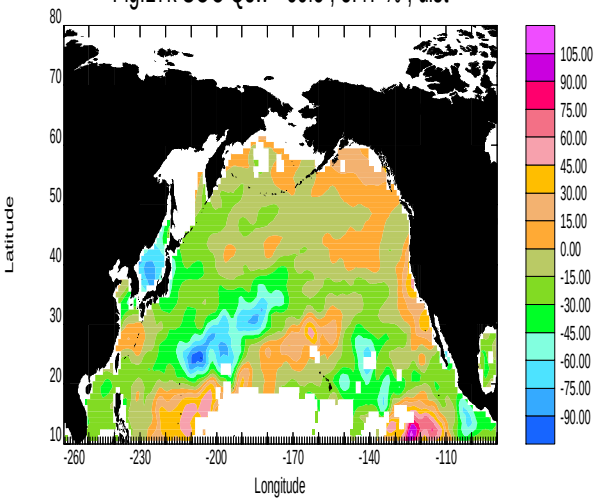

Fig.17l SOC Qsw - eof6 , 3.34 % , dist

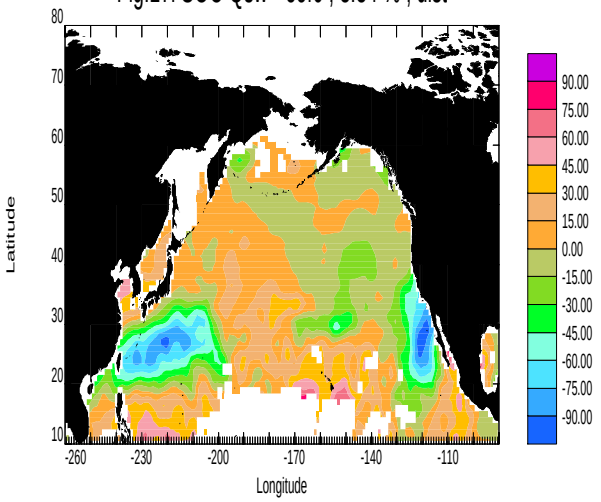

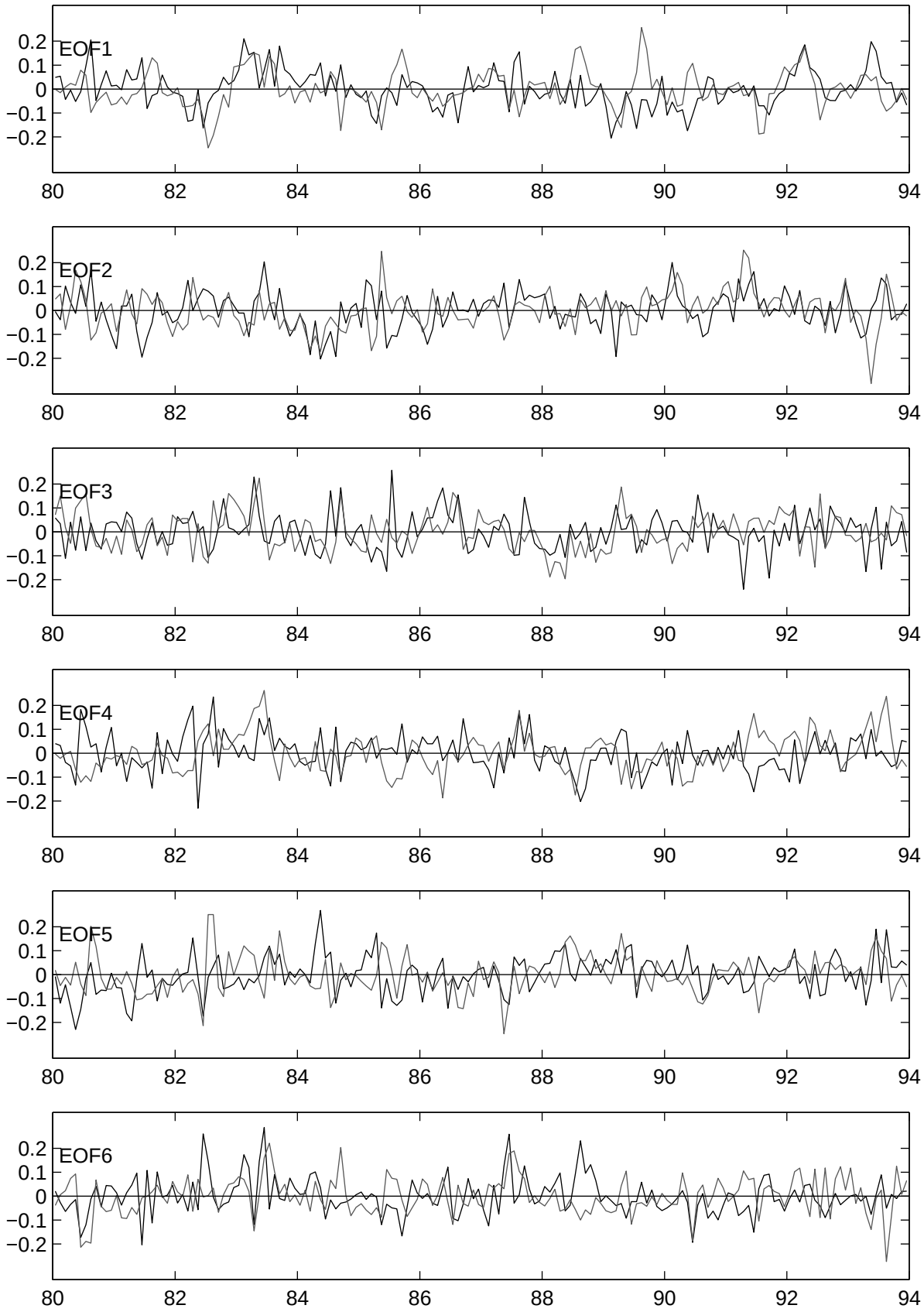

Fig. 17m Time series of North Pacific Qsw EOFs 1 to 6. SOC−black, HC−grey.

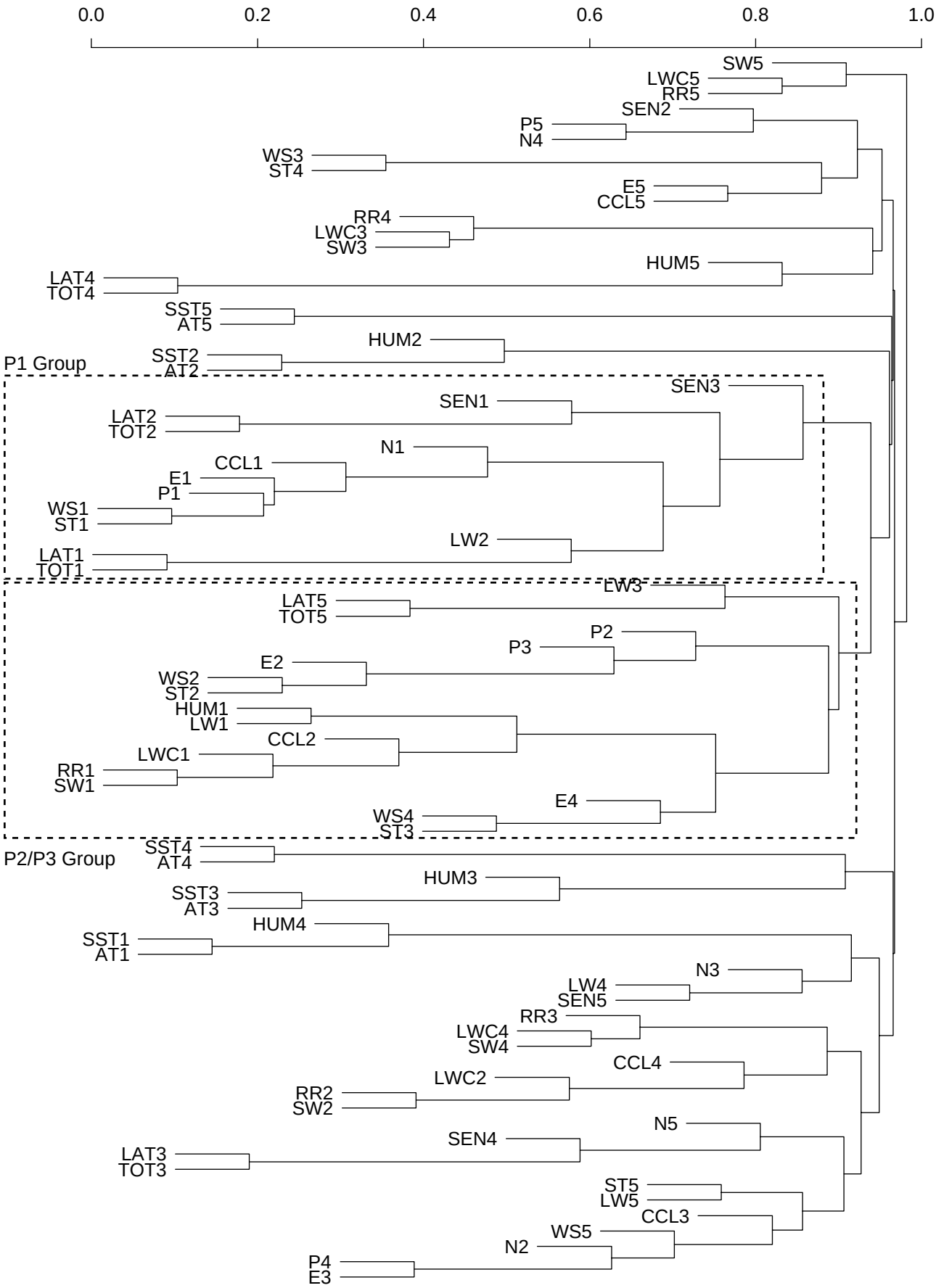

Fig. 18 Cluster analysis of HadAM3 North Pacific EOFs.

Fig.19a HC qntdm - eof1 , 5.38 % , dist

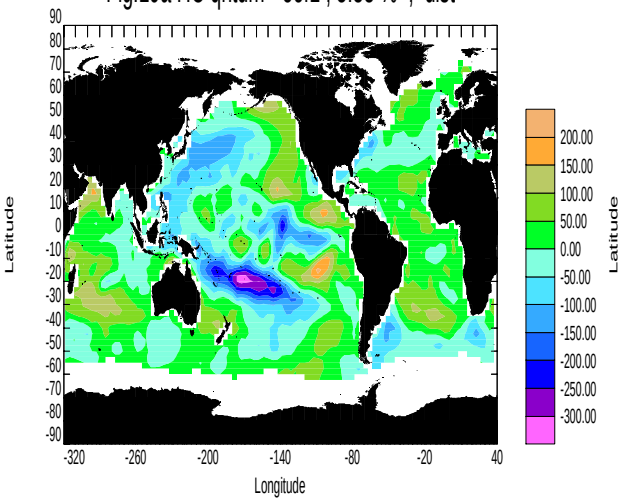

Fig.19b HC qntdm - eof2 , 3.72 % , dist

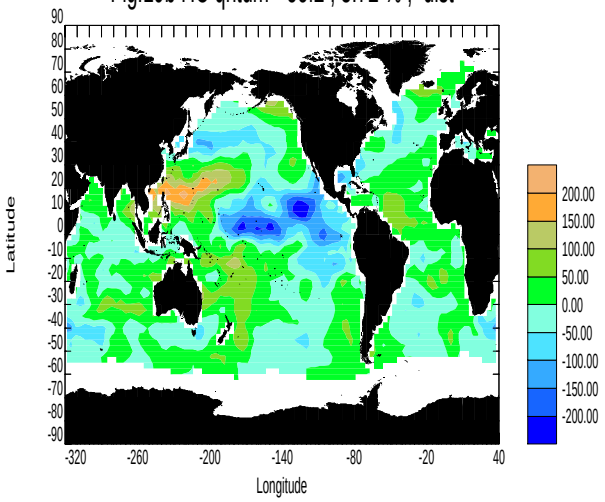

Fig.19c HC qntdm - eof3 , 3.50 % , dist

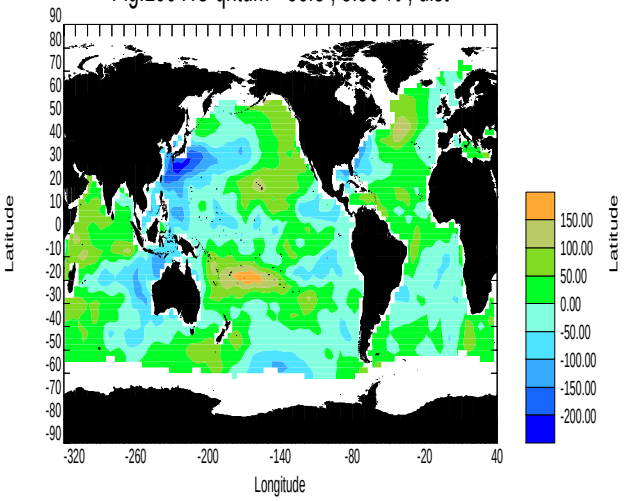

Fig.19d HC qntdm - eof4 , 3.08 % , dist

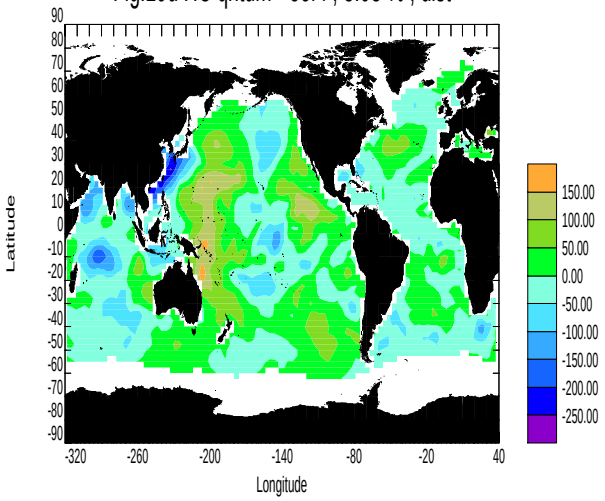

Fig.19e HC qntdm - eof5 , 2.72 % , dist

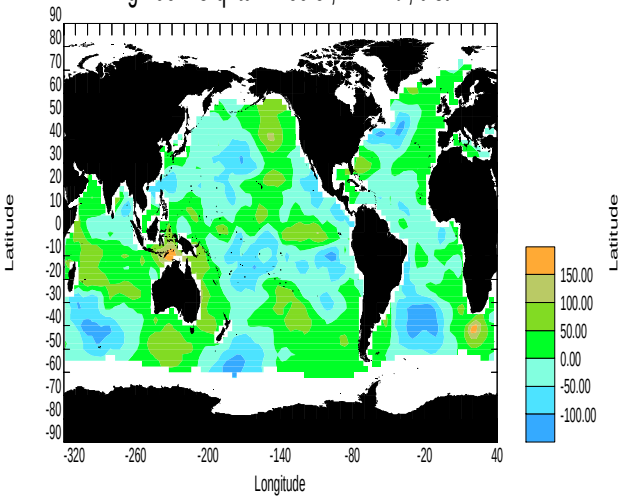

Fig.19f HC qntdm - eof6 , 2.33 % , dist

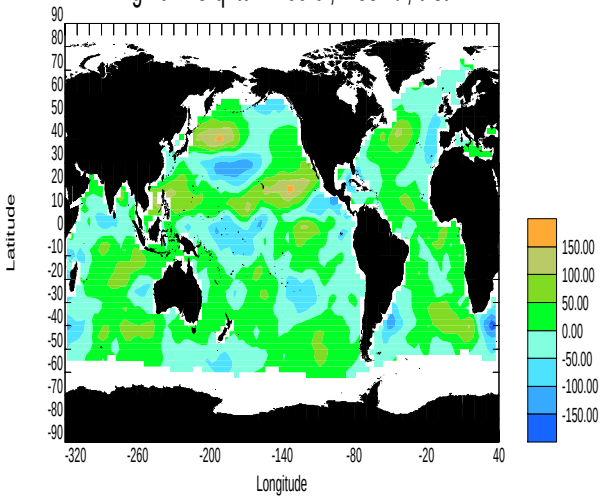

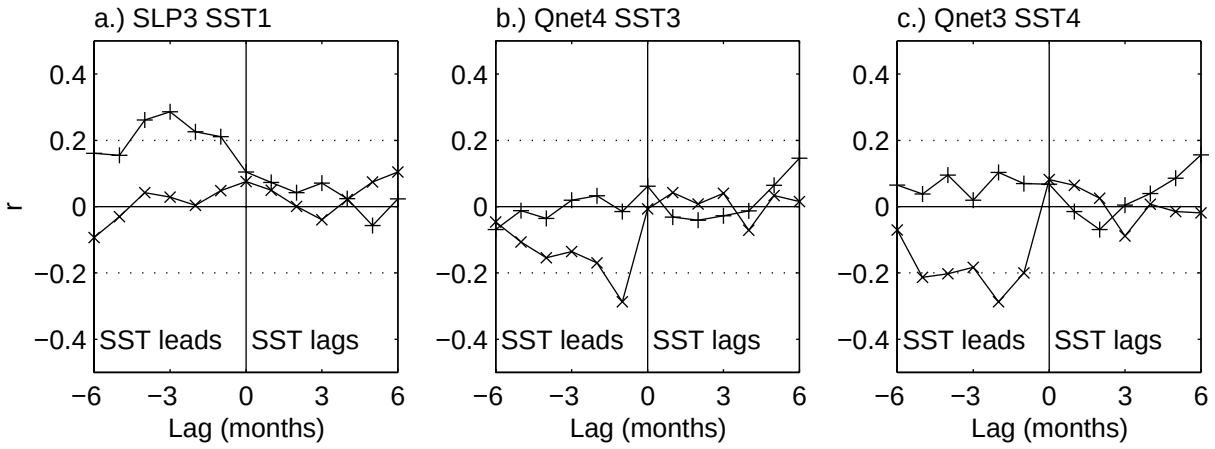

Fig.20 Lagged correlation plots for selected EOF pairs. The time axis gives the number of months by which the second member of the pair lags the first i.e. negative values imply SST leading. SOC (x symbol), HadAM3 (+ symbol).

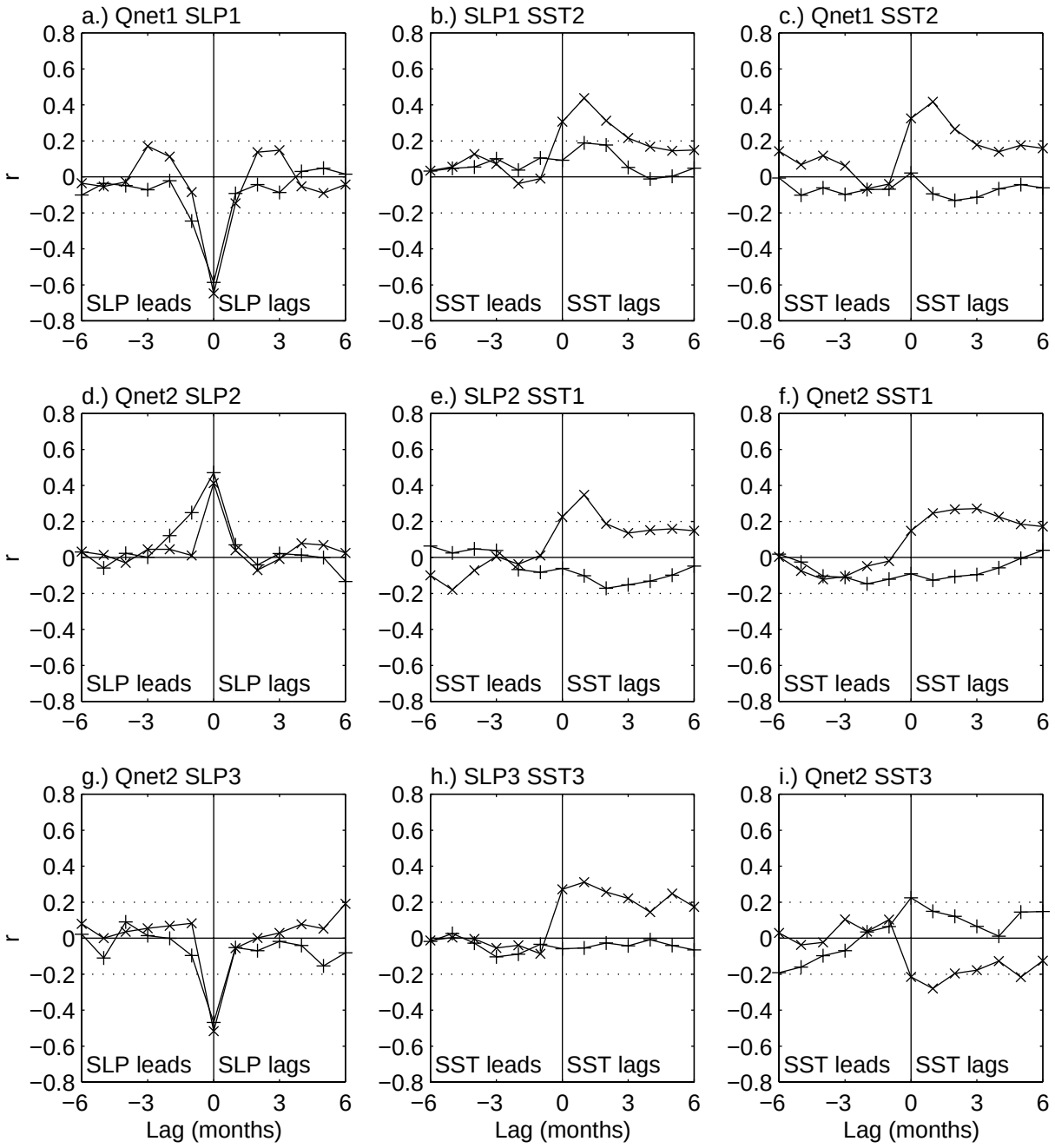

Fig.21 Lagged correlation plots for selected EOF pairs. The time axis gives the number of months by which the second member of the pair lags the first e.g. negative values imply SST leading. SOC (x symbol), HadAM3 (+ symbol).

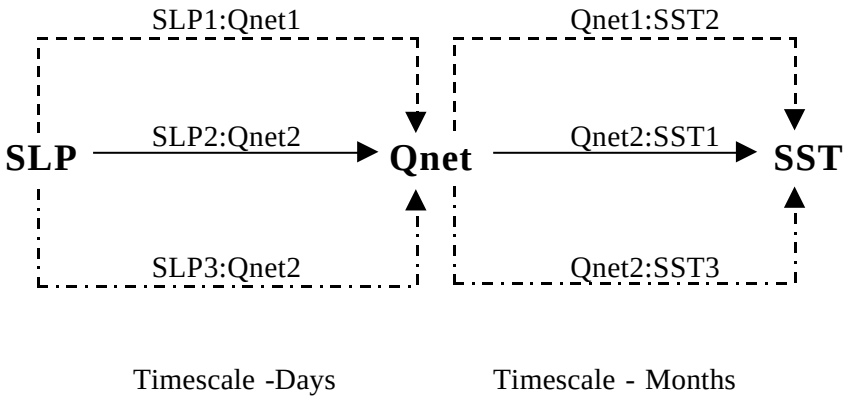

Fig.21j.) A schematic representation of the relationship between paired EOF modes that form the three groups discussed in Section 4.1.

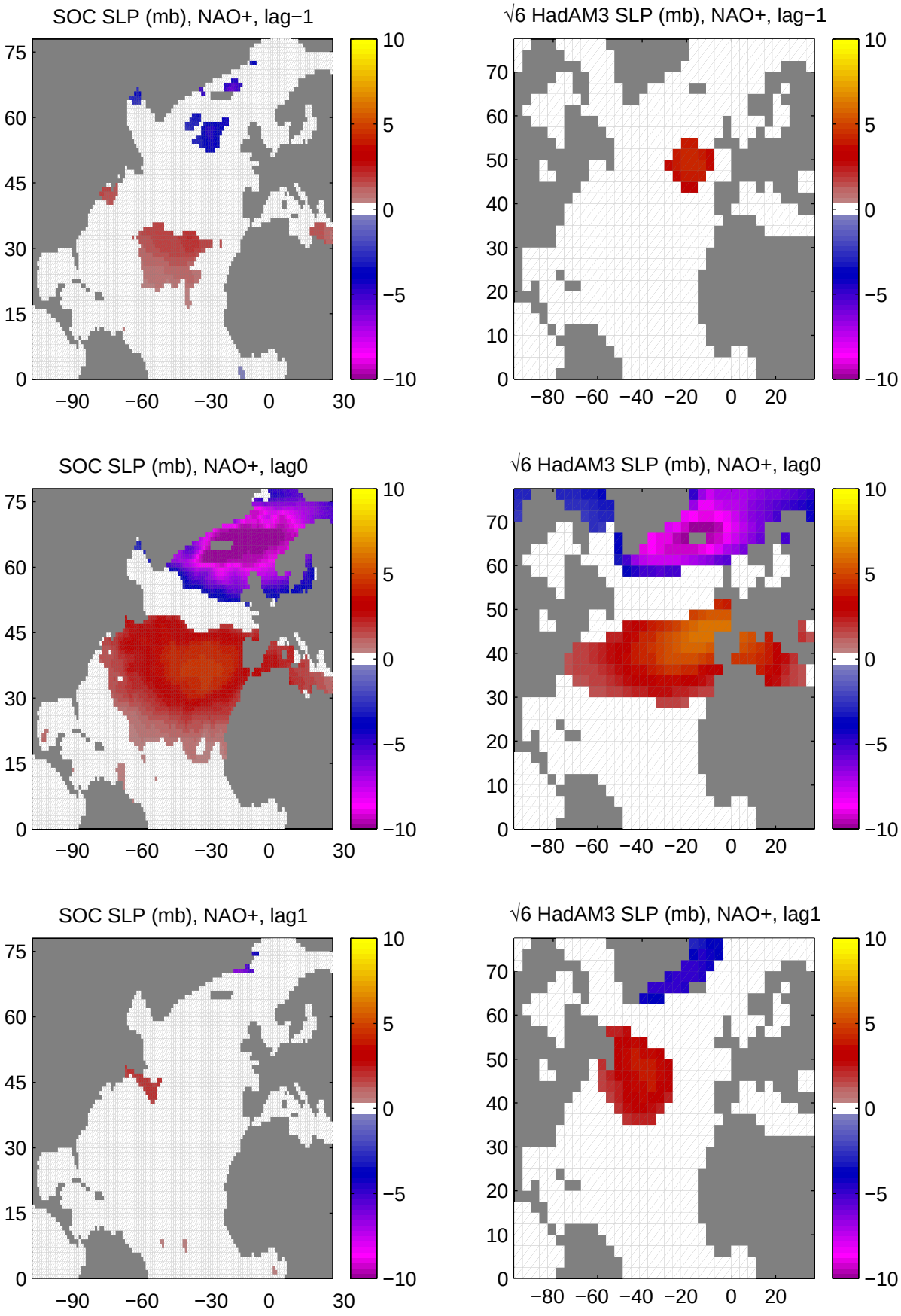

Fig.22a. SLP composite anomalies at various lags with respect to NAO+ index maximum. Only anomalies that are significant at 5% level shown, lag intervals are in units of months, negative values imply a lead interval.

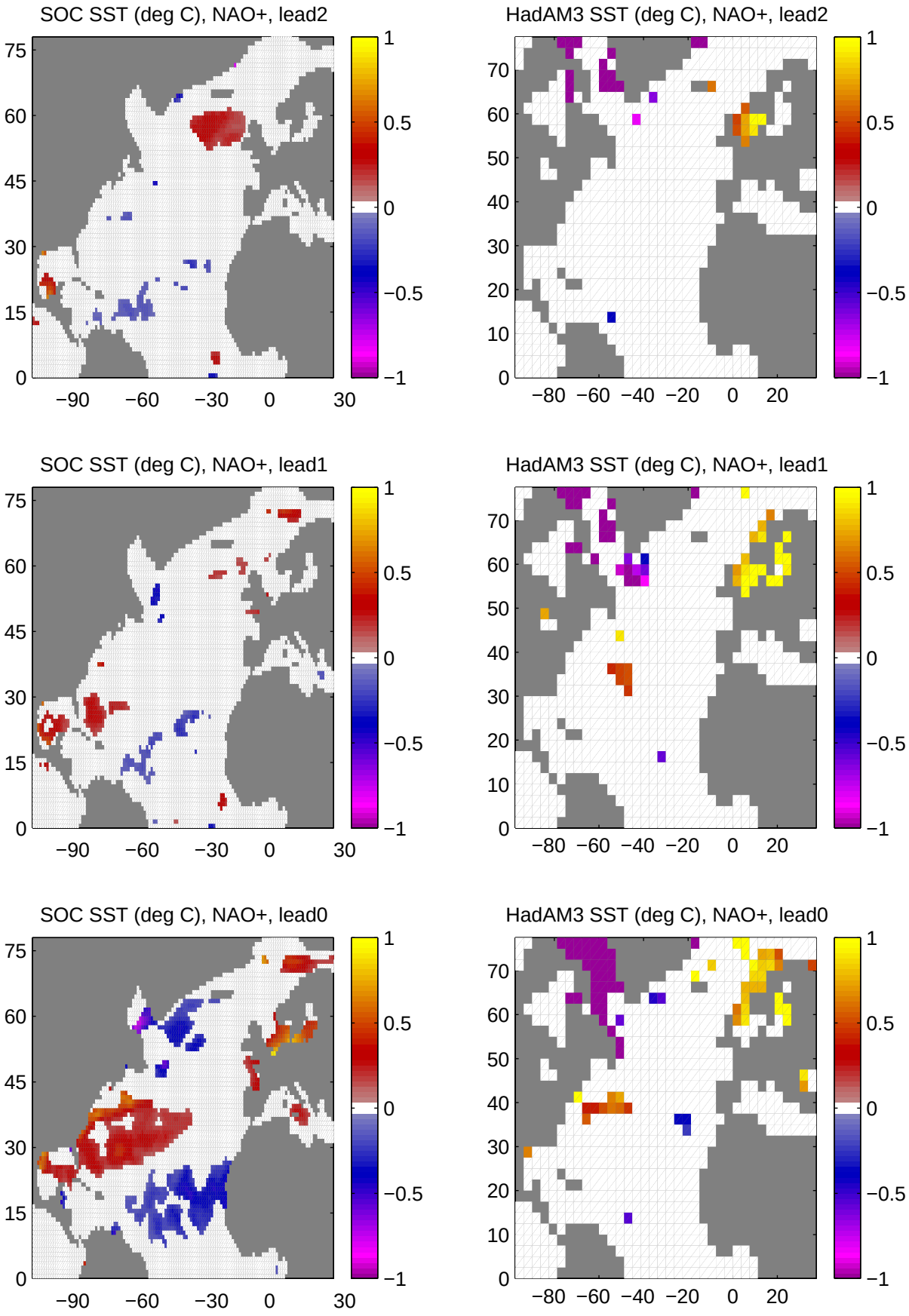

Fig.22b. SST composite anomalies at various leads with respect to NAO+ index maximum. Only anomalies that are significant at 5% level shown. Lead intervals are in units of months.

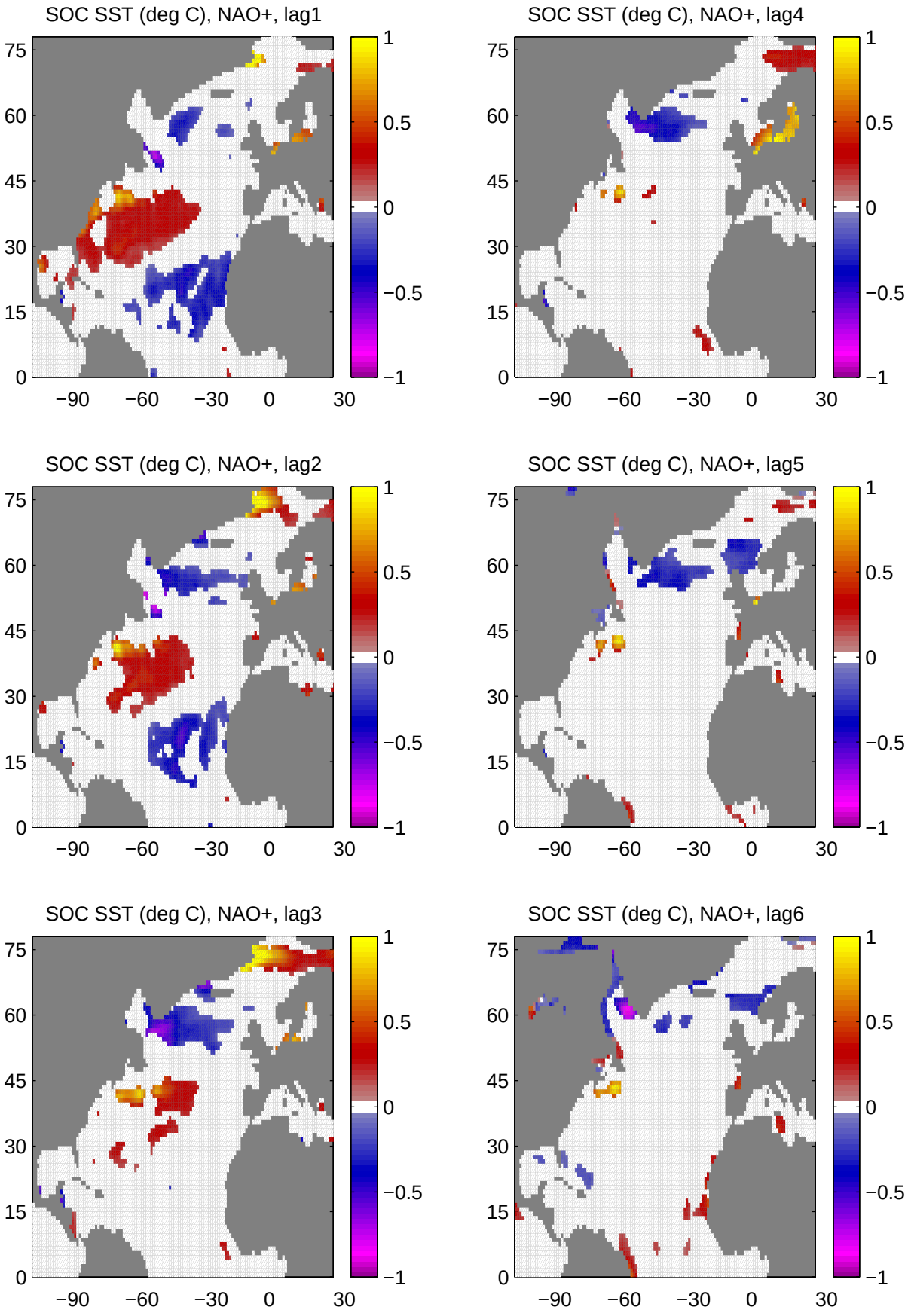

Fig.22c. SST composite anomalies at various lags with respect to NAO+ index maximum. Only anomalies that are significant at 5% level shown. Lag intervals are in units of months.

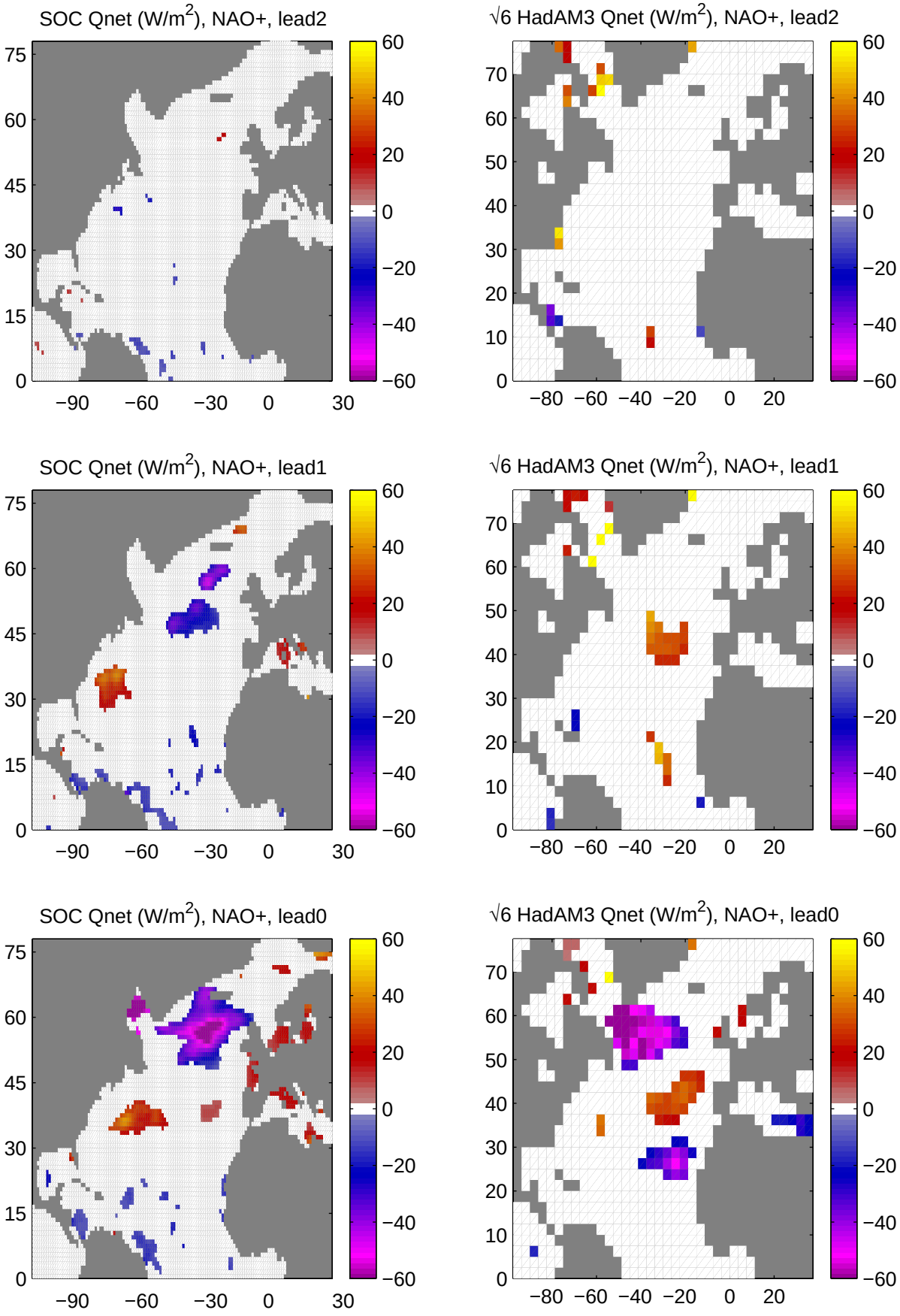

Fig.22d. Qnet composite anomalies at various leads with respect to NAO+ index maximum. Only anomalies that are significant at 5% level shown. Lead intervals are in units of months.

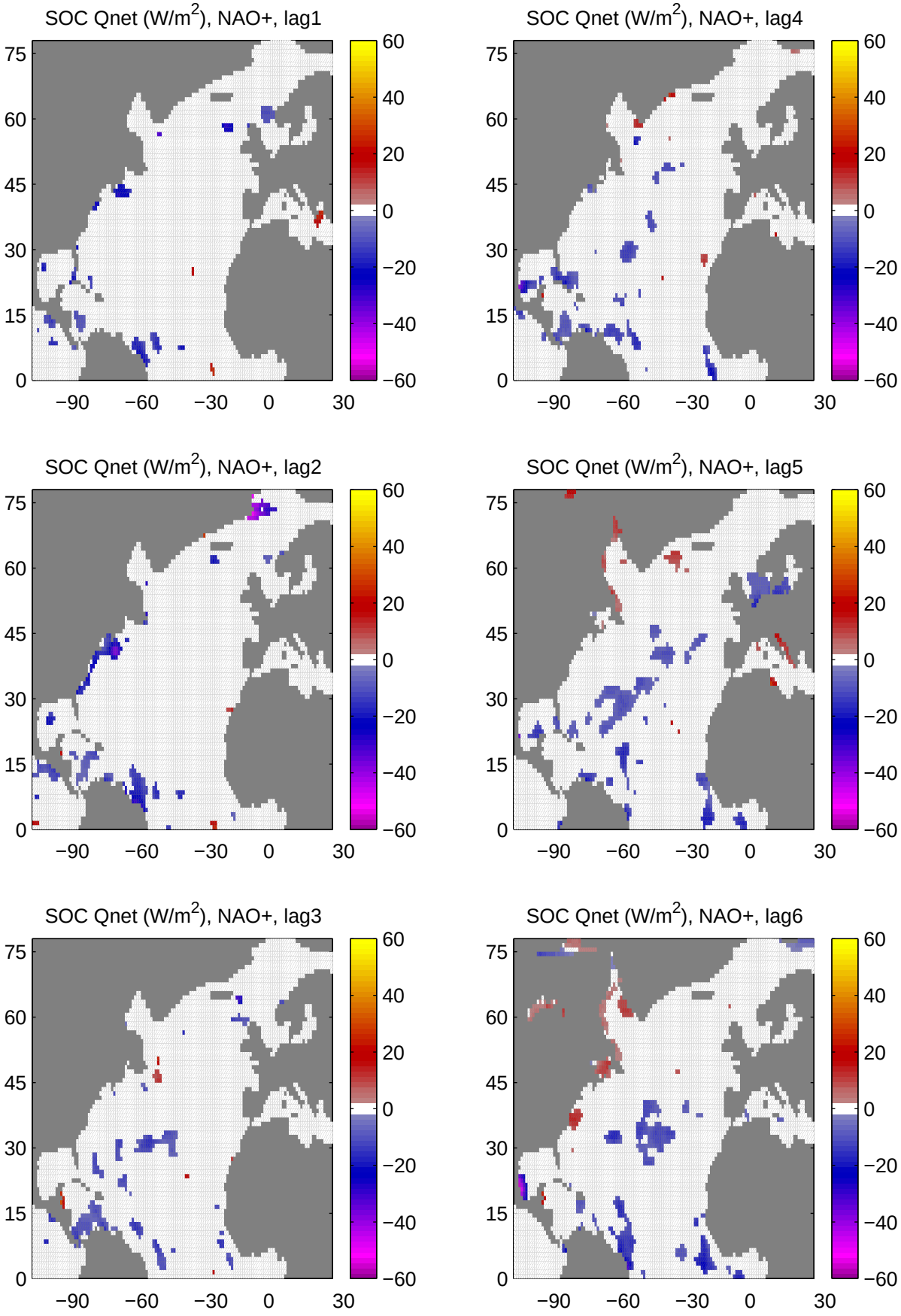

Fig.22e. Qnet composite anomalies at various lags with respect to NAO+ index maximum. Only anomalies that are significant at 5% level shown. Lag intervals are in units of months.

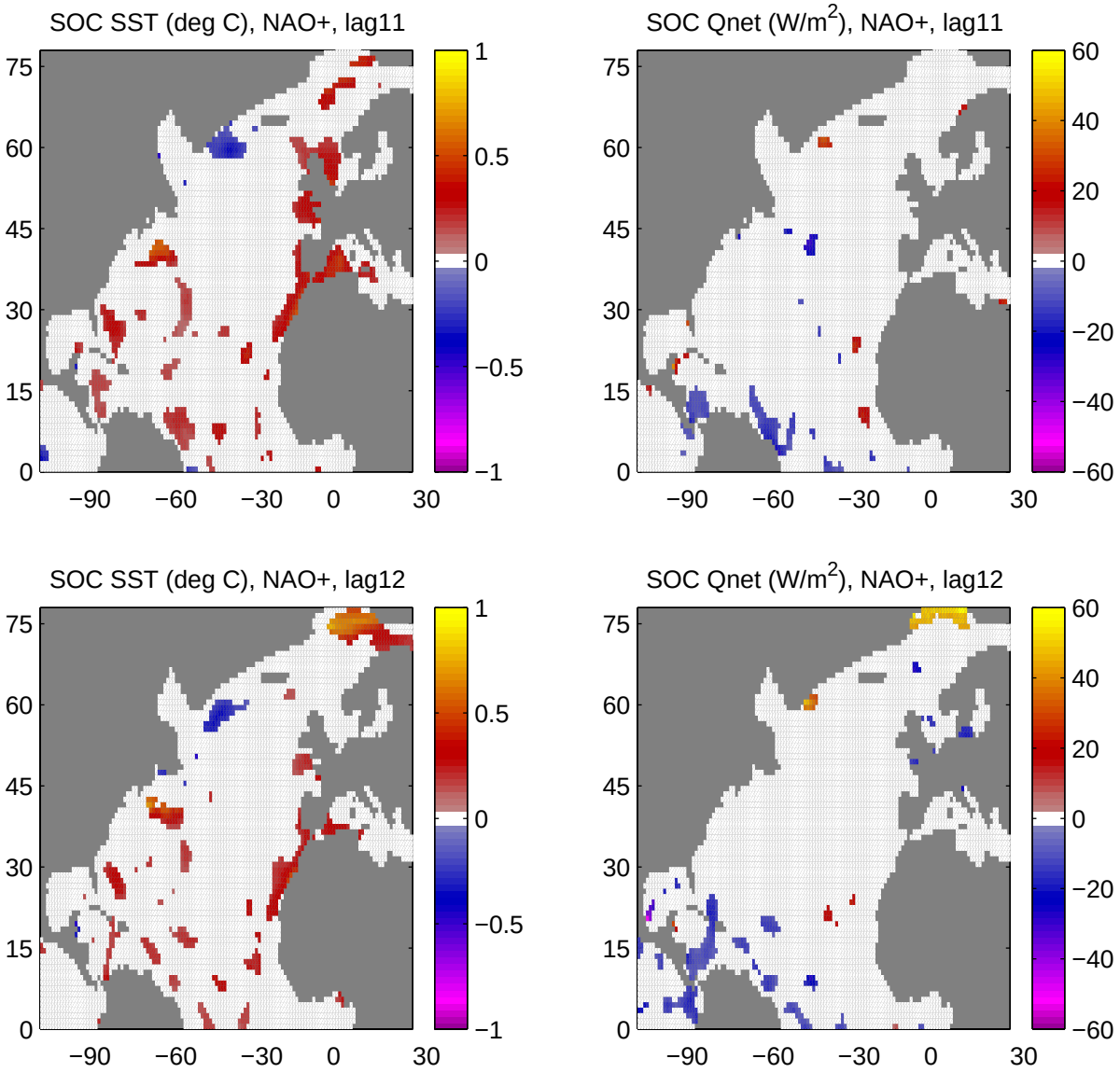

Fig.22f. SST & Qnet composite anomalies at 11−12 month lags with respect to NAO+ index maximum. Only anomalies that are significant at 5% level shown.

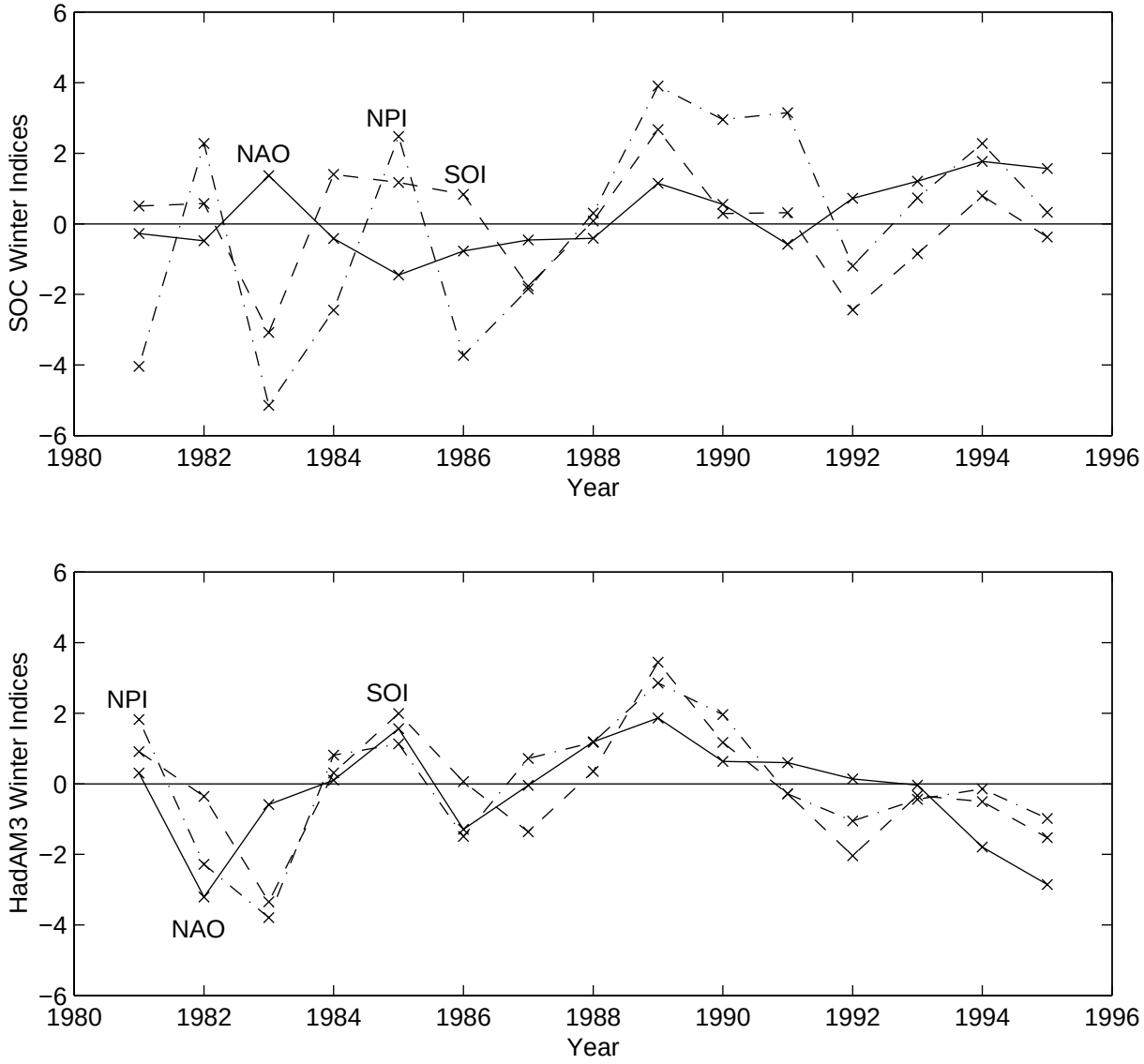

Fig. 23) Time series of NAO, NPI and SOI winter(Nov−Mar) indices in SOC and HadAM3

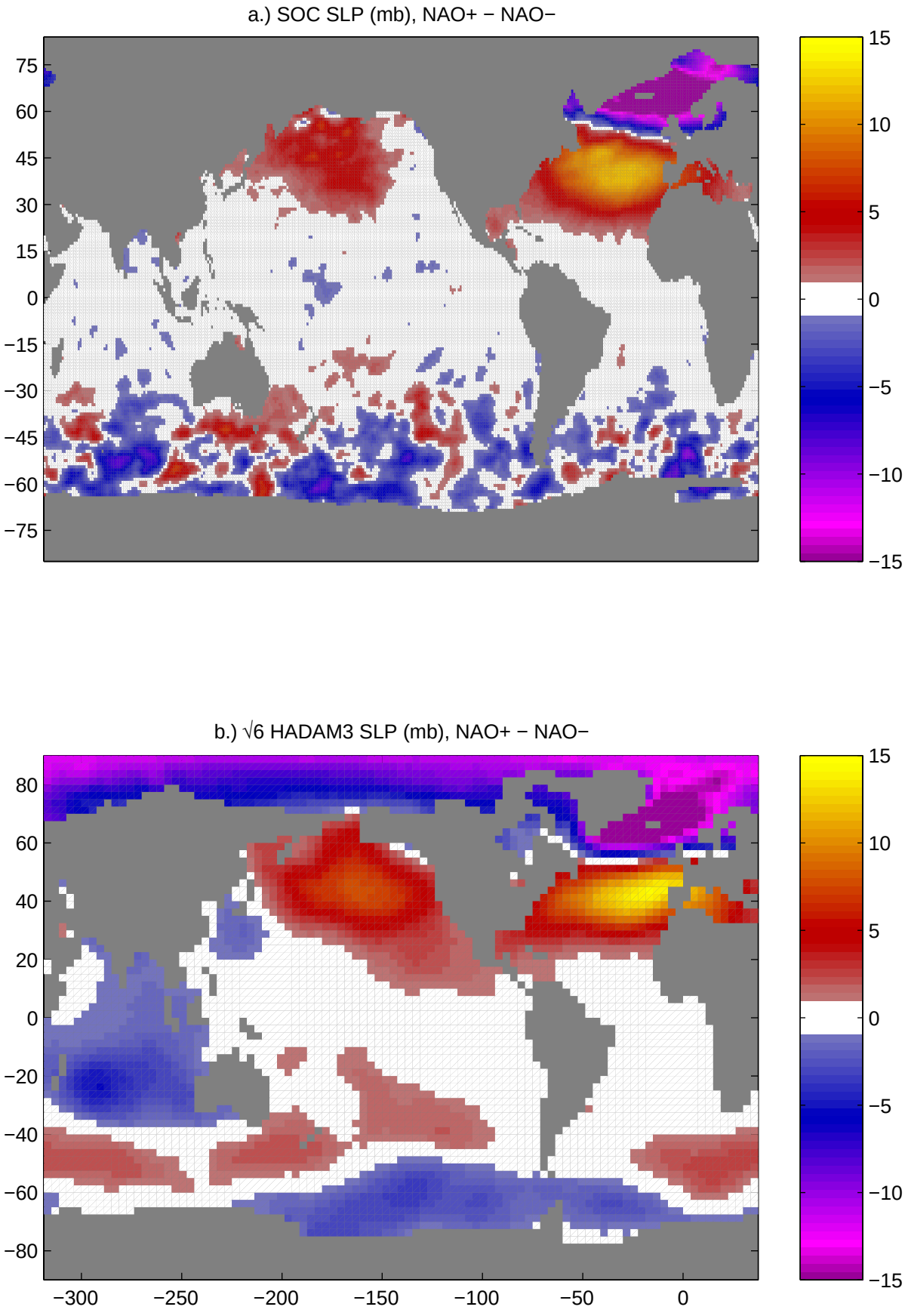

Fig. 24) Difference in global sea level pressure composite anomaly plots for NAO+ and NAO− states within the period 1980−1995.